Appendix A

Ellipsoid Potential Flow Calculations

Starting from and expanding on portions of Lamb [34] (Art.112 - Art.114) and Milne-Thomson [35] (17.50-17.52) the velocity potential and subsequent velocity of an ideal fluid around a stationary ellipsoid is determined. The work of Lamb was also the starting point for Costi and Portnoy [110], and Band and Payne [36] in their work looking at the flow around ellipsoid shapes.

The analysis starts from the equation for confocal quadratic surfaces

$$\frac{x^2}{a^2+\theta}+\frac{y^2}{b^2+\theta}+\frac{z^2}{c^2+\theta}-1=0 \tag{A.1}$$

Eq. A.1 has three roots; the first, say λ, between ∞ and $-c^2$; another root, say μ, between $-c^2$ and $-b^2$; the last root, say ν, between $-b^2$ and $-a^2$. The surface defined by Eq. A.1 when θ is between ∞ and $-c^2$ is a ellipsoid, thus when $\theta=\lambda$ the surface is ellipsoidal. The surface defined by Eq. A.1 when θ is between c^2 and $-b^2$ is a hyperboloid of one sheet; thus when $\theta=\mu$ the surface is a hyperboloid of one sheet. The surface defined by Eq. A.1 when θ is between b^2 and $-a^2$ is a hyperboloid of two sheet; thus when $\theta=\nu$ the surface is an hyperboloid of two sheets. From the definition of λ, μ and ν Eq. A.1 may also be written in the form

$$\frac{x^2}{a^2+\theta}+\frac{y^2}{b^2+\theta}+\frac{z^2}{c^2+\theta}-1=\frac{(\lambda-\theta)(\mu-\theta)(\nu-\theta)}{(a^2+\theta)(b^2+\theta)(c^2+\theta)} \tag{A.2}$$

From Eq. A.2, expressions for x^2, y^2 and z^2 may be obtained. The expression for x^2 is obtained by multiplying both sides of Eq. A.2 by $(a^2+\theta)$ and then setting $\theta=-a^2$. The

expressions for y^2 and z^2 are obtained in a similar manner, giving

$$\begin{aligned} x^2 &= \frac{(a^2+\lambda)(a^2+\mu)(a^2+\nu)}{(a^2-b^2)(a^2-c^2)} \\ y^2 &= \frac{(b^2+\lambda)(b^2+\mu)(b^2+\nu)}{(b^2-c^2)(b^2-a^2)} \\ z^2 &= \frac{(c^2+\lambda)(c^2+\mu)(c^2+\nu)}{(c^2-a^2)(c^2-b^2)} \end{aligned} \tag{A.3}$$

Partial differentiation of the expression for x^2 in Eq. A.3 with respect to λ, with μ and ν held constant, gives

$$\frac{\partial x}{\partial \lambda} = \frac{(a^2+\mu)(a^2+\nu)}{2(a^2-b^2)(a^2-c^2)\sqrt{\dfrac{(a^2+\lambda)(a^2+\mu)(a^2+\nu)}{(a^2-b^2)(a^2-c^2)}}} \tag{A.4}$$

The square root term in the denominator is x from Eq. A.3. The expression for x^2 from Eq. A.3 may be restated as

$$\frac{x^2}{(a^2+\lambda)} = \frac{(a^2+\mu)(a^2+\nu)}{(a^2-b^2)(a^2-c^2)} \tag{A.5}$$

so Eq. A.4 and the similar terms for $\dfrac{\partial y}{\partial \lambda}$ and $\dfrac{\partial z}{\partial \lambda}$ may be written as

$$\begin{aligned} \frac{\partial x}{\partial \lambda} &= \frac{x}{2(a^2+\lambda)} \\ \frac{\partial y}{\partial \lambda} &= \frac{y}{2(b^2+\lambda)} \\ \frac{\partial z}{\partial \lambda} &= \frac{z}{2(c^2+\lambda)} \end{aligned} \tag{A.6}$$

Poisson's equation in ellipsoidal coordinates is

$$\begin{aligned} \nabla^2\Phi = &\frac{-4}{(\lambda-\mu)(\mu-\nu)(\nu-\lambda)}\left[(\mu-\nu)\Delta_\lambda \frac{\partial}{\partial\lambda}\left(\Delta_\lambda \frac{\partial\Phi}{\partial\lambda}\right) + \right. \\ &\left.(\nu-\lambda)\Delta_\mu \frac{\partial}{\partial\mu}\left(\Delta_\mu \frac{\partial\Phi}{\partial\mu}\right) + (\lambda-\mu)\Delta_\nu \frac{\partial}{\partial\nu}\left(\Delta_\nu \frac{\partial\Phi}{\partial\nu}\right)\right] \end{aligned} \tag{A.7}$$

where

$$\begin{aligned} \Delta_\lambda^2 &= (a^2+\lambda)(b^2+\lambda)(c^2+\lambda) \\ \Delta_\mu^2 &= (a^2+\mu)(b^2+\mu)(c^2+\mu) \\ \Delta_\nu^2 &= (a^2+\nu)(b^2+\nu)(c^2+\nu) \end{aligned} \tag{A.8}$$

As a scalar solution of $\nabla^2\Phi = 0$ is desired, Eq. A.7 may be shortened to

$$\begin{aligned} 0 = \Bigg(&(\mu-\nu)\Delta_\lambda \frac{\partial}{\partial\lambda}\left(\Delta_\lambda \frac{\partial\Phi}{\partial\lambda}\right) + \\ &(\nu-\lambda)\Delta_\mu \frac{\partial}{\partial\mu}\left(\Delta_\mu \frac{\partial\Phi}{\partial\mu}\right) + (\lambda-\mu)\Delta_\nu \frac{\partial}{\partial\nu}\left(\Delta_\nu \frac{\partial\Phi}{\partial\nu}\right)\Bigg) \end{aligned} \tag{A.9}$$

A solution for $\Phi(\lambda,\mu,\nu)$ in Eq. A.9 is required. Lamb [34] shortens his derivation by assuming a solution of a set form. Milne-Thomson [35] provides a more detailed derivation. Milne-Thomson's solution is followed here.

If a solution of the form

$$\Phi = \eta(\lambda,\mu,\nu)\chi(\lambda) \tag{A.10}$$

is assumed, where $\eta(\lambda,\mu,\nu)$ is also a solution of Eq. A.9 (an ellipsoidal harmonic). $\chi(\lambda)$ is a function of λ. Substituting Eq. A.10 into the first term of Eq. A.9 gives

$$\begin{aligned} &(\mu-\nu)\Delta_\lambda \frac{\partial}{\partial\lambda}\left(\Delta_\lambda \frac{\partial\Phi}{\partial\lambda}\right) \\ &= (\mu-\nu)\left(\frac{\partial\Delta_\lambda}{\partial\lambda}\eta\frac{\partial\chi}{\partial\lambda} + 2\Delta_\lambda\frac{\partial\eta}{\partial\lambda}\frac{\partial\chi}{\partial\lambda} + \Delta_\lambda\eta\frac{\partial^2\chi}{\partial\lambda^2} + \chi\left(\frac{\partial\Delta_\lambda}{\partial\lambda}\frac{\partial\eta}{\partial\lambda} + \Delta_\lambda\frac{\partial^2\eta}{\partial\lambda^2}\right)\right) \\ &= (\mu-\nu)\left(\frac{\partial\Delta_\lambda}{\partial\lambda}\eta\frac{\partial\chi}{\partial\lambda} + 2\Delta_\lambda\frac{\partial\eta}{\partial\lambda}\frac{\partial\chi}{\partial\lambda} + \Delta_\lambda\eta\frac{\partial^2\chi}{\partial\lambda^2} + \chi\frac{\partial}{\partial\lambda}\left(\Delta_\lambda\frac{\partial\eta}{\partial\lambda}\right)\right) \end{aligned} \tag{A.11}$$

Substituting Eq. A.10 and Eq. A.11 into Eq. A.9 gives

$$\begin{aligned} 0 =&(\mu-\nu)\left(\frac{\partial\Delta_\lambda}{\partial\lambda}\eta\frac{\partial\chi}{\partial\lambda} + 2\Delta_\lambda\frac{\partial\eta}{\partial\lambda}\frac{\partial\chi}{\partial\lambda} + \Delta_\lambda\eta\frac{\partial^2\chi}{\partial\lambda^2}\right) + \chi\Bigg((\mu-\nu)\Delta_\lambda\frac{\partial}{\partial\lambda}\left(\Delta_\lambda\frac{\partial\eta}{\partial\lambda}\right) + \\ &(\nu-\lambda)\Delta_\mu\frac{\partial}{\partial\mu}\left(\Delta_\mu\frac{\partial\eta}{\partial\mu}\right) + (\lambda-\mu)\Delta_\nu\frac{\partial}{\partial\nu}\left(\Delta_\nu\frac{\partial\eta}{\partial\nu}\right)\Bigg) \end{aligned} \tag{A.12}$$

where the term in Eq. A.12 multiplied by χ may be set to zero, as η is a solution of Laplace's equation. Dividing the remaining terms of Eq. A.12 by $\Delta_\lambda\eta\frac{\partial\chi}{\partial\lambda}$ gives

$$0 = \frac{\frac{\partial\Delta_\lambda}{\partial\lambda}}{\Delta_\lambda} + 2\frac{\frac{\partial\eta}{\partial\lambda}}{\eta} + \frac{\frac{\partial^2\chi}{\partial\lambda^2}}{\frac{\partial\chi}{\partial\lambda}} \tag{A.13}$$

which with use of the identity $\frac{\partial}{\partial x}\left(\log_e\left[f(x)\right]\right) = \frac{f'(x)}{f(x)}$ may be reworked to

$$\frac{\partial}{\partial\lambda}\left(\log_e\left[\Delta_\lambda\frac{\partial\chi}{\partial\lambda}\right]\right) = -\frac{2}{\eta}\frac{\partial\eta}{\partial\lambda} \tag{A.14}$$

Since the left hand side of Eq. A.14 is a function of λ only, so must be the right hand side. Thus it must be possible to express

$$\eta = \eta_\lambda(\lambda) f(\mu, \nu) \tag{A.15}$$

where η_λ is a function of λ only and f is a function of only μ and ν. Substituting Eq. A.15 into Eq. A.14 results in

$$\frac{\partial}{\partial\lambda}\left(\log_e\left[\Delta_\lambda \frac{\partial\chi}{\partial\lambda}\right]\right) = \frac{\partial}{\partial\lambda}\left(\log_e\left[\frac{1}{\eta_\lambda^2}\right]\right) \tag{A.16}$$

which may be integrated w.r.t λ to give,

$$\log_e\left[\Delta_\lambda \frac{\partial\chi}{\partial\lambda}\right] = \log_e\left[\frac{1}{\eta_\lambda^2}\right] + \log_e[C] \tag{A.17}$$

When exponentiated, divided by Δ_λ and integrated again w.r.t λ this gives

$$\chi = C\int \frac{d\lambda}{\eta_\lambda^2 \Delta_\lambda} + D \tag{A.18}$$

where C and D are constants of integration.

A.1 Translation of Ellipsoid

η is a spherical harmonic, so expressions that satisfy the Laplacian include $\eta = 1, x, y, z, xy, etc.$ (see Hobson [111] for more details). Taking the case where $\eta = x$ from Eq. A.3

$$\eta \;\propto\; \sqrt{(a^2+\lambda)(a^2+\mu)(a^2+\nu)} \tag{A.19}$$

so from Eq. A.15 and Eq. A.19[1]

$$\eta_\lambda = \sqrt{(a^2+\lambda)} \tag{A.20}$$

Substituting Eq. A.18, Eq. A.19 and Eq. A.20 into Eq. A.10 results in

$$\Phi_x = C\,x\int_\lambda^\infty \frac{d\lambda^*}{(a^2+\lambda^*)\Delta_{\lambda^*}} + D \tag{A.21}$$

where the * superscript indicates a dummy variable for integration.

[1]Note in Eq. A.19 $\propto$ is proportional not alpha

The boundary condition on the surface of an ellipsoid moving parallel to the x axis is

$$\frac{\partial \Phi}{\partial \lambda} = -U_0 \frac{\partial x}{\partial \lambda} \text{ at } \lambda = 0 \tag{A.22}$$

where U_0 is the velocity in the x direction at ∞. Substituting Eq. A.21 into Eq. A.22 and further simplifying with the substitution of $\frac{\partial x}{\partial \lambda}$ from Eq. A.6 results in

$$\begin{aligned} U_0 \frac{\partial x}{\partial \lambda} &= -C \left(\frac{\partial x}{\partial \lambda} \int_\lambda^\infty \frac{d\lambda^*}{(a^2+\lambda^*)\Delta_{\lambda^*}} - \frac{x}{(a^2+\lambda)\Delta_\lambda} \right) \\ &= -C \left(\frac{\partial x}{\partial \lambda} \int_\lambda^\infty \frac{d\lambda^*}{(a^2+\lambda^*)\Delta_{\lambda^*}} - \frac{\partial x}{\partial \lambda} \frac{2}{\Delta_\lambda} \right) \end{aligned} \tag{A.23}$$

The elimination of $\frac{\partial x}{\partial \lambda}$ along with the knowledge that λ has been set to zero on the surface of the ellipsoid results in

$$U_0 = -C \left(\int_0^\infty \frac{d\lambda^*}{(a^2+\lambda^*)\Delta_{\lambda^*}} - \frac{2}{a\,b\,c} \right) \tag{A.24}$$

Thus the constant C may be expressed as

$$C = \frac{U_0\, a\, b\, c}{2-\alpha_0} \tag{A.25}$$

where

$$\alpha_\lambda = a\,b\,c \int_\lambda^\infty \frac{d\lambda^*}{(a^2+\lambda^*)\Delta_{\lambda^*}} \tag{A.26}$$

When $\lambda = 0$, $\alpha_\lambda = \alpha_0$. Substituting Eq. A.25 into Eq. A.21 produces

$$\Phi_x = \frac{U_0\, x\, a\, b\, c}{2-\alpha_0} \int_\lambda^\infty \frac{d\lambda^*}{(a^2+\lambda^*)\Delta_{\lambda^*}} + D \tag{A.27}$$

On the surface of the ellipsoid, where $\lambda = 0$, Eq. A.27 may be simplified with the substitution of Eq. A.26 to give

$$\Phi_x = \frac{U_0\, x\, \alpha_0}{2-\alpha_0} + D \tag{A.28}$$

A solution for the case when the spherical harmonic $\eta = y$ or $\eta = z$, and the boundary condition is set for the ellipsoid moving parallel to the y or z direction respectively, may be written from symmetry as

$$\Phi_y = \frac{V_0\, y\, a\, b\, c}{2-\beta_0} \int_\lambda^\infty \frac{d\lambda^*}{(b^2+\lambda^*)\Delta_{\lambda^*}} + D \tag{A.29}$$

$$\Phi_z = \frac{W_0\, z\, a\, b\, c}{2-\gamma_0} \int_\lambda^\infty \frac{d\lambda^*}{(c^2+\lambda^*)\Delta_{\lambda^*}} + D \tag{A.30}$$

where V_0 and W_0 are the velocity components at infinity in the y and z directions respectively,

and

$$\beta_0 = a\,b\,c \int_0^\infty \frac{d\lambda^*}{(b^2+\lambda^*)\Delta_{\lambda^*}} \tag{A.31}$$

$$\gamma_0 = a\,b\,c \int_0^\infty \frac{d\lambda^*}{(c^2+\lambda^*)\Delta_{\lambda^*}} \tag{A.32}$$

A.2 Calculation of α_0 and γ_0 for Spheroid

In order to calculate the velocity at the surface of the ellipsoid α_0 and γ_0 must be calculated. Substituting

$$\lambda^* = \frac{a^2}{s} - a^2 \Rightarrow \partial\lambda^* = -\frac{a^2}{s^2}\partial s \tag{A.33}$$

into Eq. A.26, adjusting the limits of integration, and multiplying numerator and denominator by $\left(\frac{\sqrt{s}}{a}\right)^3$ results in

$$\begin{aligned}
\alpha_0 &= a\,b\,c \int_0^\infty \frac{d\lambda^*}{(a^2+\lambda^*)\sqrt{(a^2+\lambda^*)(b^2+\lambda^*)(c^2+\lambda^*)}} \\
&= a\,b\,c \int_1^0 \frac{-\frac{a^2}{s^2}\,ds}{\frac{a^2}{s}\sqrt{\frac{a^2}{s}\left(b^2-a^2+\frac{a^2}{s}\right)\left(c^2-a^2+\frac{a^2}{s}\right)}} \\
&= \frac{b\,c}{a^2}\int_0^1 \frac{\sqrt{s}\,ds}{\sqrt{\left((\frac{b^2}{a^2}-1)s+1\right)}\sqrt{\left((\frac{c^2}{a^2}-1)s+1\right)}}
\end{aligned} \tag{A.34}$$

If the surface is a spheroid $b/a = c/a = t$, where t is ratio of diameter to length ($t < 1$ for a prolate spheroid). Substituting t into Eq. A.34 gives

$$\begin{aligned}
\alpha_0 &= \frac{b\,c}{a^2}\int_0^1 \frac{\sqrt{s}\,ds}{\left((\frac{b^2}{a^2}-1)s+1\right)} \\
&= t^2 \int_0^1 \frac{\sqrt{s}\,ds}{\left((t^2-1)s+1\right)}
\end{aligned} \tag{A.35}$$

If the eccentricity $e^* = \sqrt{1-t^2}$ is in turn substituted for t in Eq. A.35 and the result integrated w.r.t. s, then

$$\begin{aligned}\alpha_0 &= (1-e^{*2})\int_0^1 \frac{\sqrt{s}\,ds}{1-e^{*2}s} \\ &= (1-e^{*2})\left[\frac{-2\sqrt{s}}{e^{*2}} + \frac{2\tanh^{-1}(e^*\sqrt{s})}{e^{*3}}\right]_0^1 \\ &= \frac{(1-e^{*2})}{e^{*3}}\left(-2e^* + \log_e\left(\frac{1+e^*}{1-e^*}\right)\right)\end{aligned} \tag{A.36}$$

provides the solution of α_0 for a prolate spheroid. For γ_0 an equivalent expression may be written from Eq. A.34, giving

$$\gamma_0 = \frac{ab}{c^2}\int_0^1 \frac{\sqrt{s}\,ds}{\sqrt{\left((\frac{a^2}{c^2}-1)s+1\right)}\sqrt{\left((\frac{b^2}{c^2}-1)s+1\right)}} \tag{A.37}$$

Applying the substitution for t, then for e^* and integrating w.r.t s gives

$$\begin{aligned}\gamma_0 &= \int_0^1 \frac{\sqrt{s}\,ds}{\sqrt{\left((1-t^2)s+t^2\right)}} \\ &= \int_0^1 \frac{\sqrt{s}\,ds}{\left(e^{*2}s+1-e^{*2}\right)} \\ &= \frac{1}{e^{*2}} + \left(\frac{e^{*2}-1}{2\,e^{*3}}\right)\log_e\left(\frac{1+e^*}{1-e^*}\right)\end{aligned} \tag{A.38}$$

which provides the solution for γ_0 on a prolate spheroid where $\left(\frac{e^{*2}}{1-e^{*2}}\right)$ is greater than zero.

A.3 Calculation of α_0 and γ_0 for Ellipsoid

A solution of α_0 for the case of an ellipsoid may be obtained by substituting

$$\lambda^* = \frac{b^2-a^2}{\mu^{*2}-1} - a^2 \Rightarrow \partial\lambda^* = \frac{-2\left(b^2-a^2\right)\mu^*}{\left(\mu^{*2}-1\right)^2}\partial\mu^* \tag{A.39}$$

into Eq. A.26 as shown by Band and Payne[36], where μ^* is a dummy variable for integration. This gives

$$\begin{aligned}\alpha_0 &= \frac{-2\,a\,b\,c}{\left(a^2-b^2\right)\,\sqrt{b^2-c^2}}\int_{\frac{b}{a}}^{1}\frac{\sqrt{\left(\mu^{*2}-1\right)^3}\,\partial\mu^*}{\left(\mu^{*2}-1\right)\,\sqrt{1+\frac{\left(c^2-a^2\right)\mu^{*2}}{b^2-c^2}}} \\ &= \frac{-2\,a\,b\,c\,\Im\,E\left[\sin^{-1}\left(\sqrt{\frac{a^2-c^2}{b^2-c^2}}\,\mu\right),\frac{b^2-c^2}{a^2-c^2}\right]}{\left(b^2-a^2\right)\,\sqrt{\frac{a^2-c^2}{b^2-c^2}}\,\sqrt{b^2-c^2}}\end{aligned} \tag{A.40}$$

where E is an incomplete elliptical integral of the second kind and $\Im = \sqrt{-1}$. Care must be taken if the numerator of the first line of Eq. A.40 is divided by $\left(\mu^{*2}-1\right)$, as when $\mu < 1$ this will result in a change of sign. The result on the first line of Eq. A.40 differs from Eq.7 of Band and Payne[36]. E may be determined from tables or numerically. Elliptical integrals of the second kind are often solved numerically using the relatively recent results of Carlson [112], which conveniently solve the elliptical integral equations starting from the form of Eq. A.26. The NAG libraries [113] provide a routine implementing Carlson's algorithm in the section on special functions. This routine was used when pressure on the body of the ellipsoid was determined.

A.4 Velocity on Ellipsoid Surface due to Translation

The following section calculates the velocity and puts it in a form suggested in Band and Payne [36] and first presented by Maruhn (see [36]). The velocity of the fluid around the ellipsoid when the ellipsoid is at rest in a infinite stream of fluid at velocity U_0 in the x direction is given by

$$q_U = \nabla\left(U_0\,x + \frac{U_0\,x\,a\,b\,c}{2-\alpha_0}\int_{\lambda}^{\infty}\frac{d\lambda^*}{(a^2+\lambda^*)\Delta_{\lambda^*}}\right) \tag{A.41}$$

where q_U is the fluid velocity due to U_0. The x component of the fluid velocity due to U_0, q_{U_x}, is

$$\begin{aligned}q_{U_x} &= \frac{\partial}{\partial x}\left(U_0\,x + \frac{U_0\,x\,a\,b\,c}{2-\alpha_0}\int_{\lambda}^{\infty}\frac{d\lambda^*}{(a^2+\lambda^*)\Delta_{\lambda^*}}\right) \\ &= U_0\left(1+\frac{a\,b\,c}{2-\alpha_0}\int_{\lambda}^{\infty}\frac{d\lambda^*}{(a^2+\lambda^*)\Delta_{\lambda^*}} + \frac{x\,a\,b\,c}{(2-\alpha_0)}\frac{\partial}{\partial x}\int_{\lambda}^{\infty}\frac{d\lambda^*}{(a^2+\lambda^*)\Delta_{\lambda^*}}\right)\end{aligned} \tag{A.42}$$

The partial differentiation of Eq. A.1 w.r.t. x yields

$$\begin{aligned}\frac{\partial x}{\partial \lambda} &= \frac{\dfrac{2x}{a^2+\lambda}}{\dfrac{x^2}{(a^2+\lambda)^2}+\dfrac{y^2}{(b^2+\lambda)^2}+\dfrac{z^2}{(c^2+\lambda)^2}} \\ &= \frac{1}{h_\lambda^2}\frac{\partial \lambda}{\partial x}\end{aligned} \tag{A.43}$$

where

$$h_\theta^2 = \frac{1}{4}\left(\frac{x^2}{(a^2+\theta)^2}+\frac{y^2}{(b^2+\theta)^2}+\frac{z^2}{(c^2+\theta)^2}\right); \quad \theta = \lambda, \mu, \nu \tag{A.44}$$

and h_λ, h_μ, h_ν are metric coefficients. Milne-Thomson [35] provides a clear graphical representation of the relation between $\dfrac{\partial x}{\partial \lambda}$ and $\dfrac{\partial \lambda}{\partial x}$. The unit normal to the surface of the ellipsoid, $\bar{n} = (n_x, n_y, n_z)$, may be expressed in terms of h_θ,

$$\begin{aligned}\bar{n} &= \left(\frac{2x}{a^2+\lambda}, \frac{2y}{b^2+\lambda}, \frac{2z}{c^2+\lambda}\right)\frac{1}{|\bar{n}|} \\ &= \left(\frac{\partial x}{\partial \lambda}, \frac{\partial y}{\partial \lambda}, \frac{\partial z}{\partial \lambda}\right)\frac{1}{h_\lambda}\end{aligned} \tag{A.45}$$

where $\bar{n}$ is the normal vector.

The last term of Eq. A.42 may be simplified with the substitution of Eq. A.6, Eq. A.43 and Eq. A.45, giving

$$\begin{aligned}\frac{x\,a\,b\,c}{(2-\alpha_0)}\frac{\partial}{\partial x}\int_\lambda^\infty \frac{d\lambda^*}{(a^2+\lambda^*)\Delta_{\lambda^*}} &= \frac{x\,a\,b\,c}{(2-\alpha_0)}\frac{\partial \lambda}{\partial x}\frac{\partial}{\partial \lambda}\int_\lambda^\infty \frac{d\lambda^*}{(a^2+\lambda^*)\Delta_{\lambda^*}} \\ &= -\frac{x\,a\,b\,c}{(2-\alpha_0)}\frac{\partial \lambda}{\partial x}\frac{1}{(a^2+\lambda)\Delta_\lambda} \\ &= -\frac{a\,b\,c}{(2-\alpha_0)}\frac{1}{\Delta_\lambda}\frac{1}{h_\lambda^2}\frac{\partial x}{\partial \lambda}\left(\frac{x}{(a^2+\lambda)}\right) \\ &= -\frac{a\,b\,c}{(2-\alpha_0)}\frac{2}{\Delta_\lambda}\frac{1}{h_\lambda^2}\frac{\partial x}{\partial \lambda}\frac{\partial x}{\partial \lambda} \\ &= -\frac{a\,b\,c}{(2-\alpha_0)}\frac{2}{\Delta_\lambda}\,n_x\,n_x\end{aligned} \tag{A.46}$$

Substituting Eq. A.46 into Eq. A.42 gives

$$\begin{aligned}q_{U_x} &= U_0\left(1+\frac{a\,b\,c}{2-\alpha_0}\int_\lambda^\infty \frac{d\lambda^*}{(a^2+\lambda^*)\Delta_{\lambda^*}} - \frac{a\,b\,c}{(2-\alpha_0)}\frac{2}{\Delta_\lambda}\,n_x\,n_x\right) \\ &= U_0\left(1+\frac{\alpha_\lambda}{2-\alpha_0} - \frac{a\,b\,c}{(2-\alpha_0)}\frac{2}{\Delta_\lambda}\,n_x\,n_x\right).\end{aligned} \tag{A.47}$$

The y and z components of the fluid velocity due to U_0, q_{U_y} and q_{U_z} respectively, are calculated

in a similar manner, giving

$$
\begin{aligned}
q_{U_y} &= \frac{\partial}{\partial y}\left(U_0\, x + \frac{U_0\, x\, a\, b\, c}{2-\alpha_0}\int_\lambda^\infty \frac{d\lambda^*}{(a^2+\lambda^*)\Delta_{\lambda^*}}\right) \\
&= U_0\left(\frac{x\, a\, b\, c}{(2-\alpha_0)}\frac{\partial}{\partial y}\int_\lambda^\infty \frac{d\lambda^*}{(a^2+\lambda^*)\Delta_{\lambda^*}}\right) \\
&= U_0\left(\frac{x\, a\, b\, c}{(2-\alpha_0)}\frac{\partial\lambda}{\partial y}\frac{\partial}{\partial\lambda}\int_\lambda^\infty \frac{d\lambda^*}{(a^2+\lambda^*)\Delta_{\lambda^*}}\right) \\
&= -U_0\left(\frac{a\, b\, c}{(2-\alpha_0)}\frac{2}{\Delta_\lambda}\frac{1}{h_\lambda^2}\frac{\partial y}{\partial\lambda}\frac{\partial x}{\partial\lambda}\right) \\
&= -U_0\left(\frac{a\, b\, c}{(2-\alpha_0)}\frac{2}{\Delta_\lambda}\, n_y\, n_x\right)
\end{aligned}
\tag{A.48}
$$

$$
q_{U_z} = -U_0\left(\frac{a\, b\, c}{(2-\alpha_0)}\frac{2}{\Delta_\lambda}\, n_z\, n_x\right) \tag{A.49}
$$

Applying Eq. A.47, Eq. A.48 and Eq. A.49 on the surface of the ellipsoid, where $\lambda = 0$, gives

$$
q_{U_0} = \frac{2\, U_0}{(2-\alpha_0)}\left((1,0,0) - n_x\left(n_x, n_y, n_z\right)\right) \tag{A.50}
$$

and from symmetry

$$
q_{V_0} = \frac{2\, V_0}{(2-\beta_0)}\left((0,1,0) - n_y\left(n_x, n_y, n_z\right)\right) \tag{A.51}
$$

$$
q_{W_0} = \frac{2\, W_0}{(2-\gamma_0)}\left((0,0,1) - n_z\left(n_x, n_y, n_z\right)\right). \tag{A.52}
$$

Appendix B

Uncertainty Calculations for Surface Pressure Measurements

B.1 Inaccuracy Estimates

One source of inaccuracy in these measurements is due to the pressure sensor. The Validyne DP15 was used to measure both the pressure at the tappings and the dynamic pressure from the pitot-static tube when the contraction factor was determined. This sensor has a stated accuracy of ±0.25% of full scale that includes non-linearity, hysteresis and non-repeatability. The inaccuracy of C_{P_i}, $\varepsilon_{C_{P_i}}$ may be determined from

$$\varepsilon_{C_{P_i}} \simeq \varepsilon_{C_{V_{1\_ref}}}\left(\frac{\partial C_{P_1}}{\partial C_{V_{1\_ref}}}\right) + \varepsilon_{C_{V_{2\_ref}}}\left(\frac{\partial C_{P_2}}{\partial C_{V_{2\_ref}}}\right) + \varepsilon_{C_{V_{i\_ref}}}\left(\frac{\partial C_{P_i}}{\partial C_{V_{i\_ref}}}\right) + \varepsilon_{k_{cont}}\left(\frac{\partial C_{P_i}}{\partial k_{cont}}\right)$$

$$\simeq \frac{C_{V_{i\_ref}}}{k_{cont}\left(C_{V_{2\_ref}} - C_{V_{1\_ref}}\right)^2} \times \left(\varepsilon_{C_{V_{2\_ref}}} + \varepsilon_{C_{V_{1\_ref}}}\right) + \frac{1}{k_{cont}\left(C_{V_{2\_ref}} - C_{V_{1\_ref}}\right)} \times \varepsilon_{C_{V_{i\_ref}}} + \frac{C_{V_{i\_ref}}}{k_{cont}^2\left(C_{V_{2\_ref}} - C_{V_{1\_ref}}\right)} \times \varepsilon_{k_{cont}} \tag{B.1}$$

where $C_{V_{i\_ref}}$ is dimensionless pressure measurement that has been zero corrected for drift in the Validyne pressure transducer and temporal corrected for fluctuations in the test section

dynamic pressure. $\varepsilon_{C_{V_{i\_ref}}}$ is the inaccuracy of $C_{V_{i\_ref}}$ determined from

$$\begin{aligned}\varepsilon_{C_{V_{i\_ref}}} \simeq\ & \varepsilon_{V_{P_i-P_{ref}}}\left(\frac{\partial C_{V_{i\_ref}}}{\partial V_{P_i-P_{ref}}}\right)+\ \varepsilon_{V_{P_0-P_{ref}}}\left(\frac{\partial C_{V_{i\_ref}}}{\partial V_{P_0-P_{ref}}}\right)+ \\ & \varepsilon_{V_{i_{Rose}}}\left(\frac{\partial C_{V_{i\_ref}}}{\partial V_{P_{i_{Rose}}}}\right)+\ \varepsilon_{V_{P_{Rose\_zero}}}\left(\frac{\partial C_{V_{i\_ref}}}{\partial V_{P_{Rose\_zero}}}\right) \\ \simeq & \frac{\left(V_{P_i-P_{ref}}-V_{P_0-P_{ref}}\right)}{\left(V_{P_{i_{Rose}}}-V_{P_{Rose\_zero}}\right)^2}\times\left(\varepsilon_{V_{i_{Rose}}}+\varepsilon_{V_{i_{Rose\_zero}}}\right) \\ & +\frac{1}{\left(V_{P_{i_{Rose}}}-V_{P_{Rose\_zero}}\right)}\times\left(\varepsilon_{V_{P_i-P_{ref}}}+\varepsilon_{V_{P_0-P_{ref}}}\right)\end{aligned} \tag{B.2}$$

where $\varepsilon_{V_{i_{Rose}}}$, $\varepsilon_{V_{i_{Rose\_zero}}}$, $\varepsilon_{V_{P_i-P_{ref}}}$ and $\varepsilon_{V_{P_0-P_{ref}}}$ are the inaccuracies associated with $V_{P_{i_{Rose}}}$, $V_{P_{Rose\_zero}}$, $V_{P_i-P_{ref}}$ and $V_{P_0-P_{ref}}$ respectively. $\varepsilon_{k_{cont}}$ is the inaccuracy associated with the calculation of the contraction factor. Propagation of the errors associated with Eq. 4.8 results in

$$\begin{aligned}\varepsilon_{k_{cont}} = & \frac{1}{C_{V_{2\_ref}}-C_{V_{1\_ref}}}\times\left(\varepsilon_{C_{V_{4\_ref}}}+\varepsilon_{C_{V_{3\_ref}}}\right) \\ & +\frac{C_{V_{4\_ref}}-C_{V_{3\_ref}}}{\left(C_{V_{2\_ref}}-C_{V_{1\_ref}}\right)^2}\times\left(\varepsilon_{C_{V_{2\_ref}}}+\varepsilon_{C_{V_{1\_ref}}}\right)\end{aligned} \tag{B.3}$$

Substitution of Eqs. B.2 and B.3 into Eq. B.1 allows a formal estimate of inaccuracy. However, this neglects that a large portion of the error due to nonlinearity over the full scale should be eliminated as we do a local "calibration" when we convert it to a C_p. In addition any hysteresis will only be on a sub-hysteresis curve as the sensor is not being cycled across the full span of the transducer. (The maximum range occurs between the nose tap, $C_p \approx 1$, and a tapping on the side of the body $C_p \gtrapprox -0.4$.) At the lowest Reynolds numbers where the total pressure is only a small percent of the range of the transducer; applying the inaccuracy associated with the full scale has a significant influence on the uncertainty estimate. All this neglects the uncertainty due to the sensitivity of the laminar-turbulent transition which is significant at the rear of the model. The analysis provided in the main body is believed to provide a better estimate of the inaccuracy.

B.2 Imprecision Estimates

Analysis of Eqs. 4.6 and 4.7 allow the precision of the measurements of the surface pressure to be estimated. The slow variation of k_{cont} with Reynolds number results in a negligible

contribution to the imprecision of the measurements. High precision allows small variations with Reynolds number to be observed. The precision of the mean (standard error) may be estimated using

$$\sigma_{\overline{C}_{P_i}} = \frac{\sigma_{C_{P_i}}}{\sqrt{N}} \tag{B.4}$$

where N is the number of samples and the standard deviation of C_{P_i}, $\sigma_{C_{P_i}}$, is determined using the error propagation equation [56]

$$\begin{aligned}
\sigma^2_{C_{P_i}} &\simeq \sigma^2_{C_{V_{1_ref}}}\left(\frac{\partial C_{P_1}}{\partial C_{V_{1_ref}}}\right)^2 + \sigma^2_{C_{V_{2_ref}}}\left(\frac{\partial C_{P_2}}{\partial C_{V_{2_ref}}}\right)^2 + \sigma^2_{C_{V_{i_ref}}}\left(\frac{\partial C_{P_i}}{\partial C_{V_{i_ref}}}\right)^2 \\
&\simeq \frac{C^2_{V_{i_ref}}}{k^2_{cont}\left(C_{V_{2_ref}} - C_{V_{1_ref}}\right)^4} \times \left(\sigma^2_{C_{V_{1_ref}}} + \sigma^2_{C_{V_{2_ref}}}\right) \\
&\quad + \frac{1}{k^2_{cont}\left(C_{V_{2_ref}} - C_{V_{1_ref}}\right)^2} \times \sigma^2_{C_{V_{i_ref}}}.
\end{aligned} \tag{B.5}$$

$\sigma_{C_{V_{i\_ref}}}$ is the standard deviation of $C_{V_{i\_ref}}$ determined from

$$\begin{aligned}
\sigma^2_{C_{V_{i_ref}}} &\simeq \sigma^2_{V_{P_i-P_{ref}}}\left(\frac{\partial C_{V_{i_ref}}}{\partial V_{P_i-P_{ref}}}\right)^2 + \sigma^2_{V_{P_0-P_{ref}}}\left(\frac{\partial C_{V_{i_ref}}}{\partial V_{P_0-P_{ref}}}\right)^2 + \\
&\quad \sigma^2_{V_{i_{Rose}}}\left(\frac{\partial C_{V_{i_ref}}}{\partial V_{P_{i_{Rose}}}}\right)^2 + \sigma^2_{V_{P_{Rose_zero}}}\left(\frac{\partial C_{V_{i_ref}}}{\partial V_{P_{Rose_zero}}}\right)^2 \\
&\simeq \frac{\left(V_{P_i-P_{ref}} - V_{P_0-P_{ref}}\right)^2}{\left(V_{P_{i_{Rose}}} - V_{P_{Rose_zero}}\right)^4} \times \left(\sigma^2_{V_{i_{Rose}}} + \sigma^2_{V_{i_{Rose_zero}}}\right) \\
&\quad + \frac{1}{\left(V_{P_{i_{Rose}}} - V_{P_{Rose_zero}}\right)^2} \times \left(\sigma^2_{V_{P_i-P_{ref}}} + \sigma^2_{V_{P_0-P_{ref}}}\right)
\end{aligned} \tag{B.6}$$

where $\sigma_{V_{i_{Rose}}}$, $\sigma_{V_{i_{Rose\_zero}}}$, $\sigma_{V_{P_i-P_{ref}}}$ and $\sigma_{V_{P_0-P_{ref}}}$ are the standard deviations associated with $V_{P_{i_{Rose}}}$, $V_{P_{Rose\_zero}}$, $V_{P_i-P_{ref}}$ and $V_{P_0-P_{ref}}$ respectively.

Appendix C

Spheroid Surface Pressure Measurements: Constant Azimuth Plots

C.1 Spheroid Surface Pressure Distrubutions at $\alpha = -6.2°$

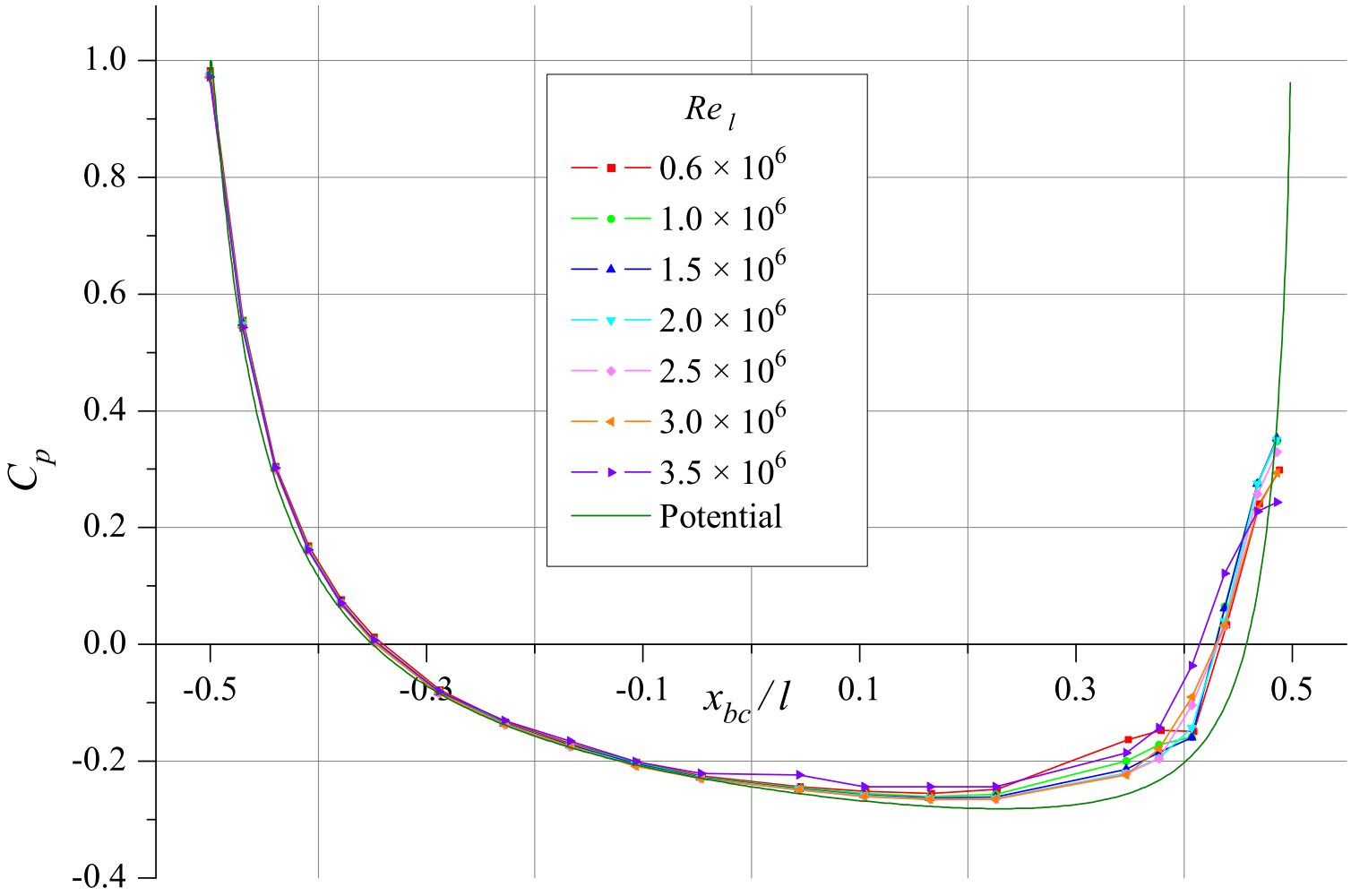

Figure C.1: Surface pressure distribution on spheroid at $\alpha = -6.2°$, $\varphi_e = 0°$

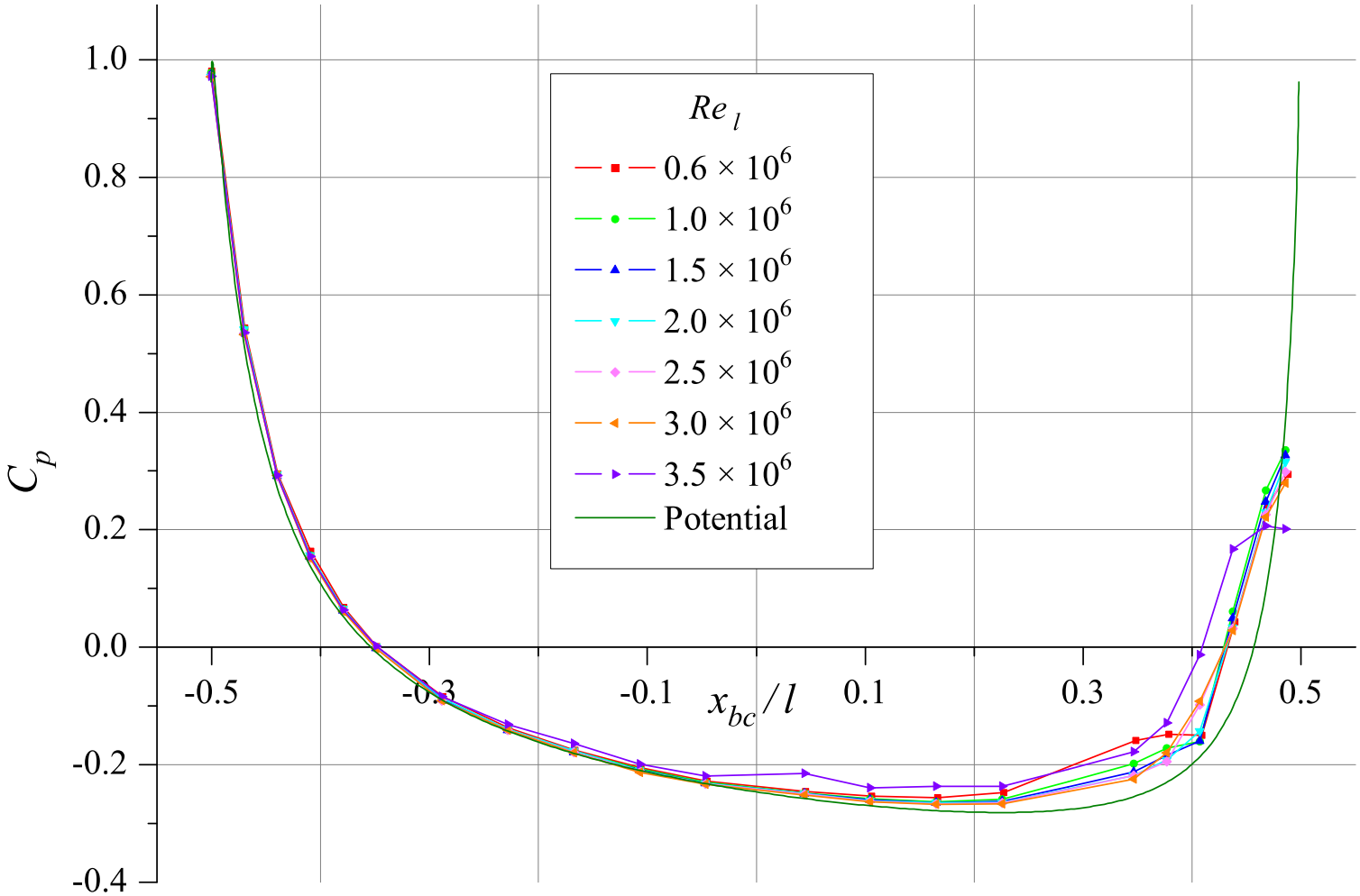

Figure C.2: Surface pressure distribution on spheroid at $\alpha = -6.2°$, $\varphi_e = -15°$

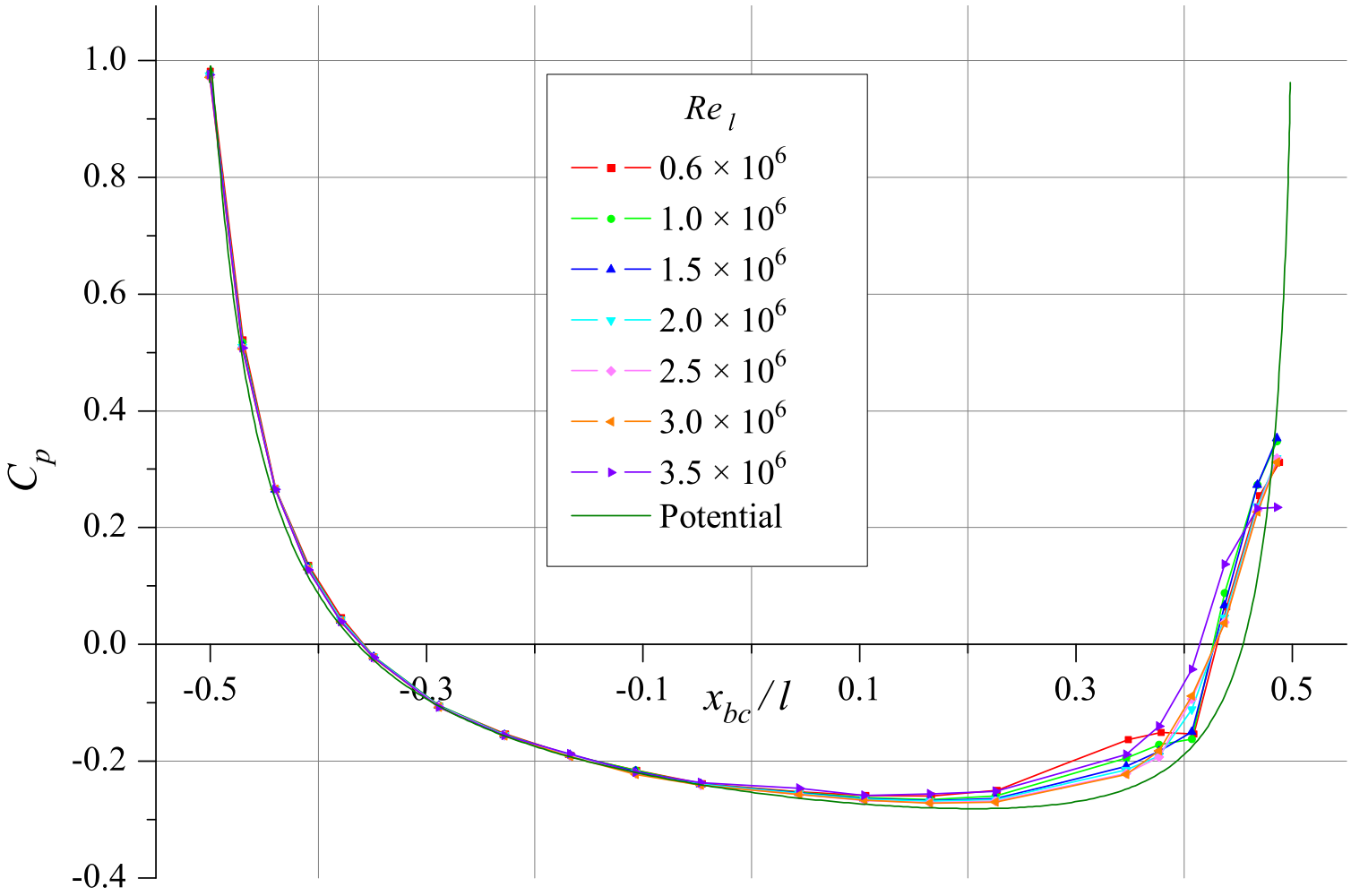

Figure C.3: Surface pressure distribution on spheroid at $\alpha = -6.2°$, $\varphi_e = -30°$

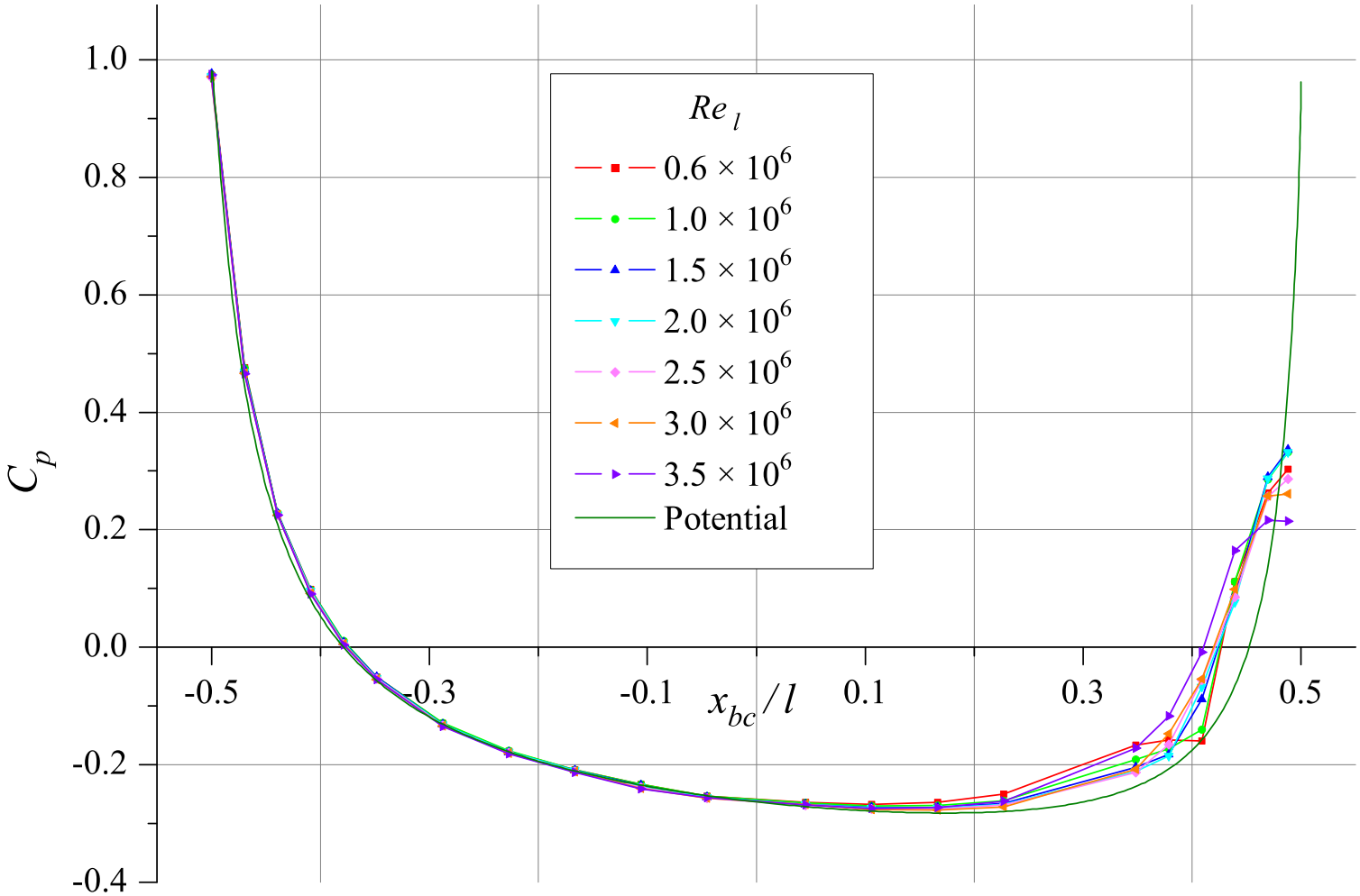

Figure C.4: Surface pressure distribution on spheroid at $\alpha = -6.2°$, $\varphi_e = -45°$

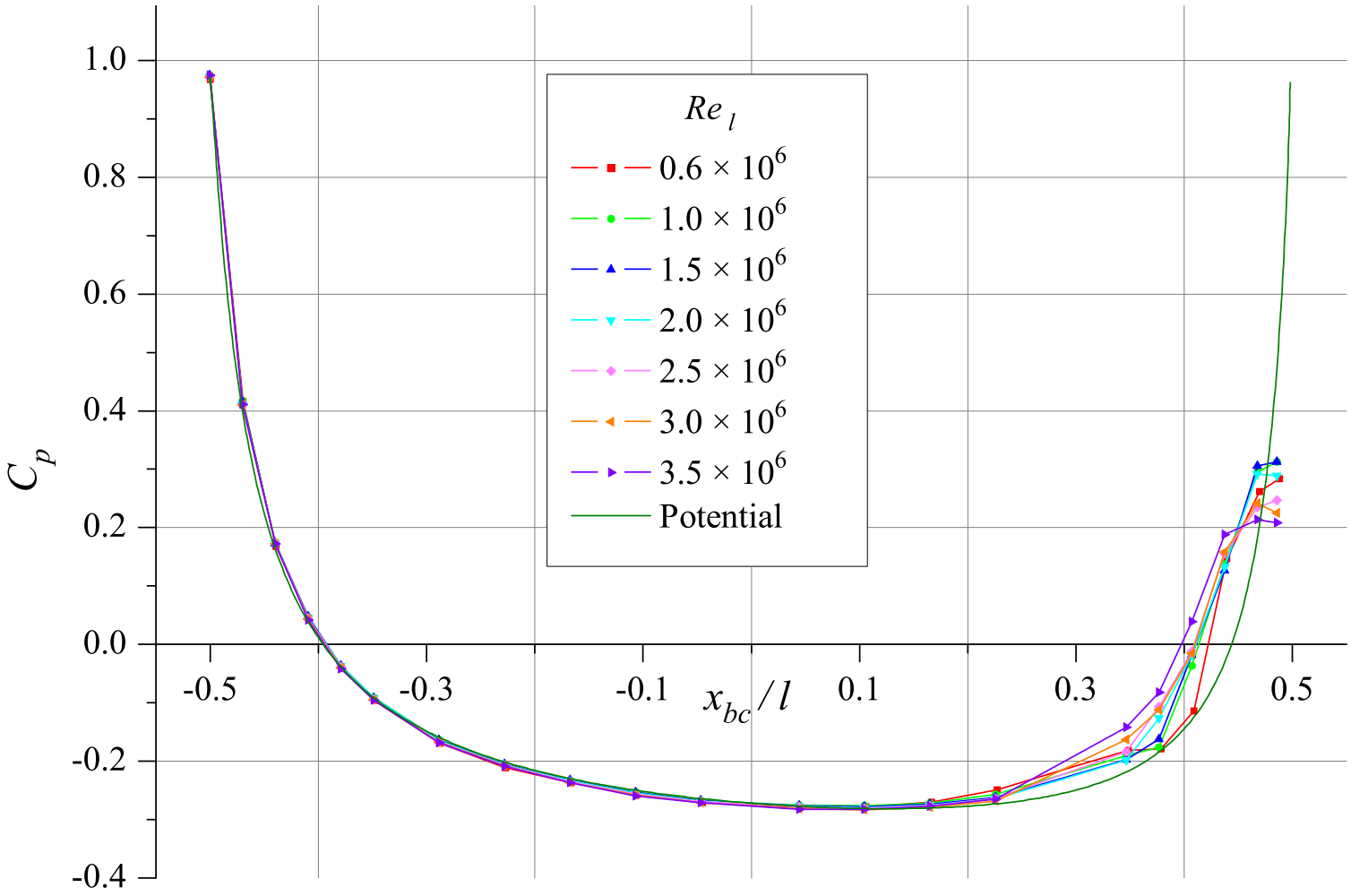

Figure C.5: Surface pressure distribution on spheroid at $\alpha = -6.2°$, $\varphi_e = -60°$

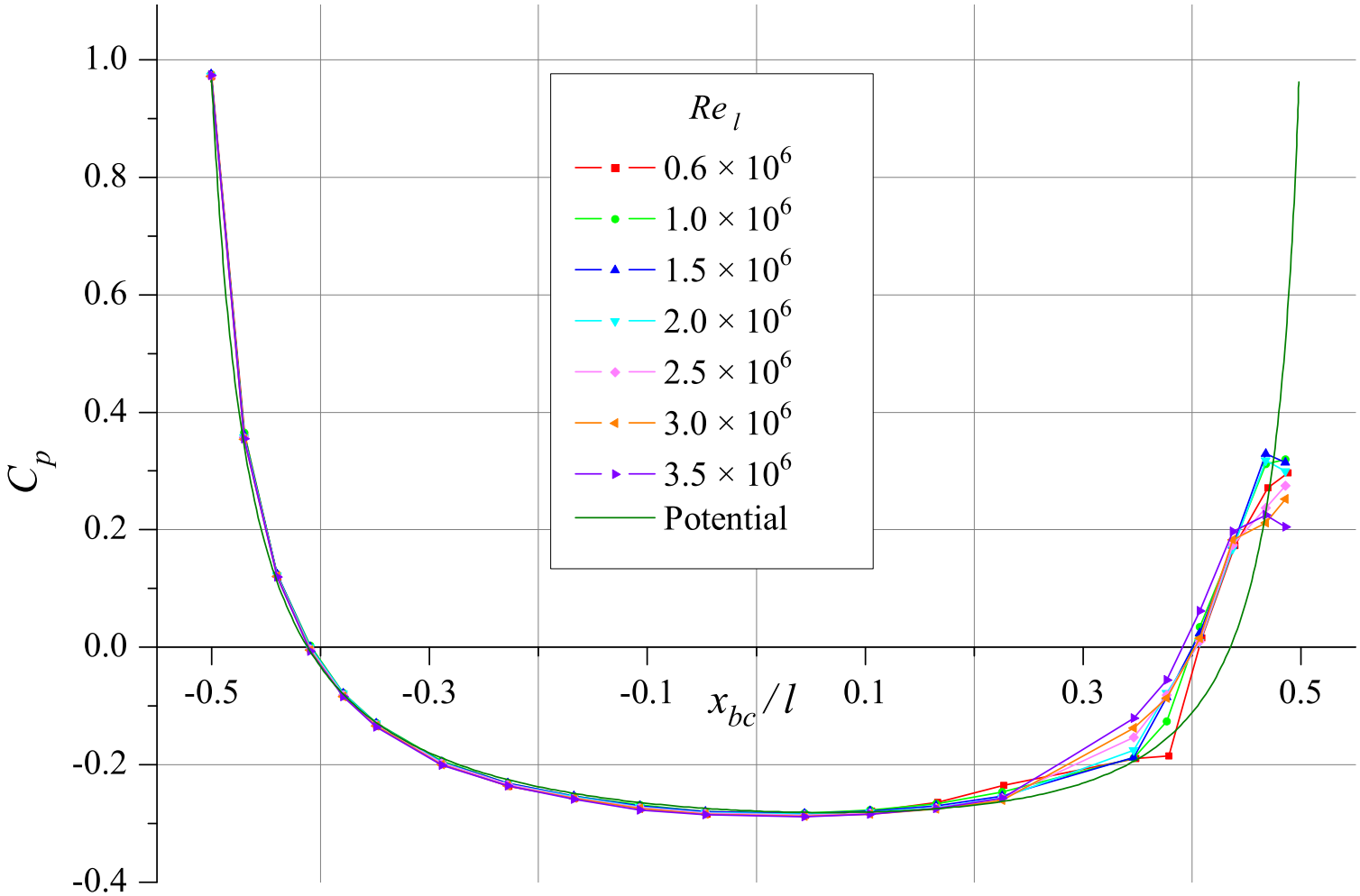

Figure C.6: Surface pressure distribution on spheroid at $\alpha = -6.2°$, $\varphi_e = -75°$

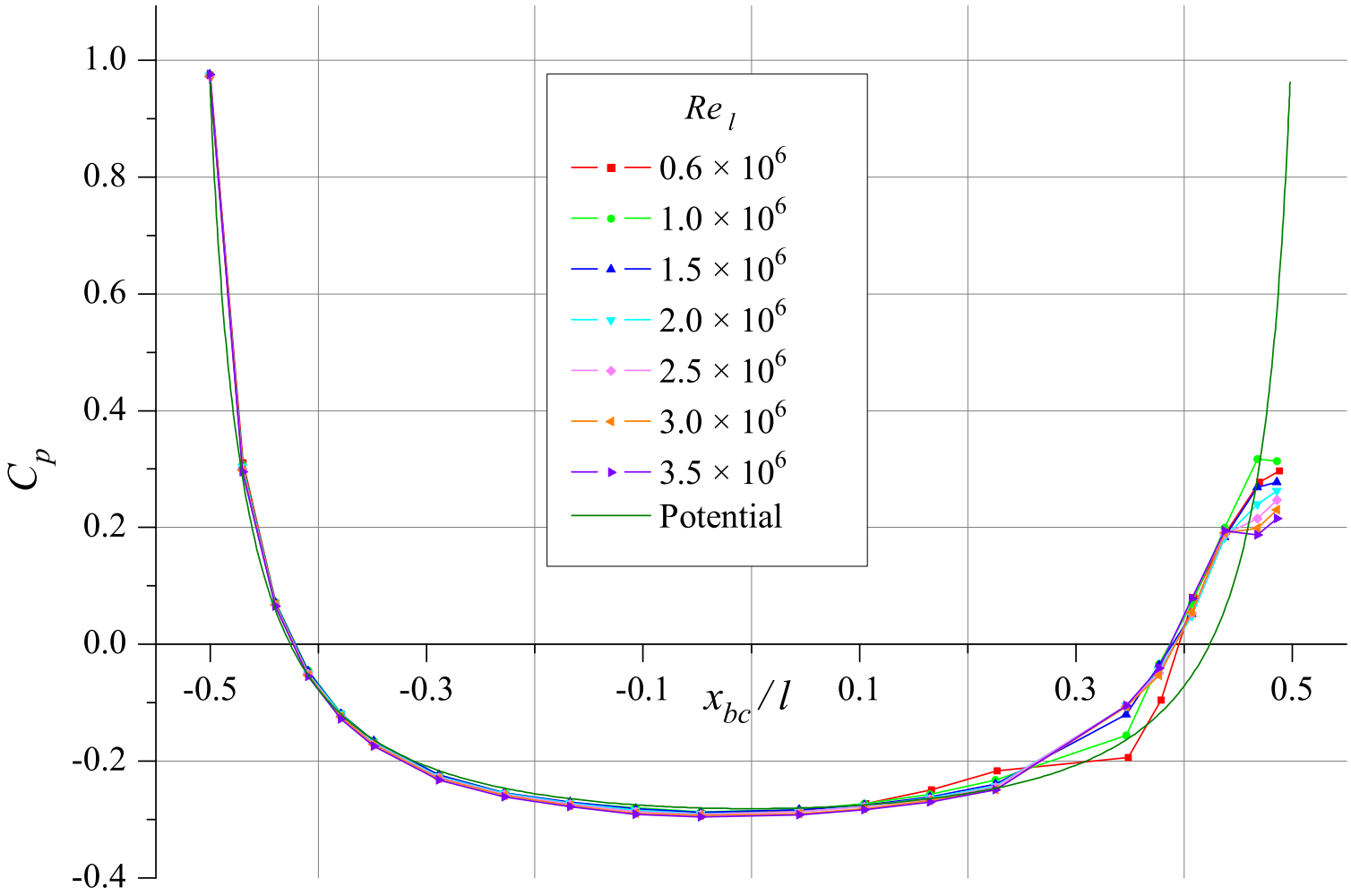

Figure C.7: Surface pressure distribution on spheroid at $\alpha = -6.2°$, $\varphi_e = -90°$

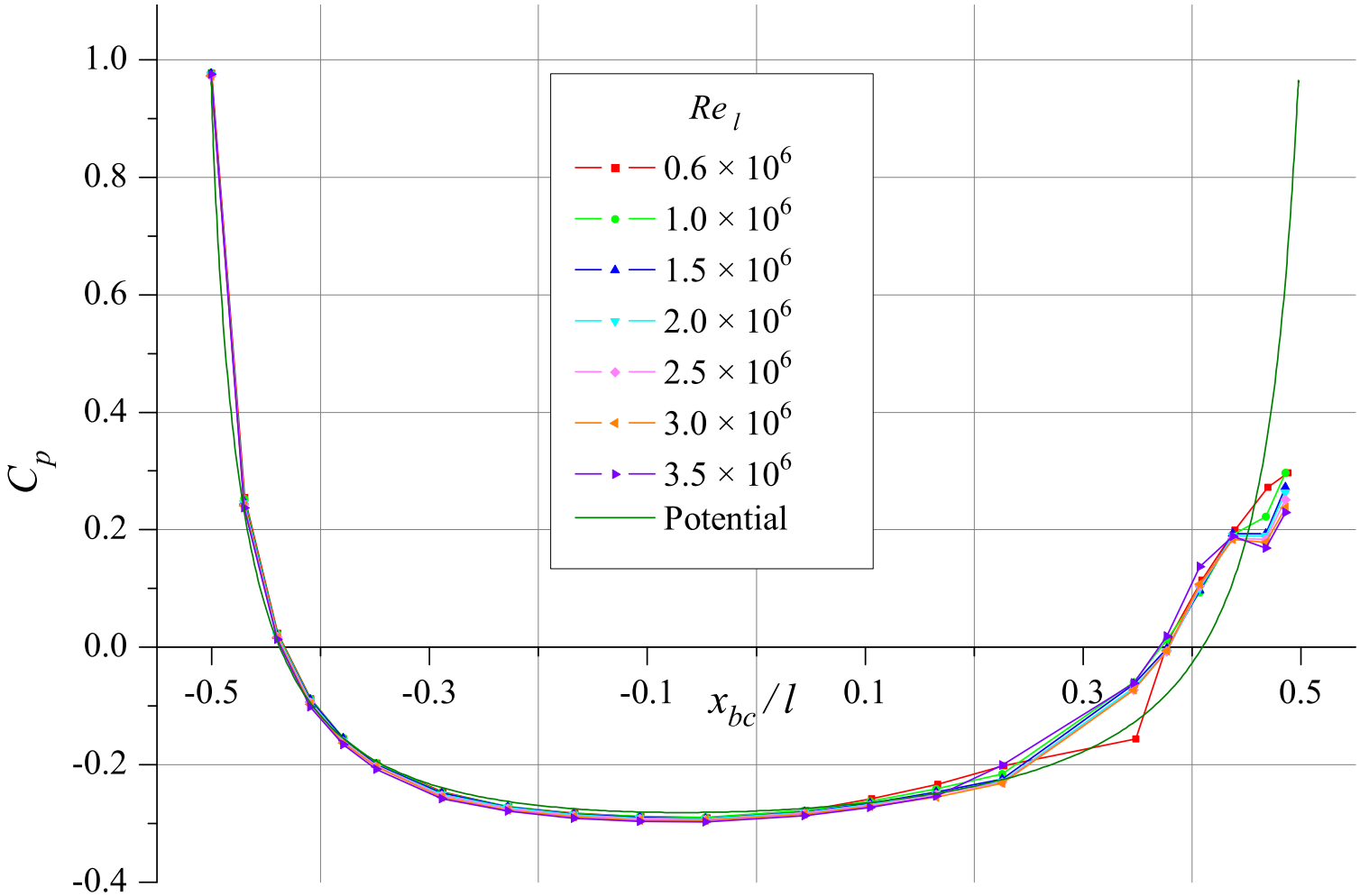

Figure C.8: Surface pressure distribution on spheroid at $\alpha = -6.2°$, $\varphi_e = -105°$

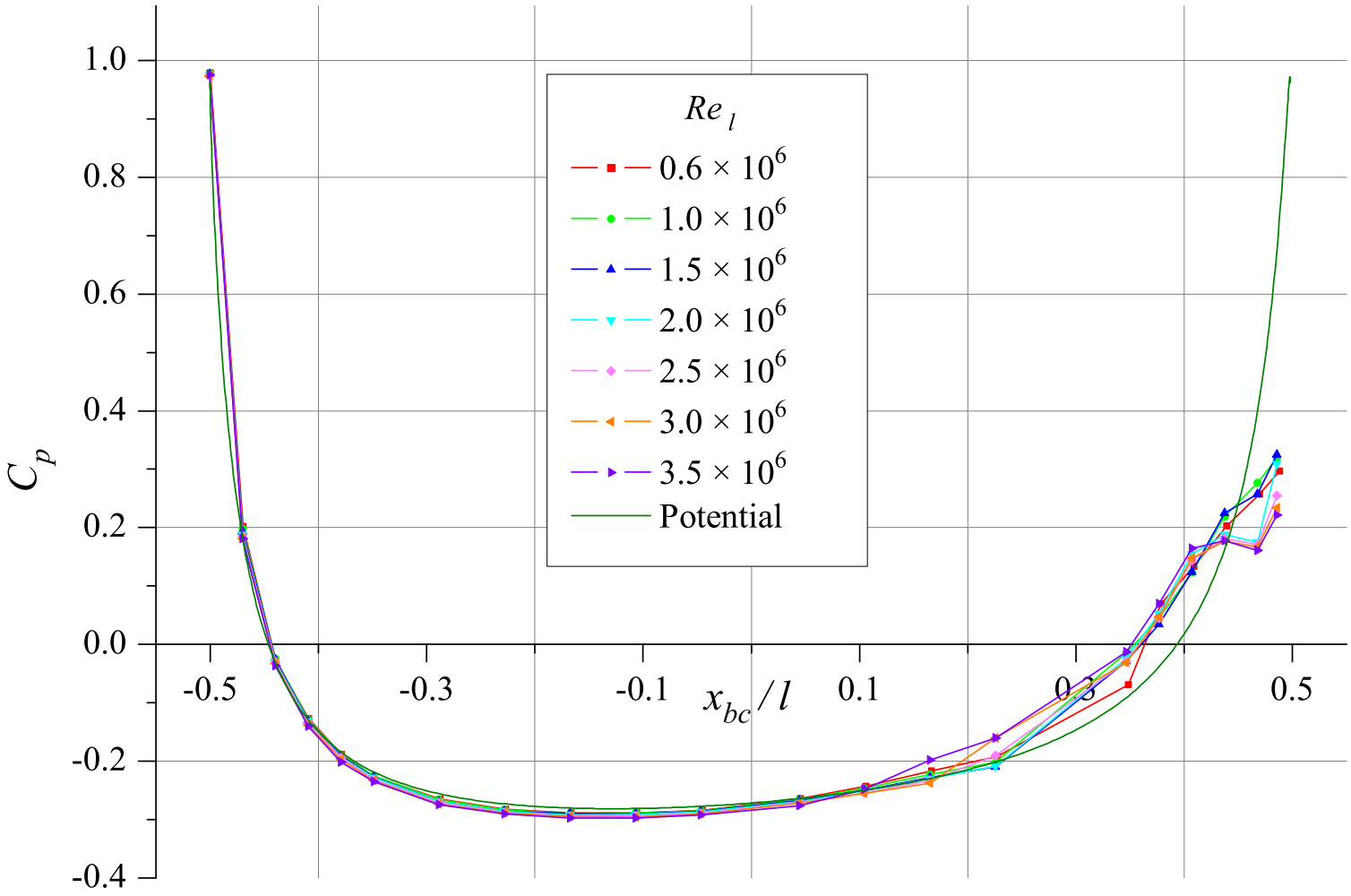

Figure C.9: Surface pressure distribution on spheroid at $\alpha = -6.2°$, $\varphi_e = -120°$

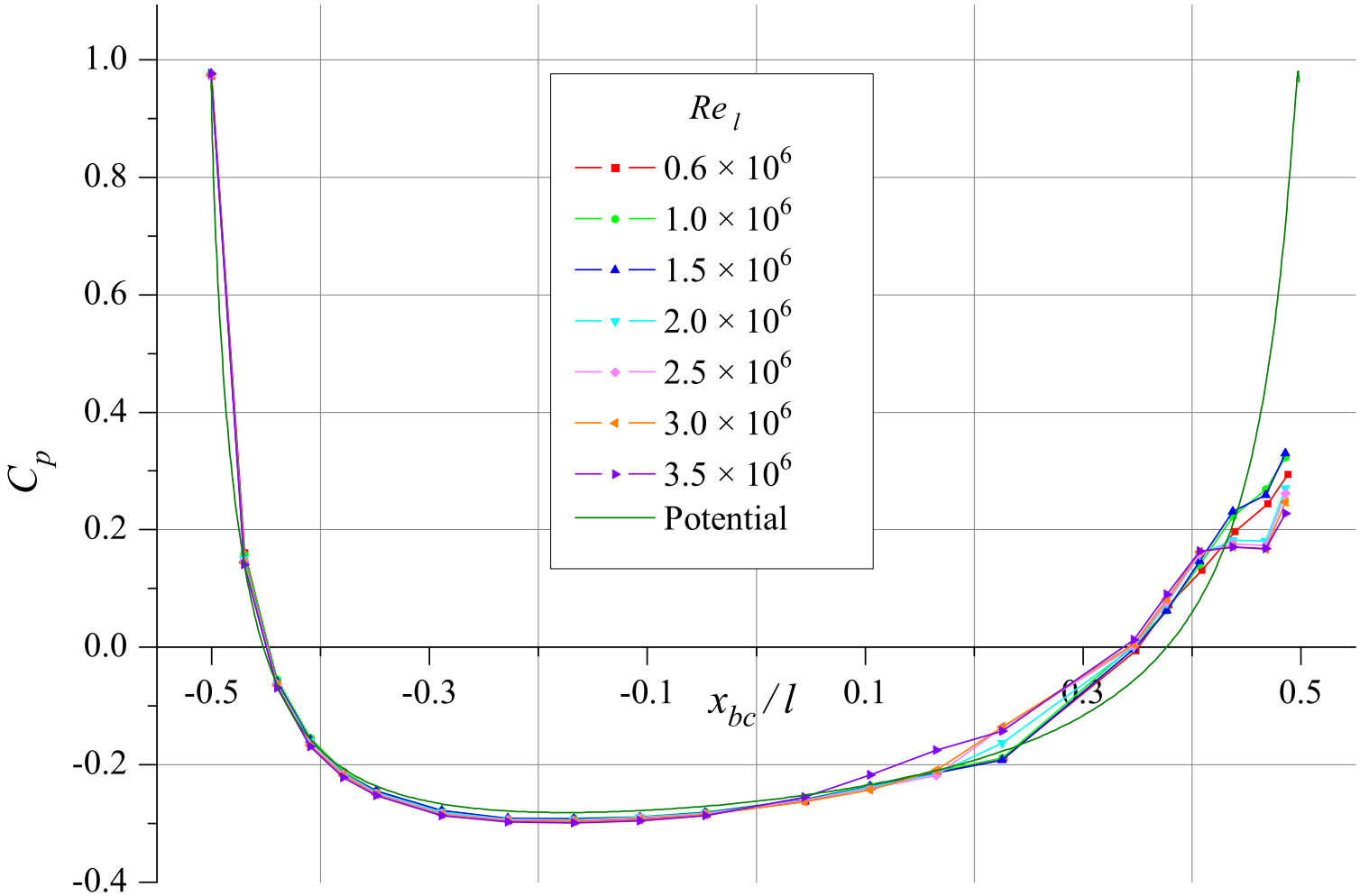

Figure C.10: Surface pressure distribution on spheroid at $\alpha = -6.2°$, $\varphi_e = -135°$

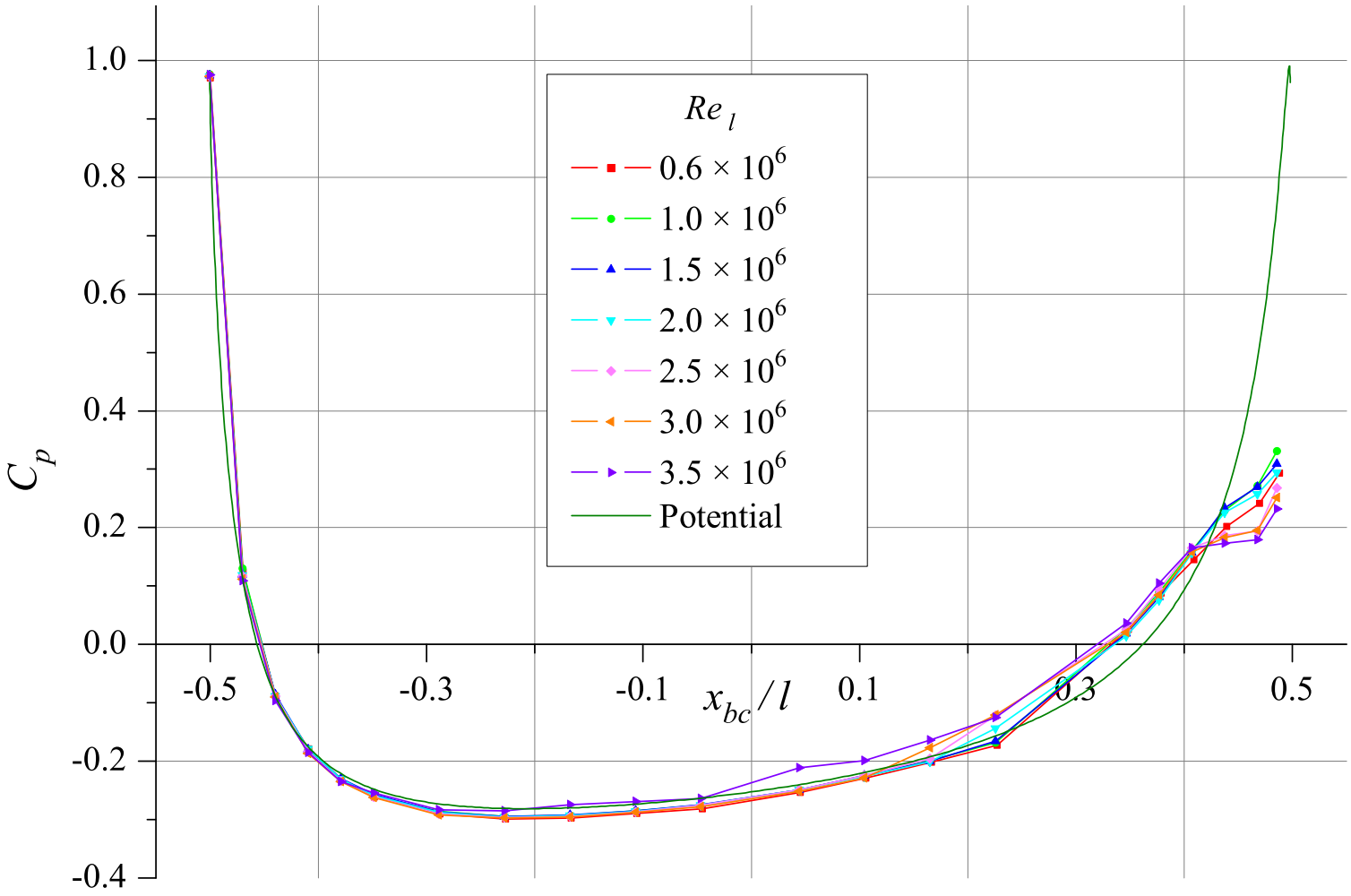

Figure C.11: Surface pressure distribution on spheroid at $\alpha = -6.2°$, $\varphi_e = -150°$

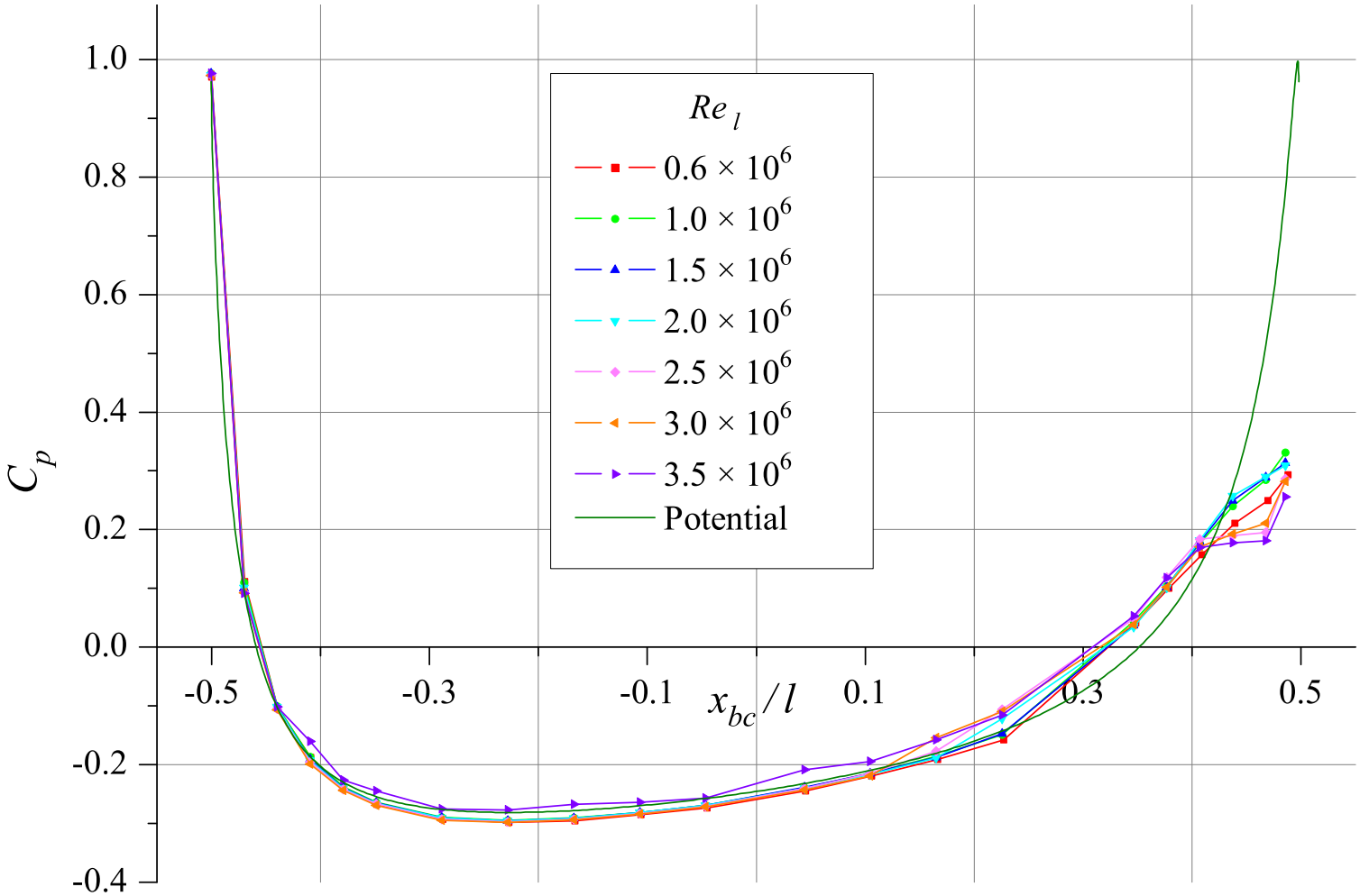

Figure C.12: Surface pressure distribution on spheroid at $\alpha = -6.2°$, $\varphi_e = -165°$

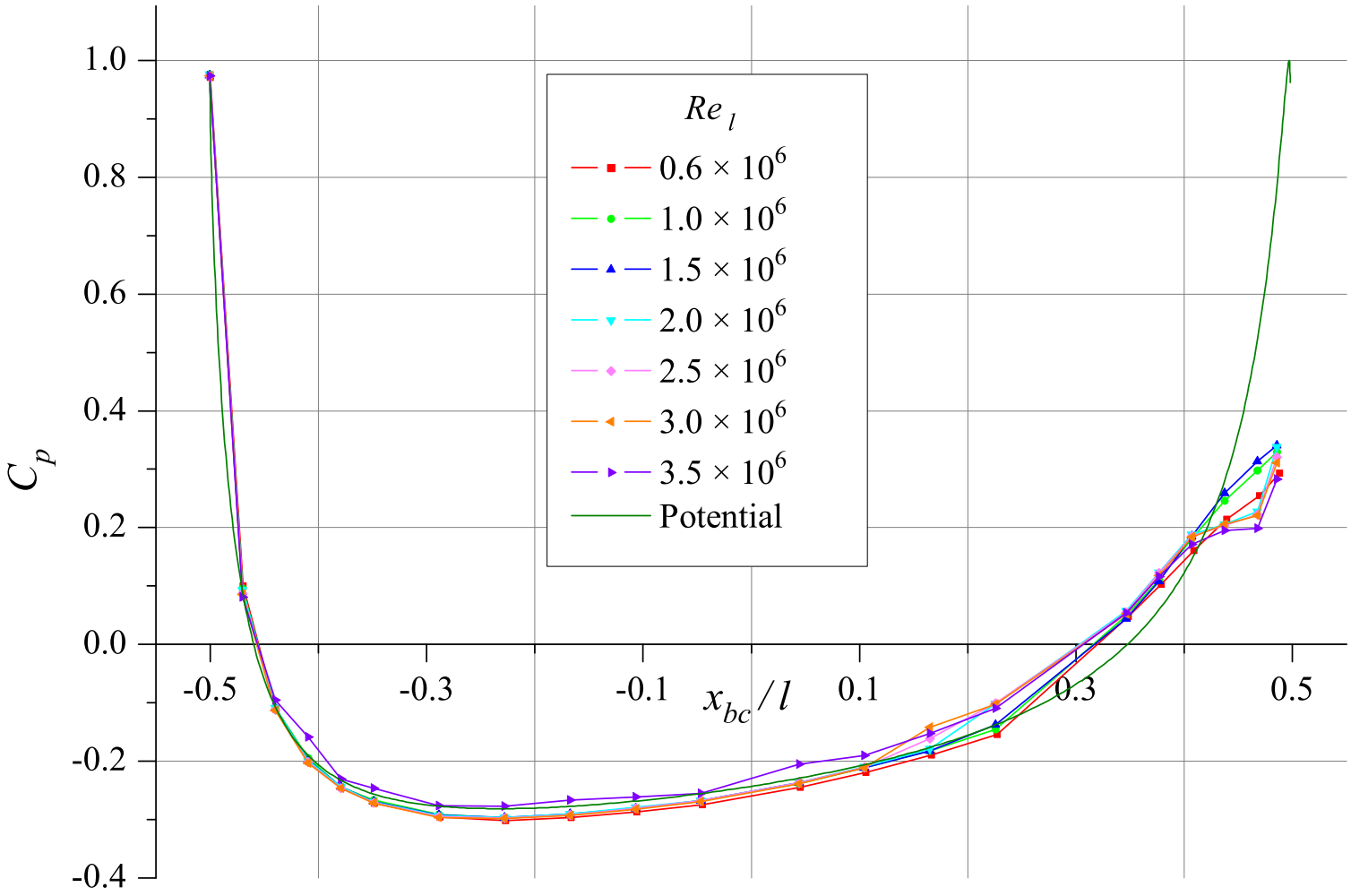

Figure C.13: Surface pressure distribution on spheroid at $\alpha = -6.2°$, $\varphi_e = -180°$

C.2 Spheroid Surface Pressure Distrubutions at $\alpha = -10.2°$

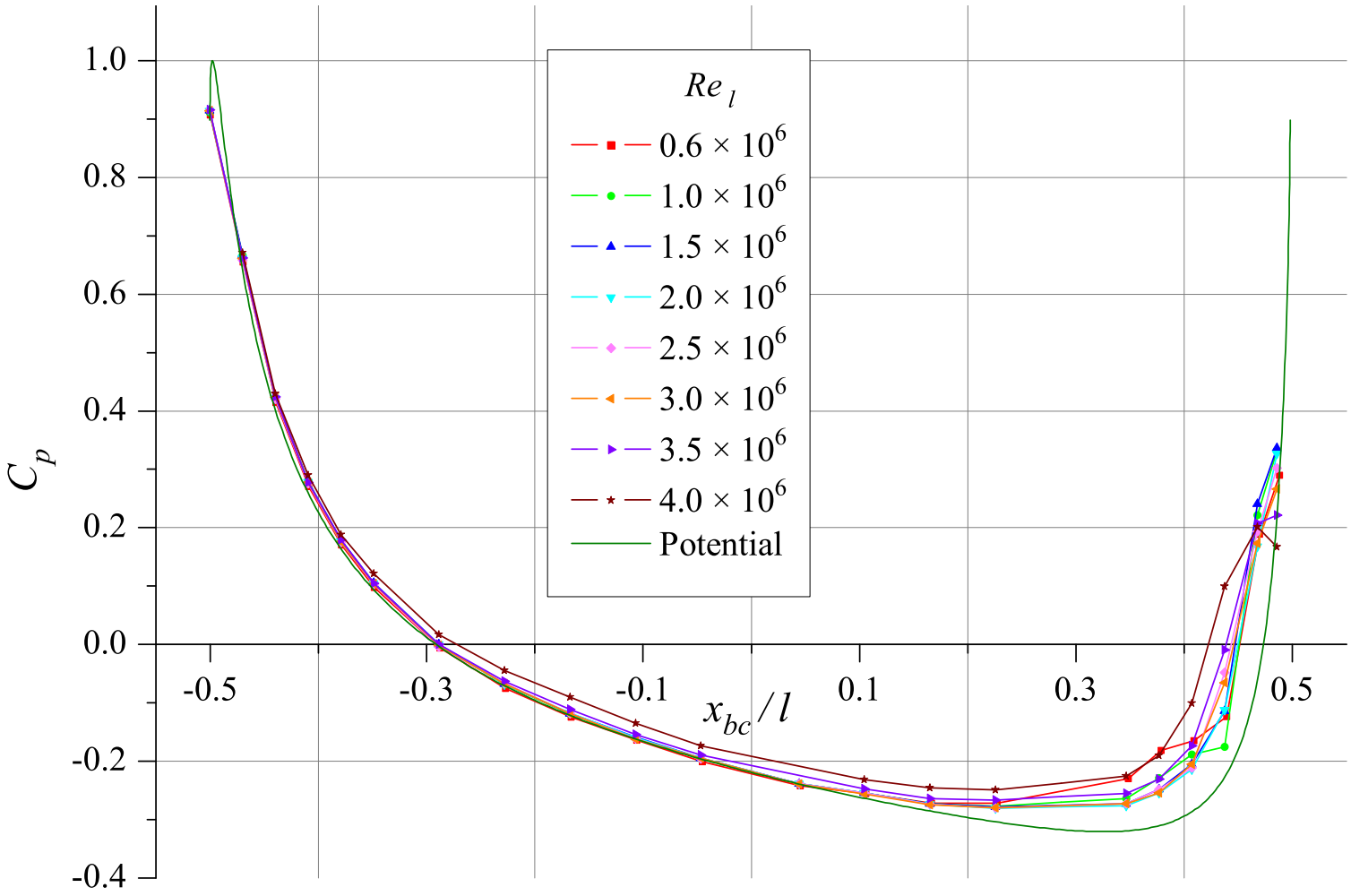

Figure C.14: Surface pressure distribution on spheroid at $\alpha = -10.2°$, $\varphi_e = 0°$

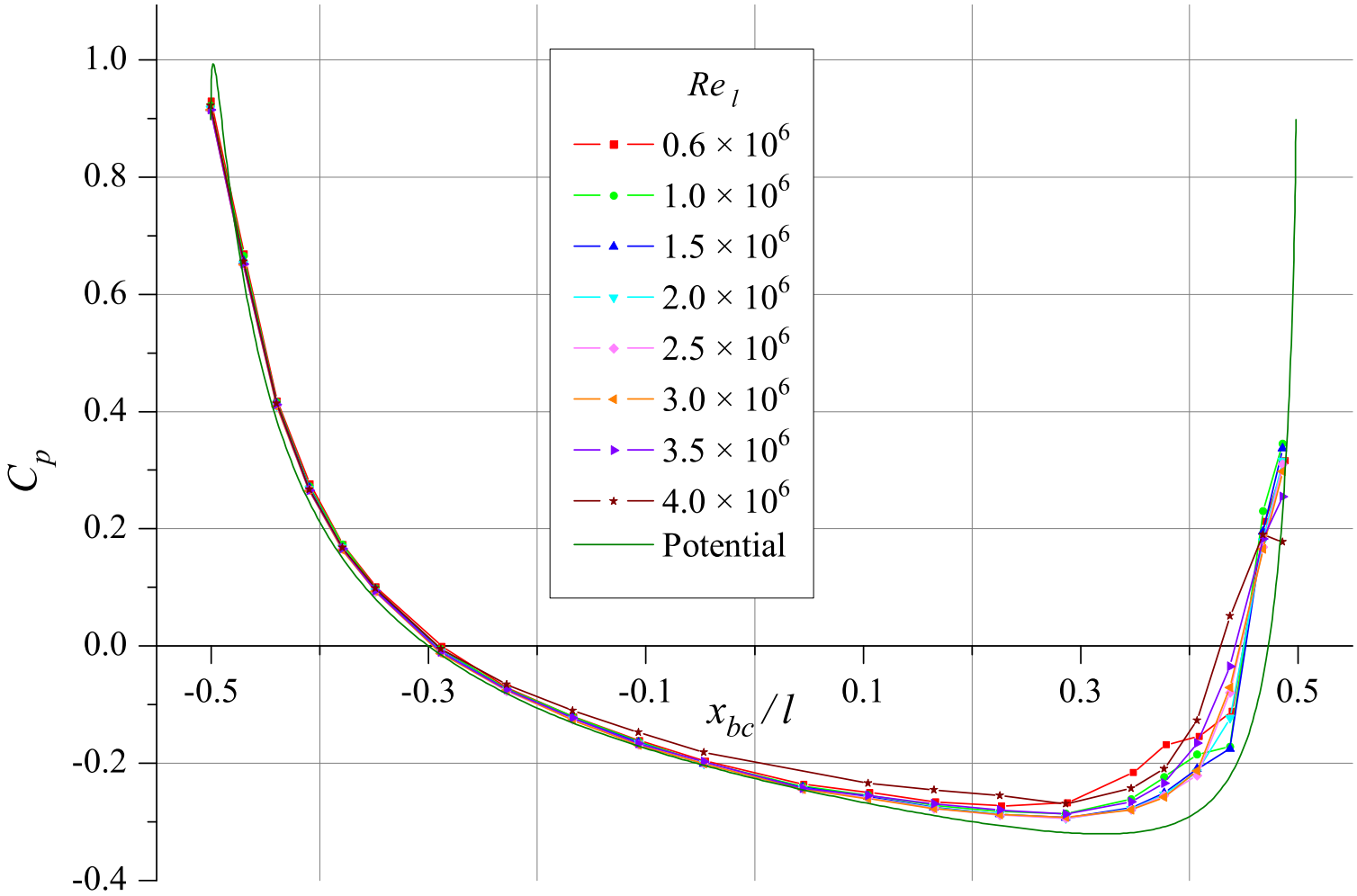

Figure C.15: Surface pressure distribution on spheroid at $\alpha = -10.2°$, $\varphi_e = -15°$

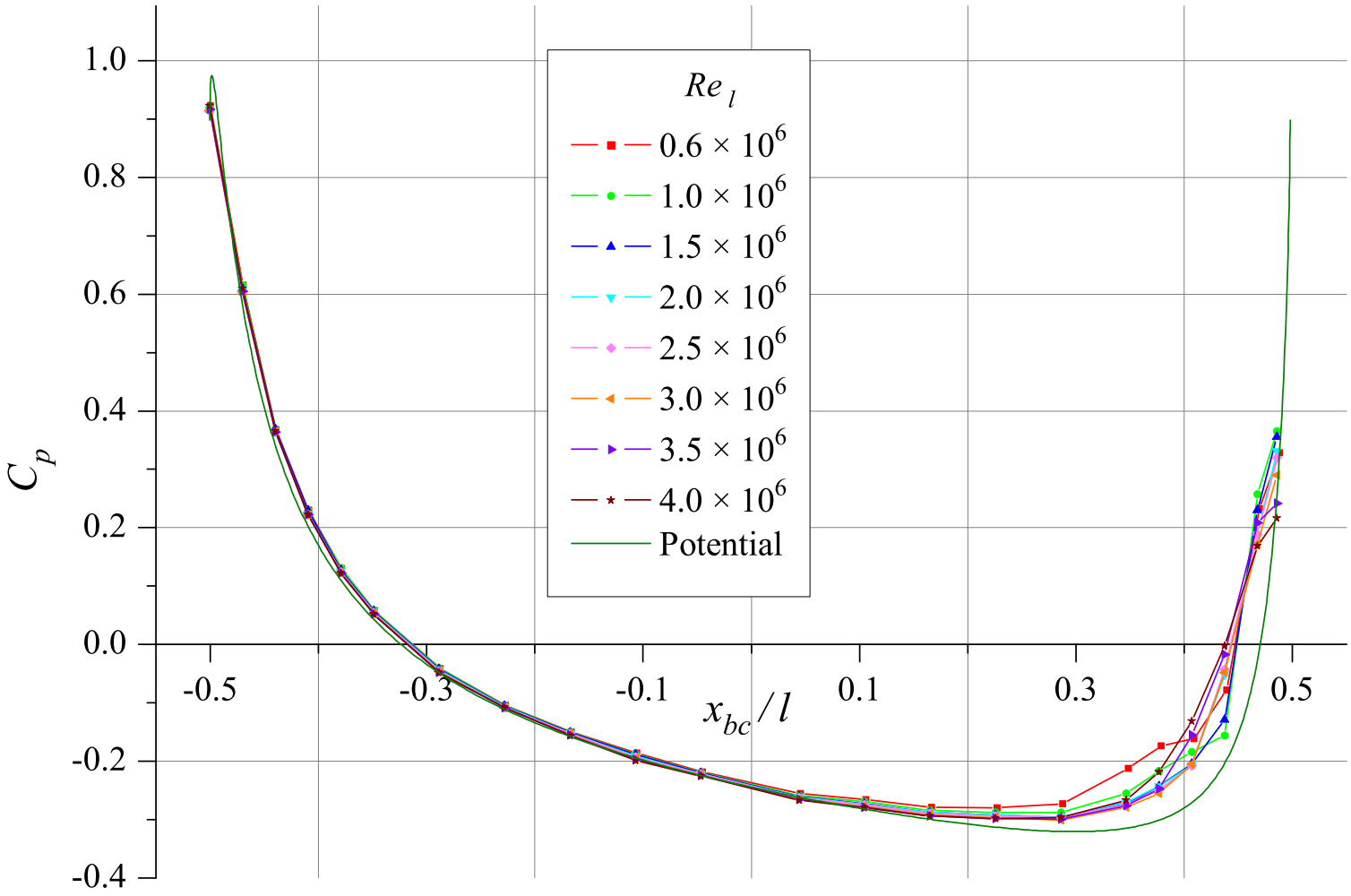

Figure C.16: Surface pressure distribution on spheroid at $\alpha = -10.2°$, $\varphi_e = -30°$

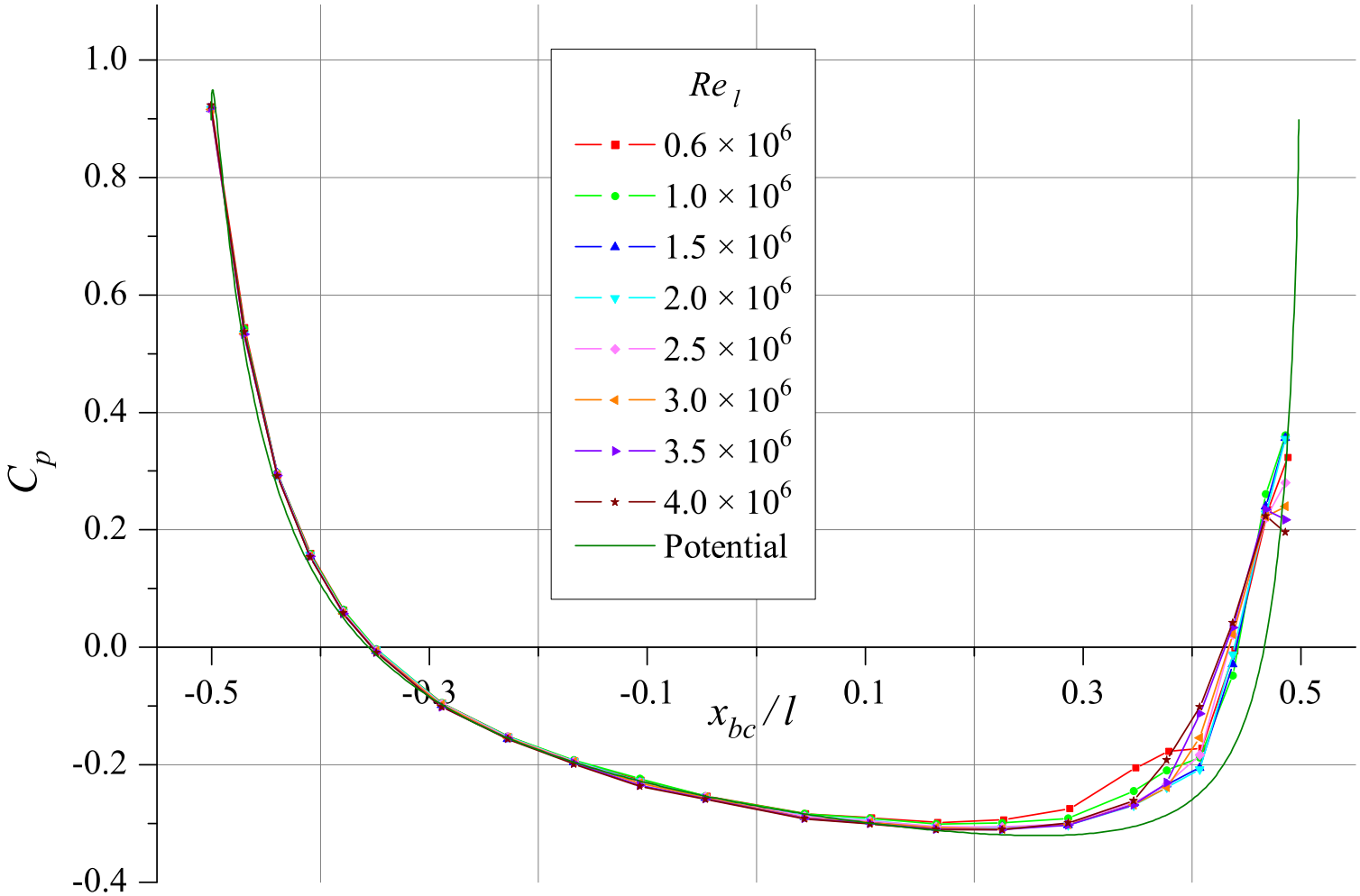

Figure C.17: Surface pressure distribution on spheroid at $\alpha = -10.2°$, $\varphi_e = -45°$

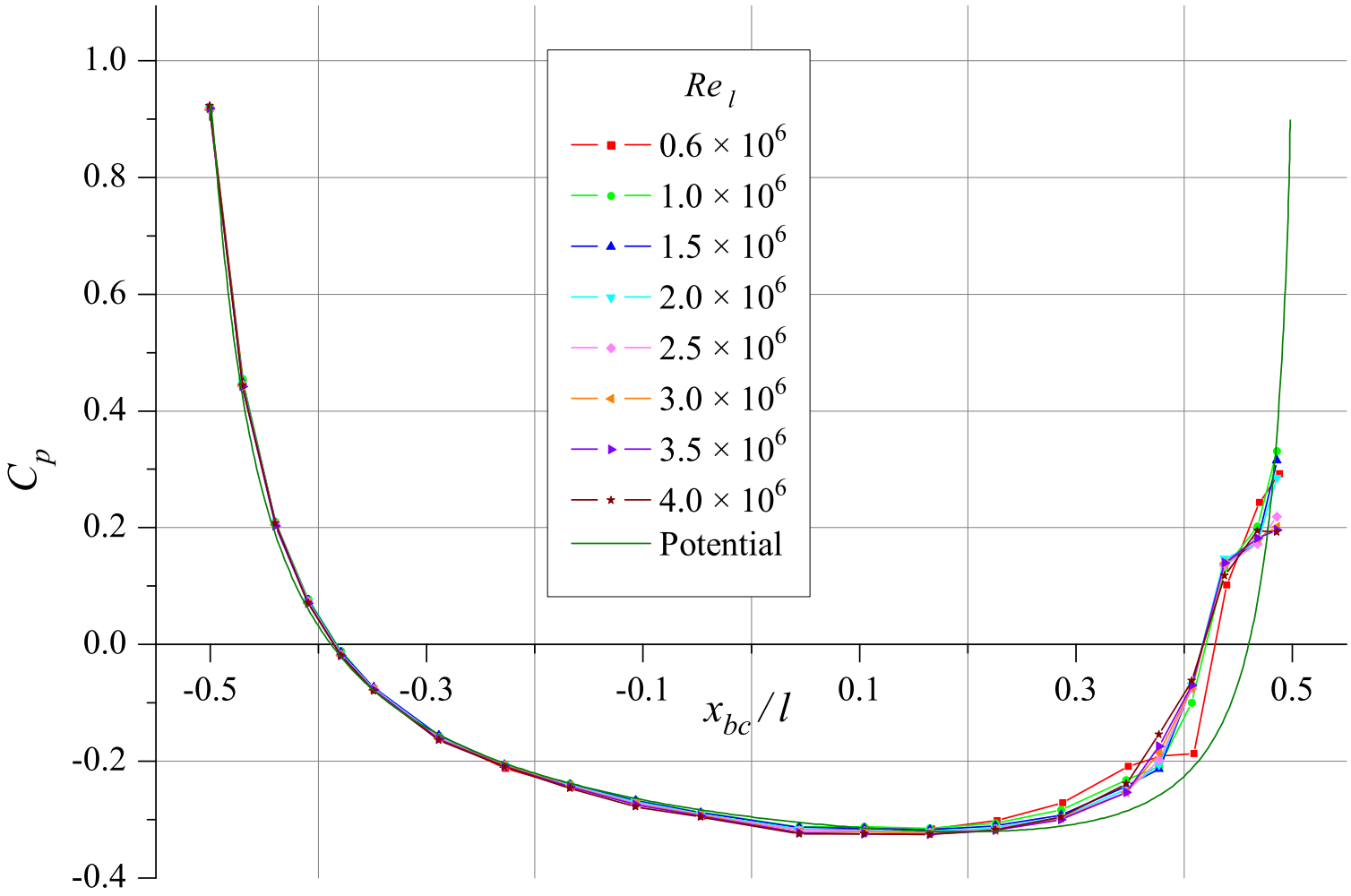

Figure C.18: Surface pressure distribution on spheroid at $\alpha = -10.2°$, $\varphi_e = -60°$

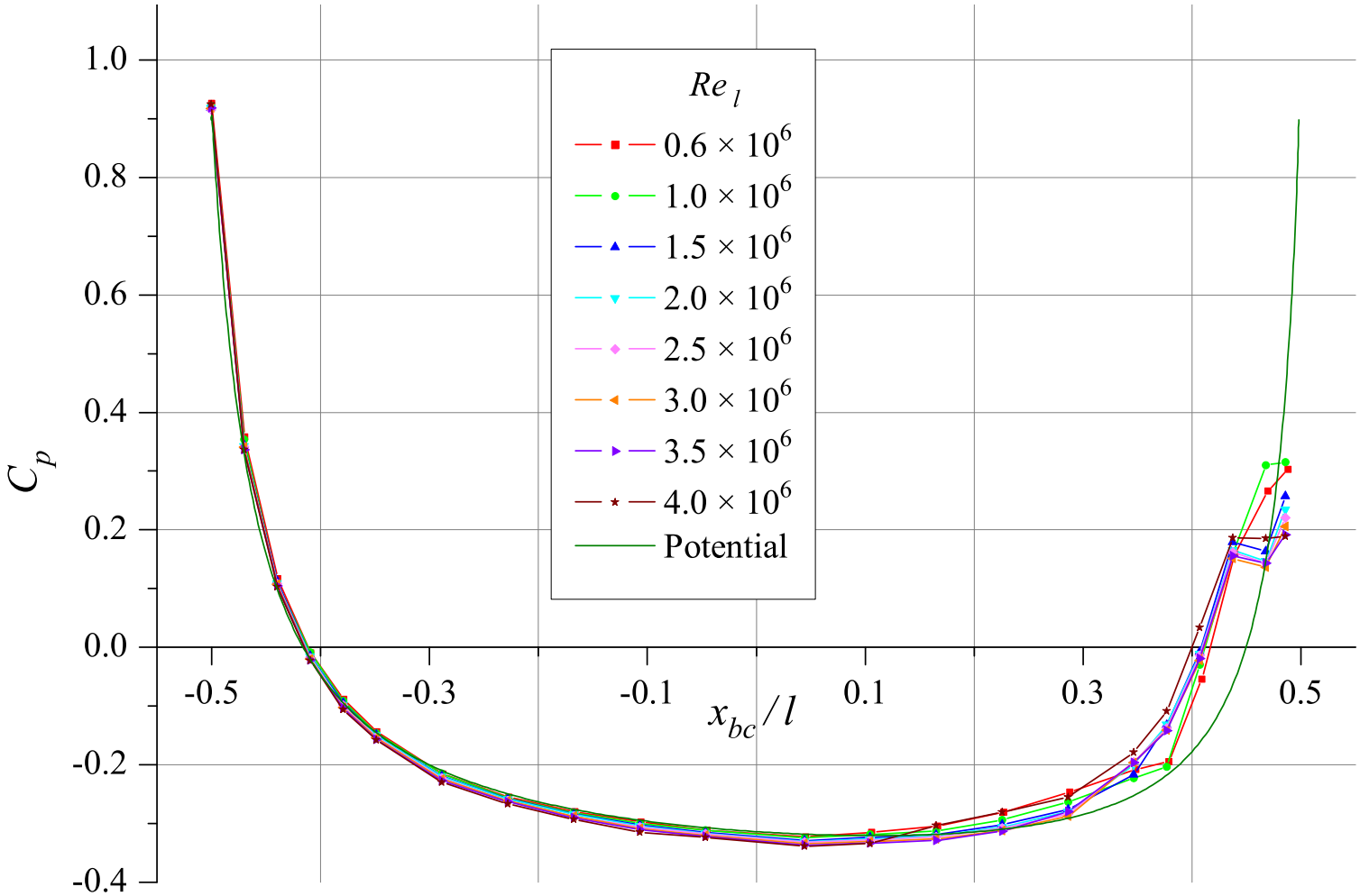

Figure C.19: Surface pressure distribution on spheroid at $\alpha = -10.2°$, $\varphi_e = -75°$

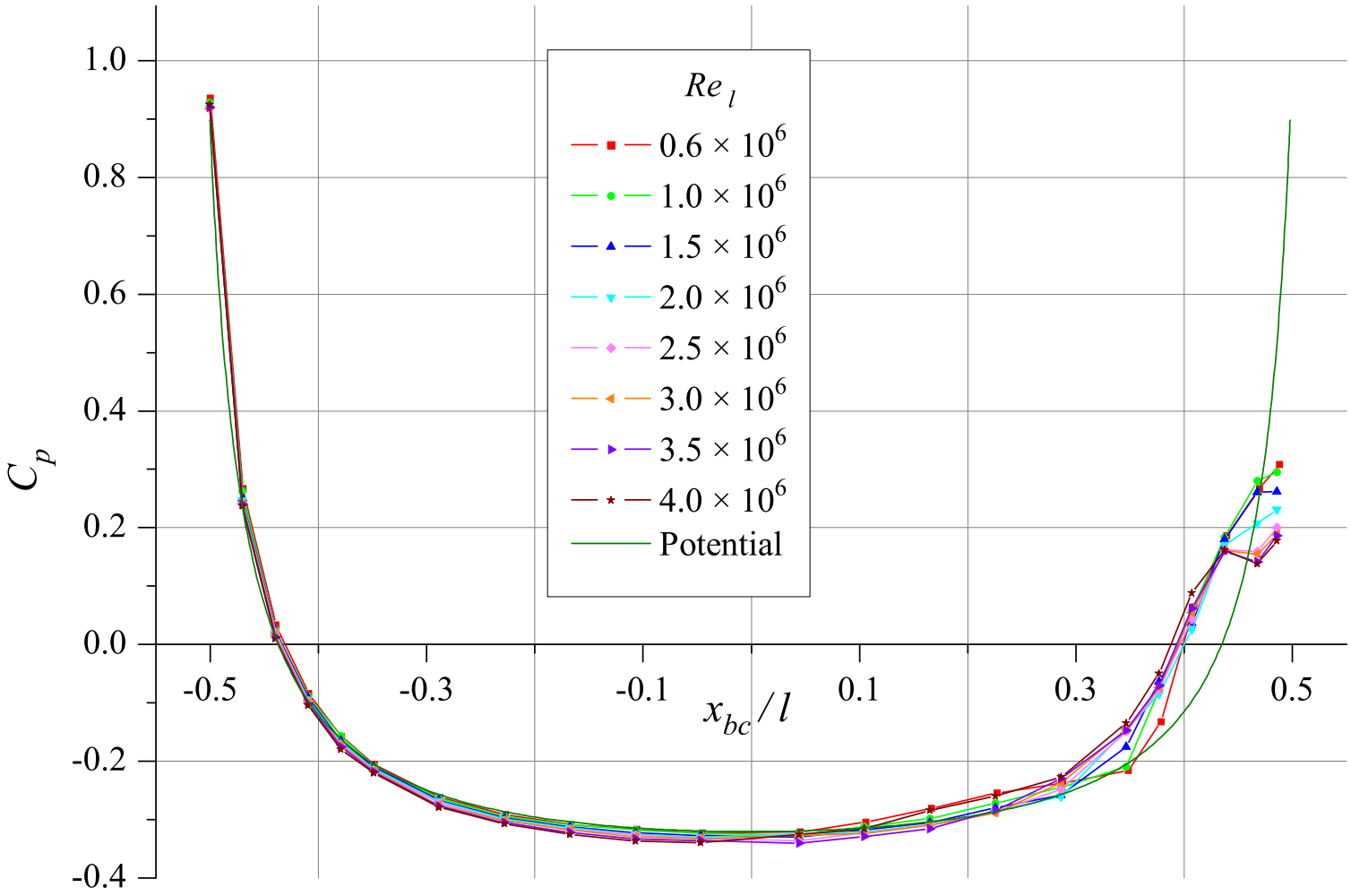

Figure C.20: Surface pressure distribution on spheroid at $\alpha = -10.2°$, $\varphi_e = -90°$

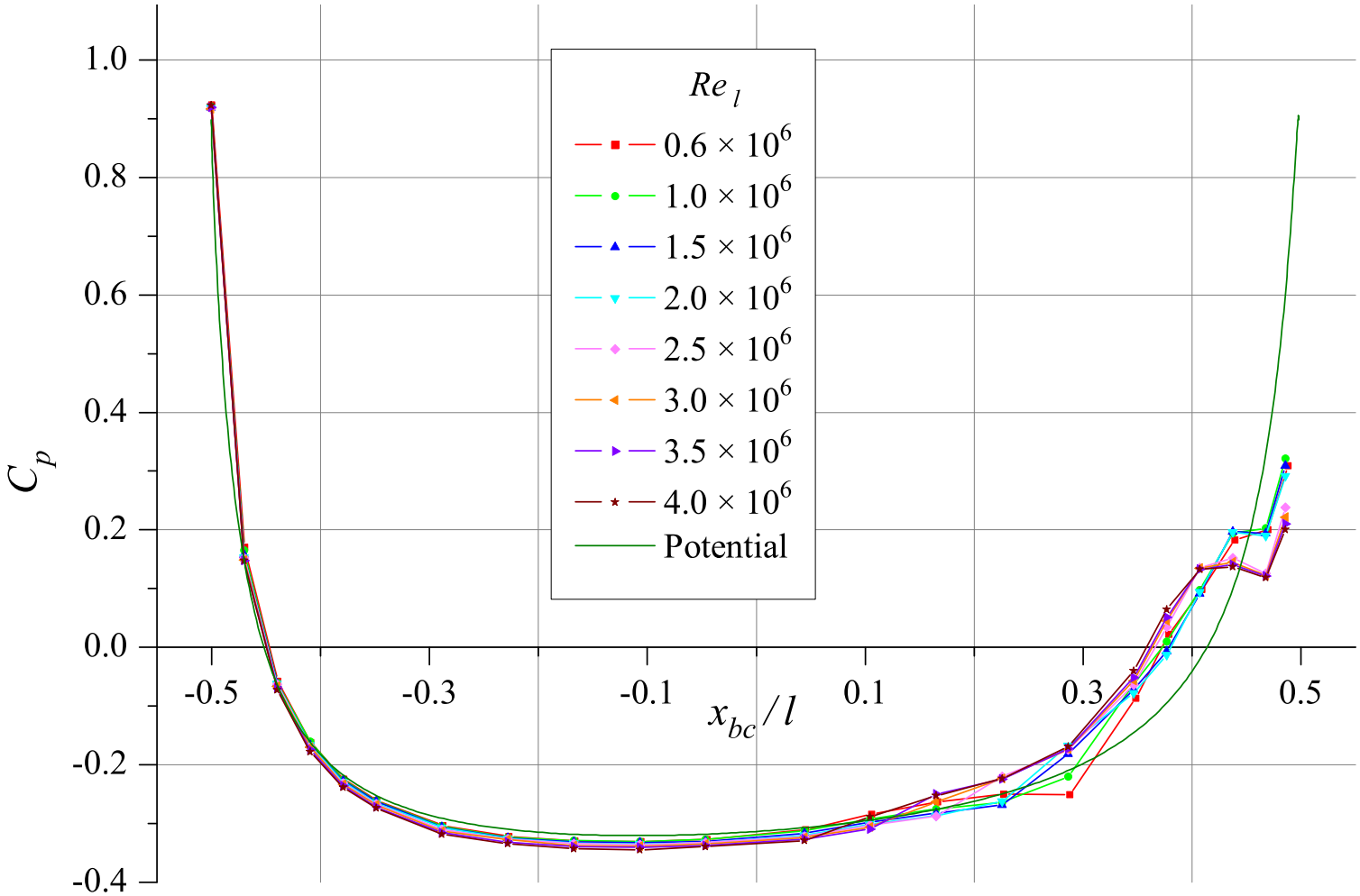

Figure C.21: Surface pressure distribution on spheroid at $\alpha = -10.2°$, $\varphi_e = -105°$

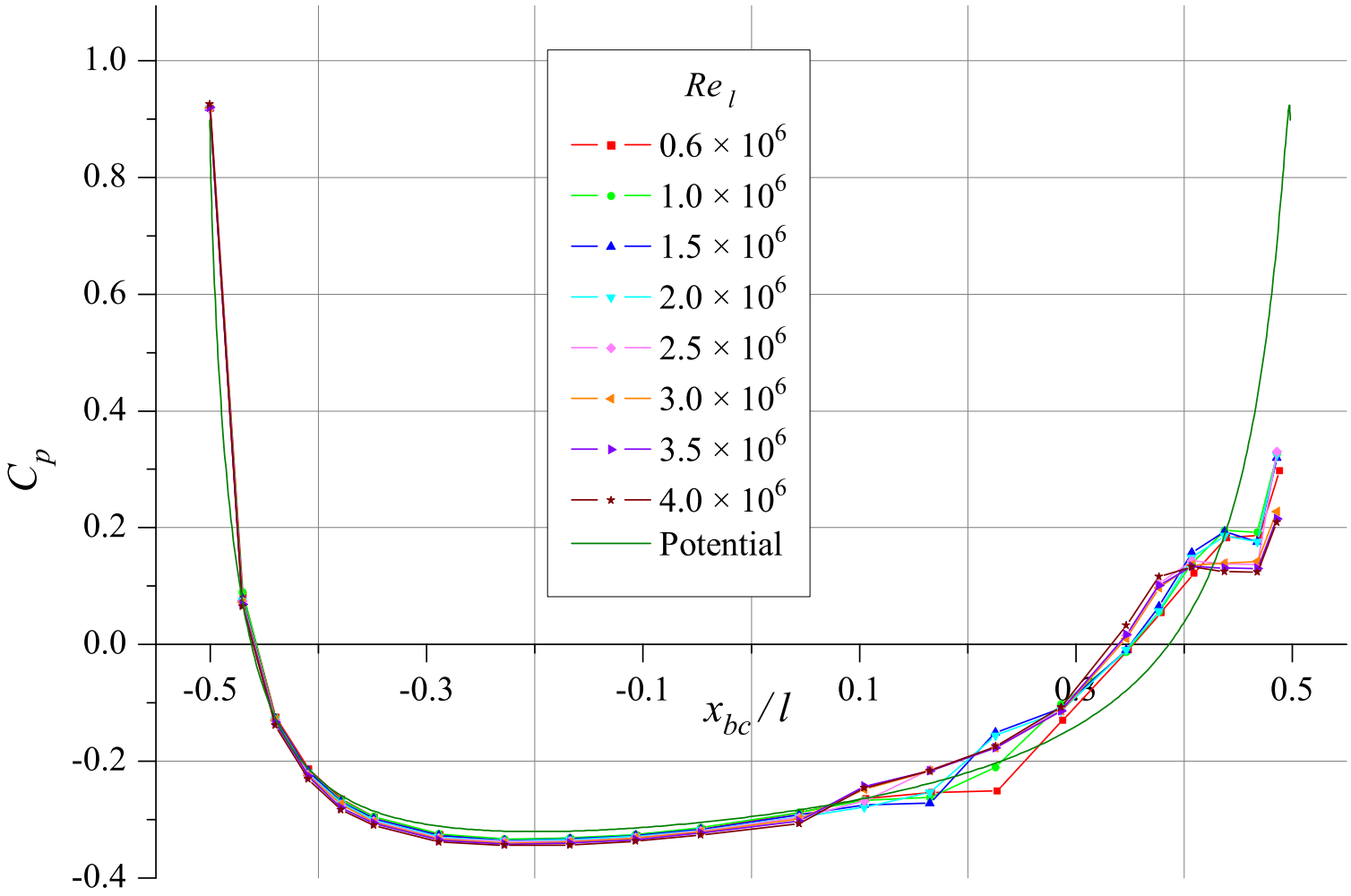

Figure C.22: Surface pressure distribution on spheroid at $\alpha = -10.2°$, $\varphi_e = -120°$

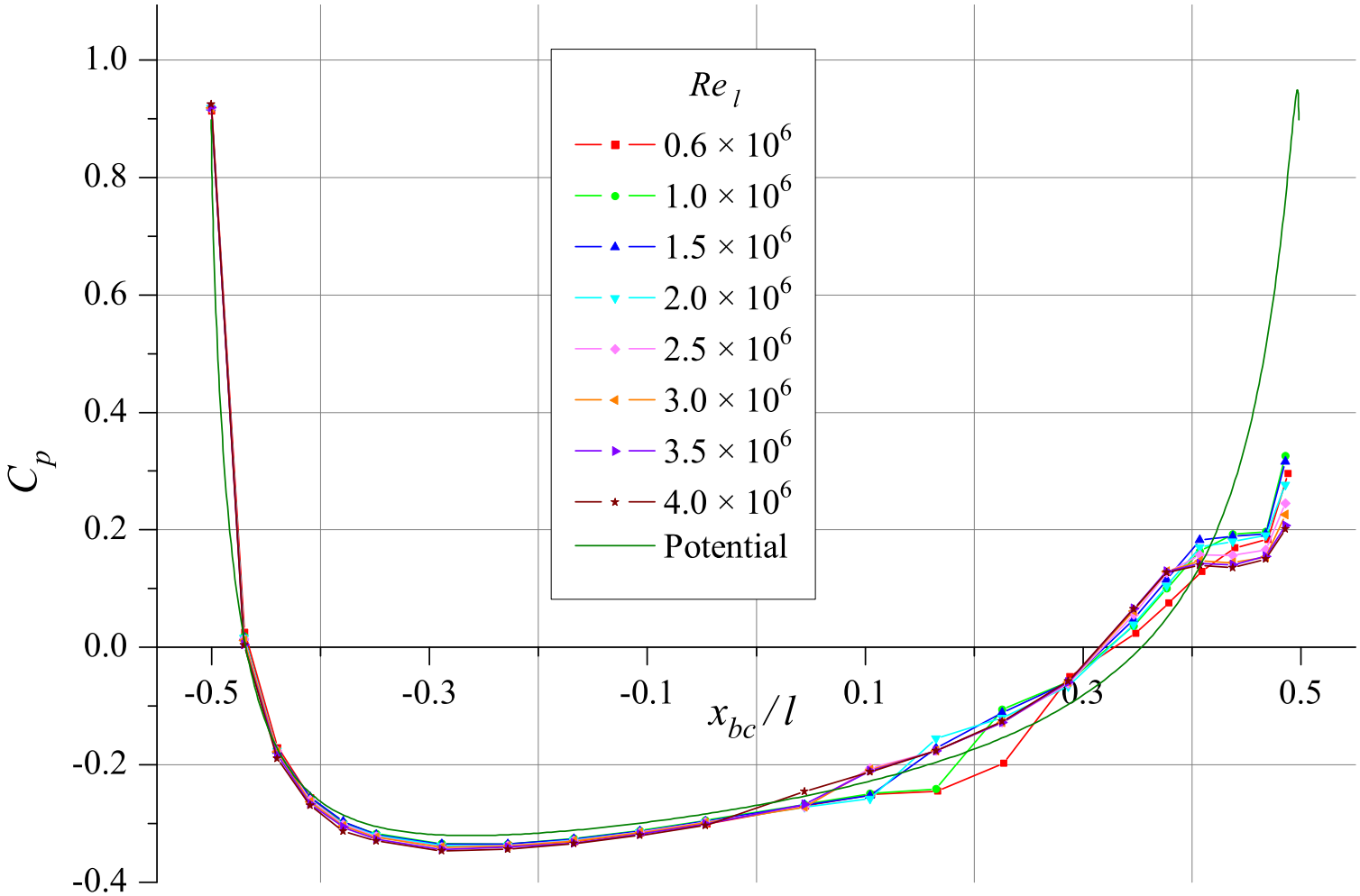

Figure C.23: Surface pressure distribution on spheroid at $\alpha = -10.2°$, $\varphi_e = -135°$

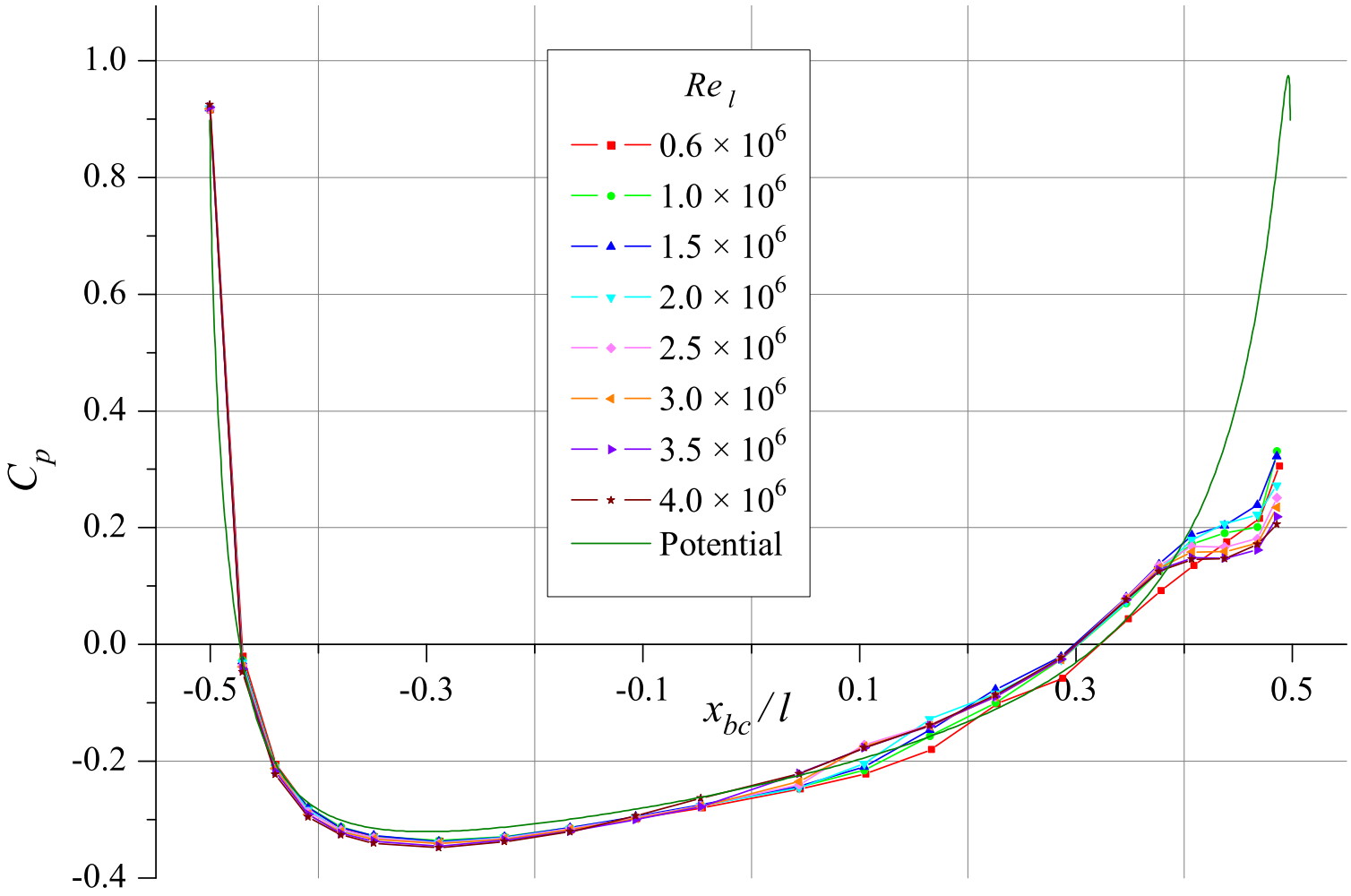

Figure C.24: Surface pressure distribution on spheroid at $\alpha = -10.2°$, $\varphi_e = -150°$

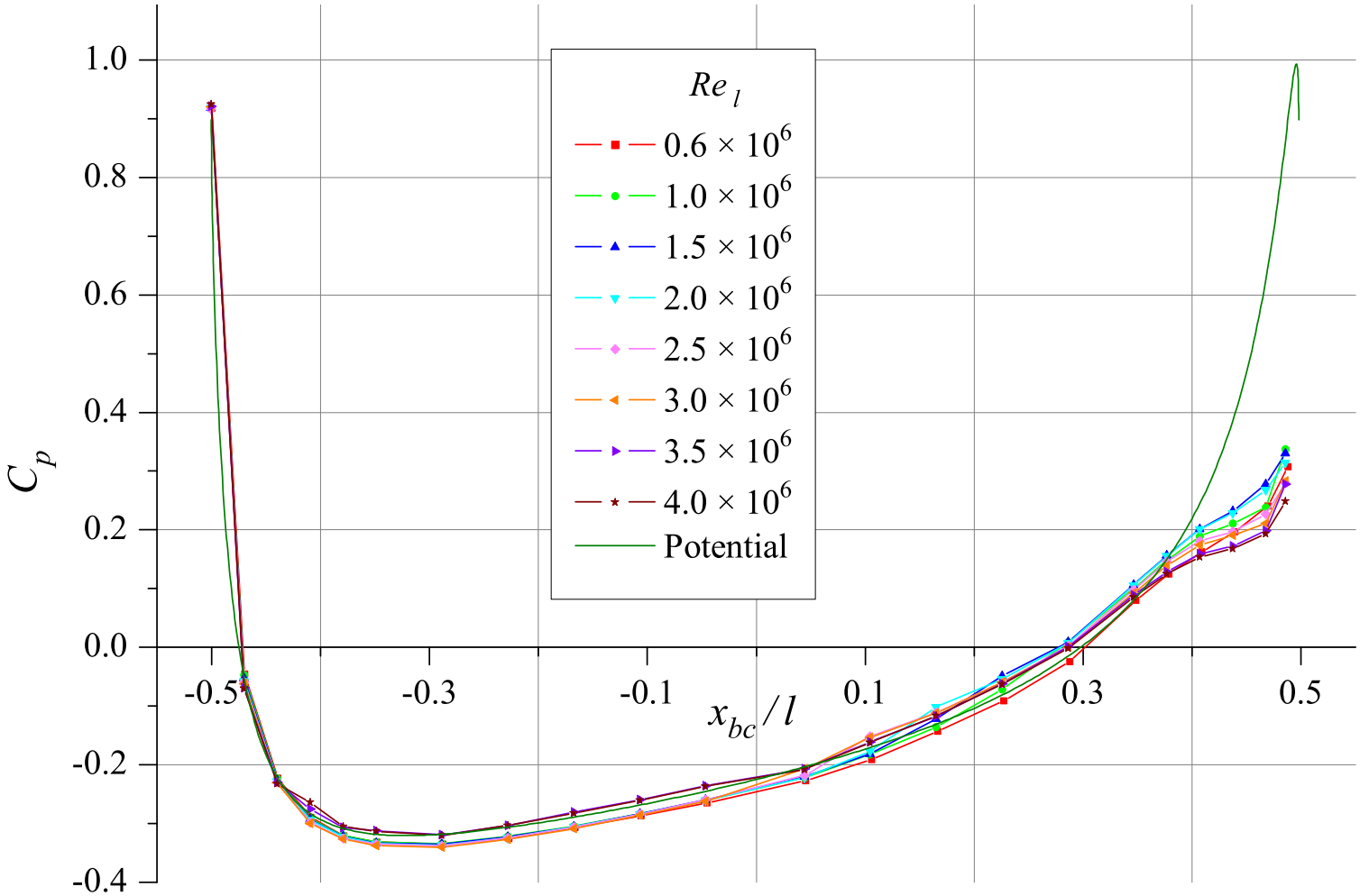

Figure C.25: Surface pressure distribution on spheroid at $\alpha = -10.2°$, $\varphi_e = -165°$

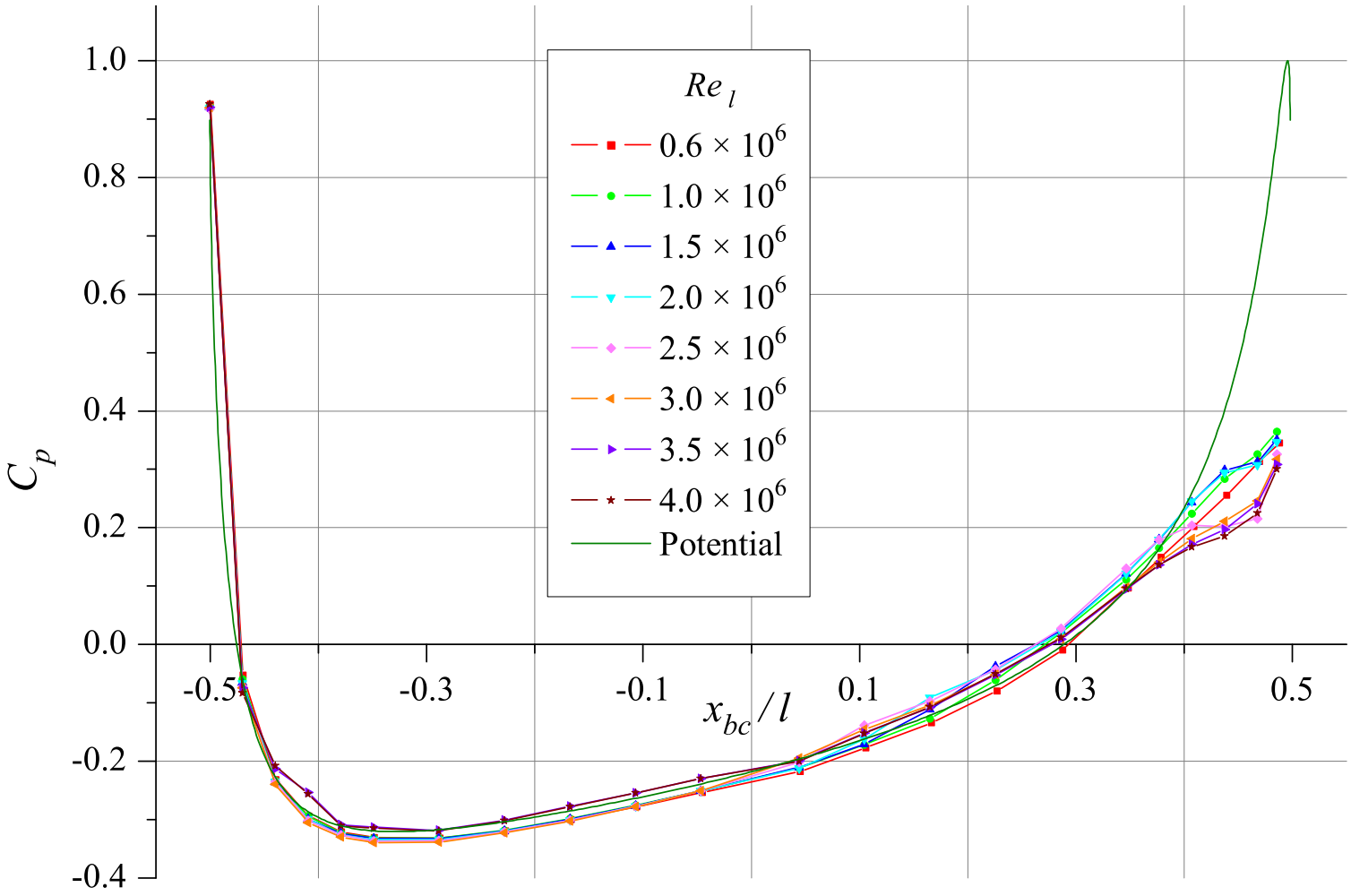

Figure C.26: Surface pressure distribution on spheroid at $\alpha = -10.2°$, $\varphi_e = -180°$

C.3 Spheroid Surface Pressure at $\alpha = -10.2°$, Tripped $x_{bc}/l = -0.3$

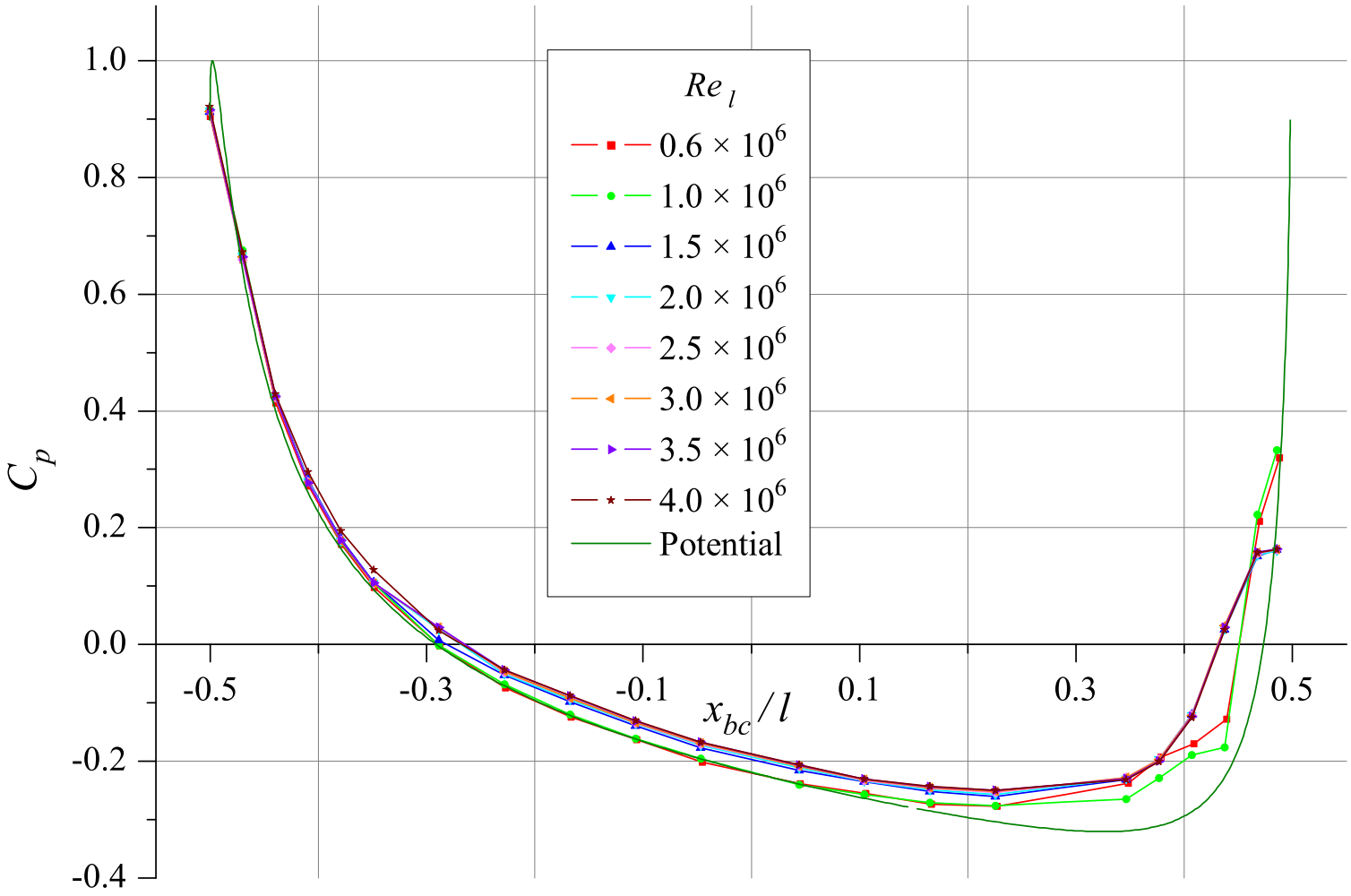

Figure C.27: Surface pressure distribution on spheroid at $\alpha = -10.2°$, $\varphi_e = 0°$, tripped at $x_{bc}/l = -0.3$

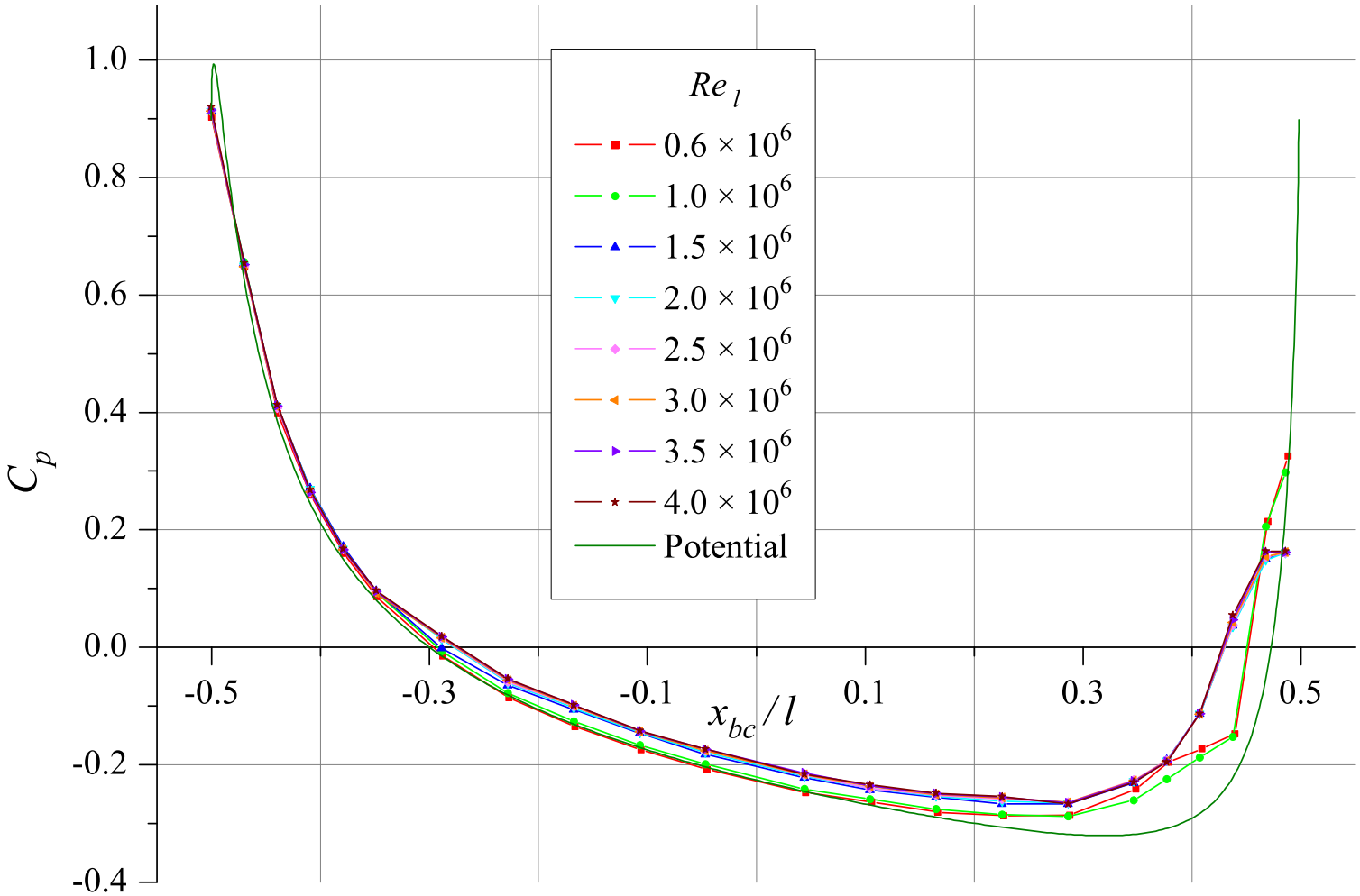

Figure C.28: Surface pressure distribution on spheroid at $\alpha = -10.2°$, $\varphi_e = -15°$, tripped at $x_{bc}/l = -0.3$

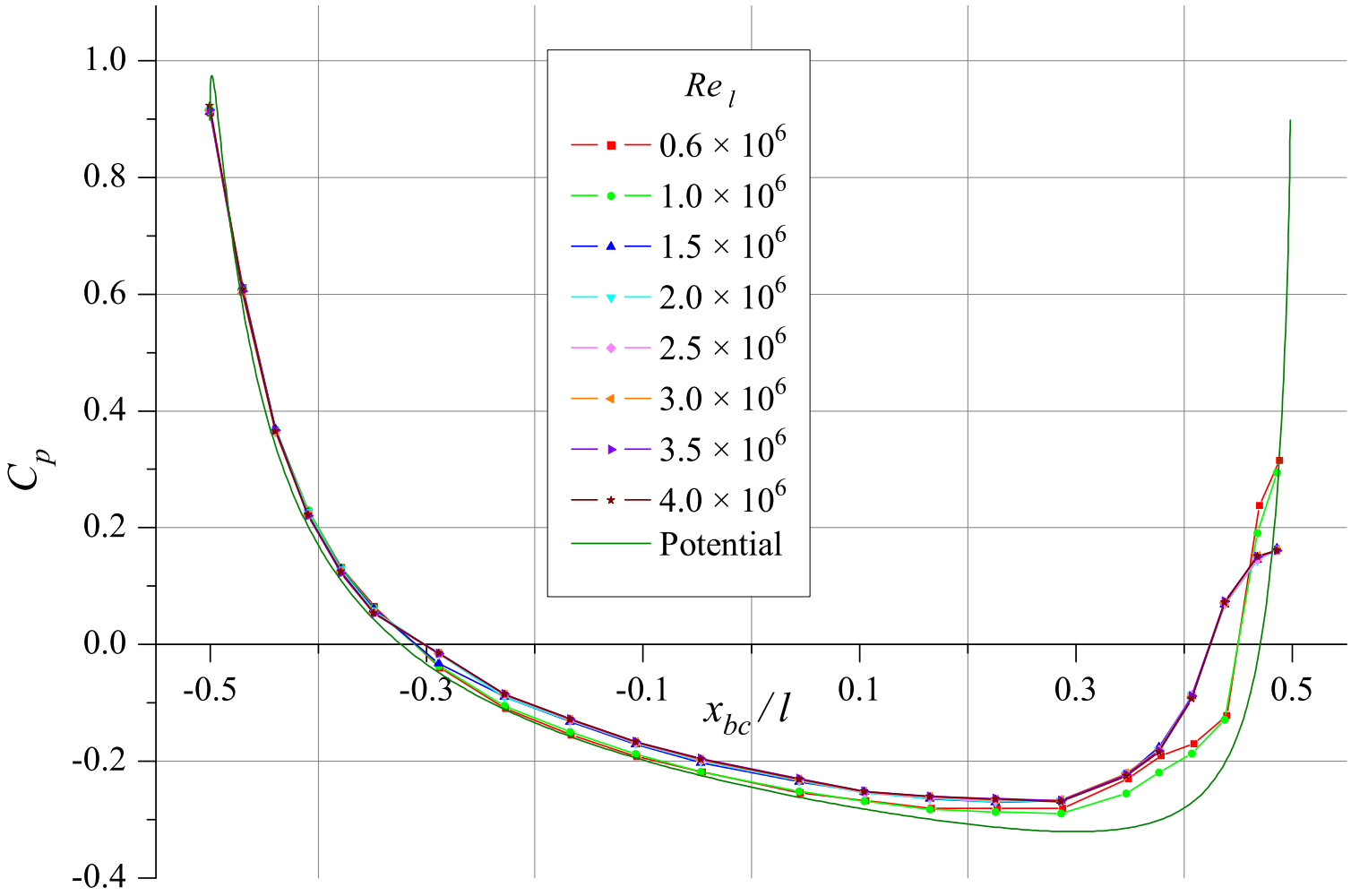

Figure C.29: Surface pressure distribution on spheroid at $\alpha = -10.2°$, $\varphi_e = -30°$, tripped at $x_{bc}/l = -0.3$

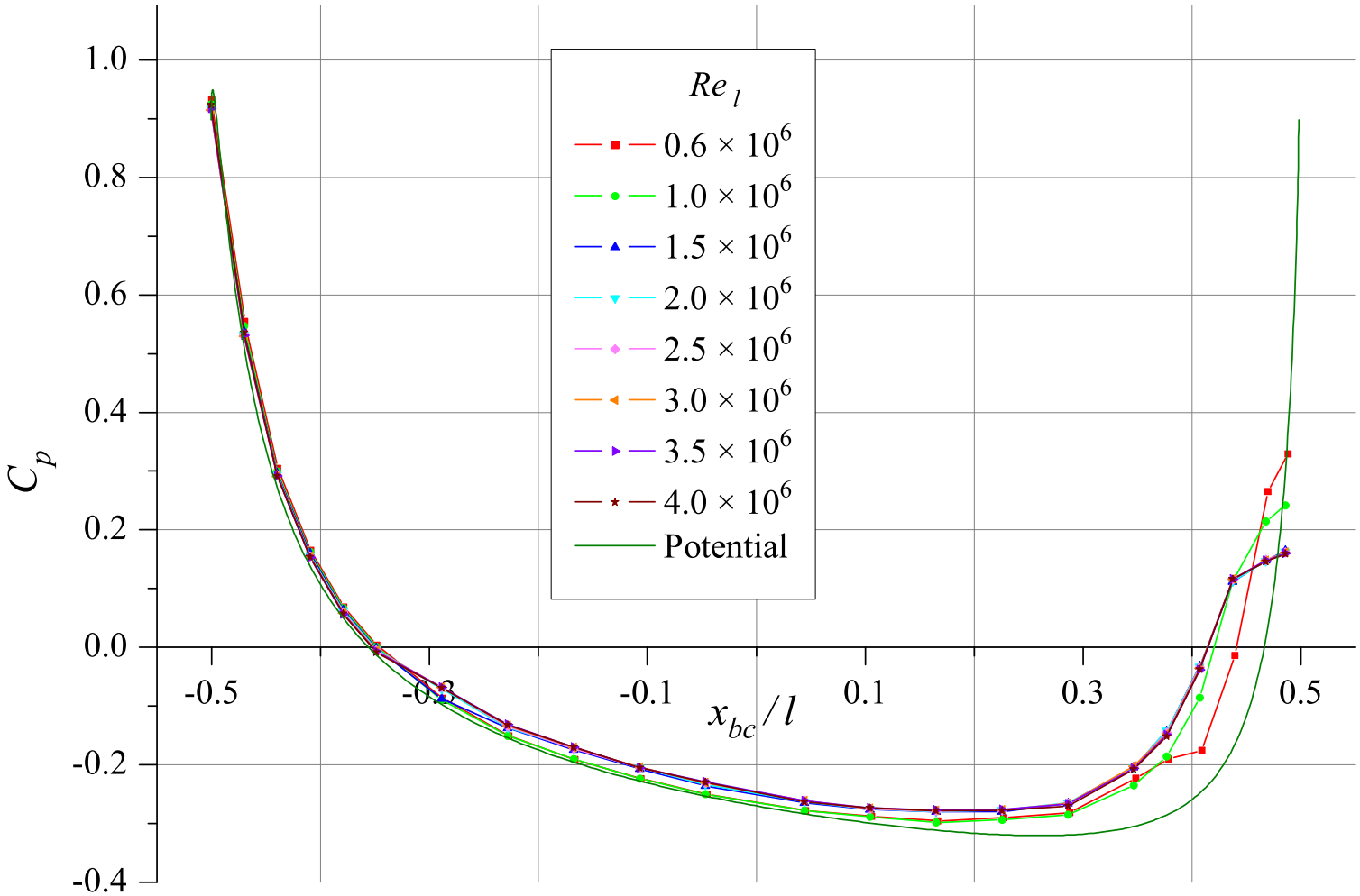

Figure C.30: Surface pressure distribution on spheroid at $\alpha = -10.2°$, $\varphi_e = -45°$, tripped at $x_{bc}/l = -0.3$

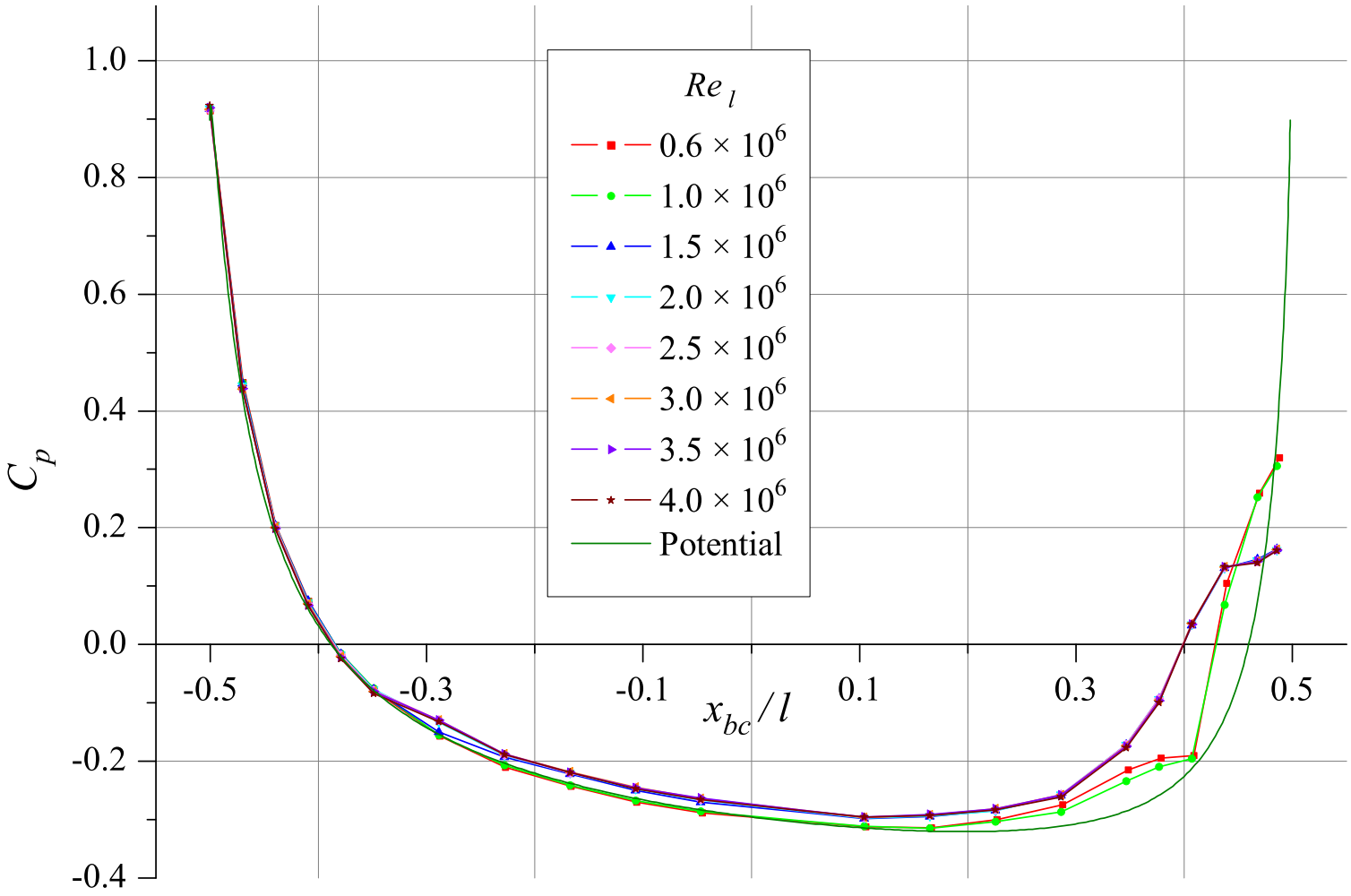

Figure C.31: Surface pressure distribution on spheroid at $\alpha = -10.2°$, $\varphi_e = -60°$, tripped at $x_{bc}/l = -0.3$

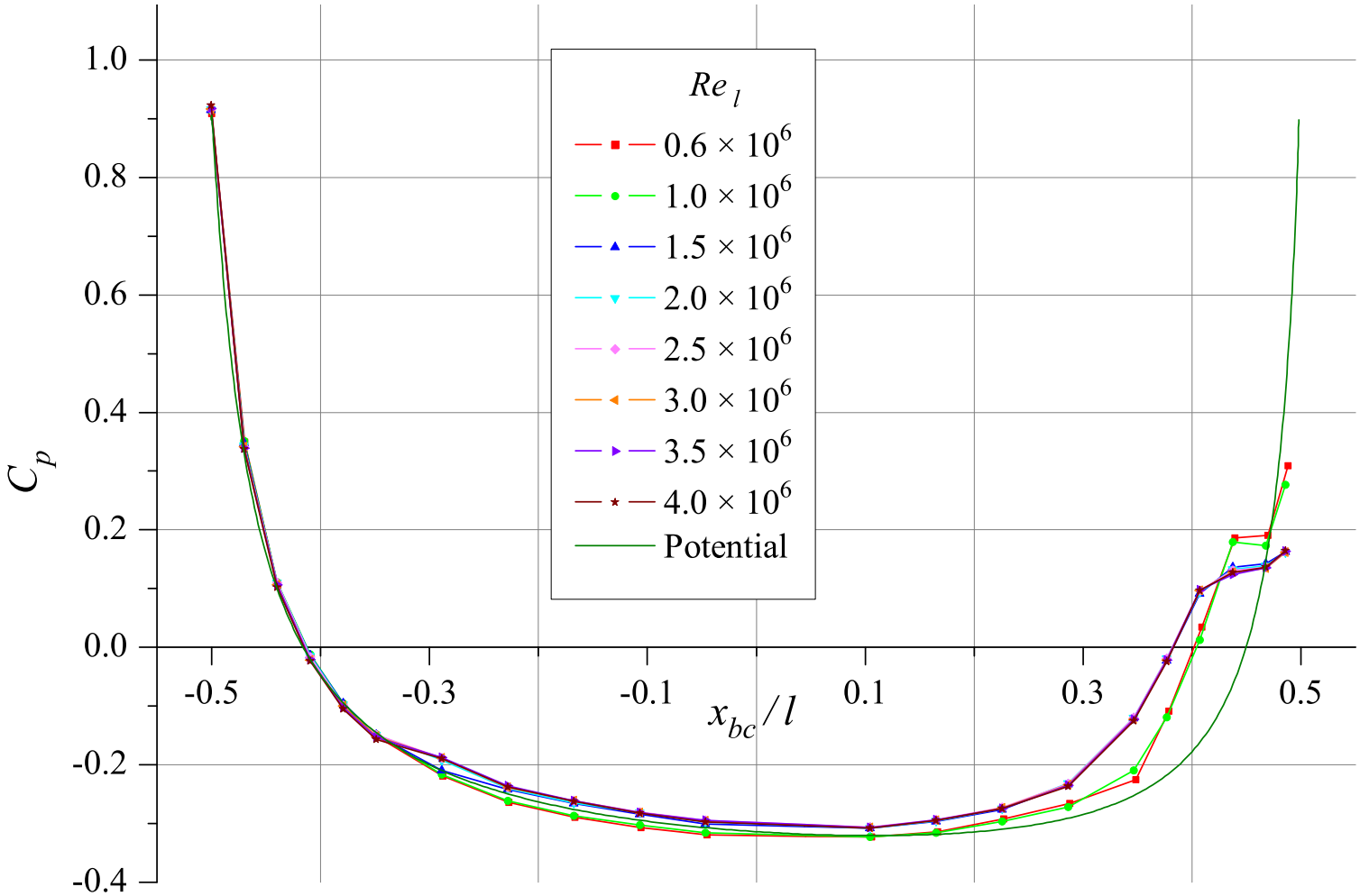

Figure C.32: Surface pressure distribution on spheroid at $\alpha = -10.2°$, $\varphi_e = -75°$, tripped at $x_{bc}/l = -0.3$

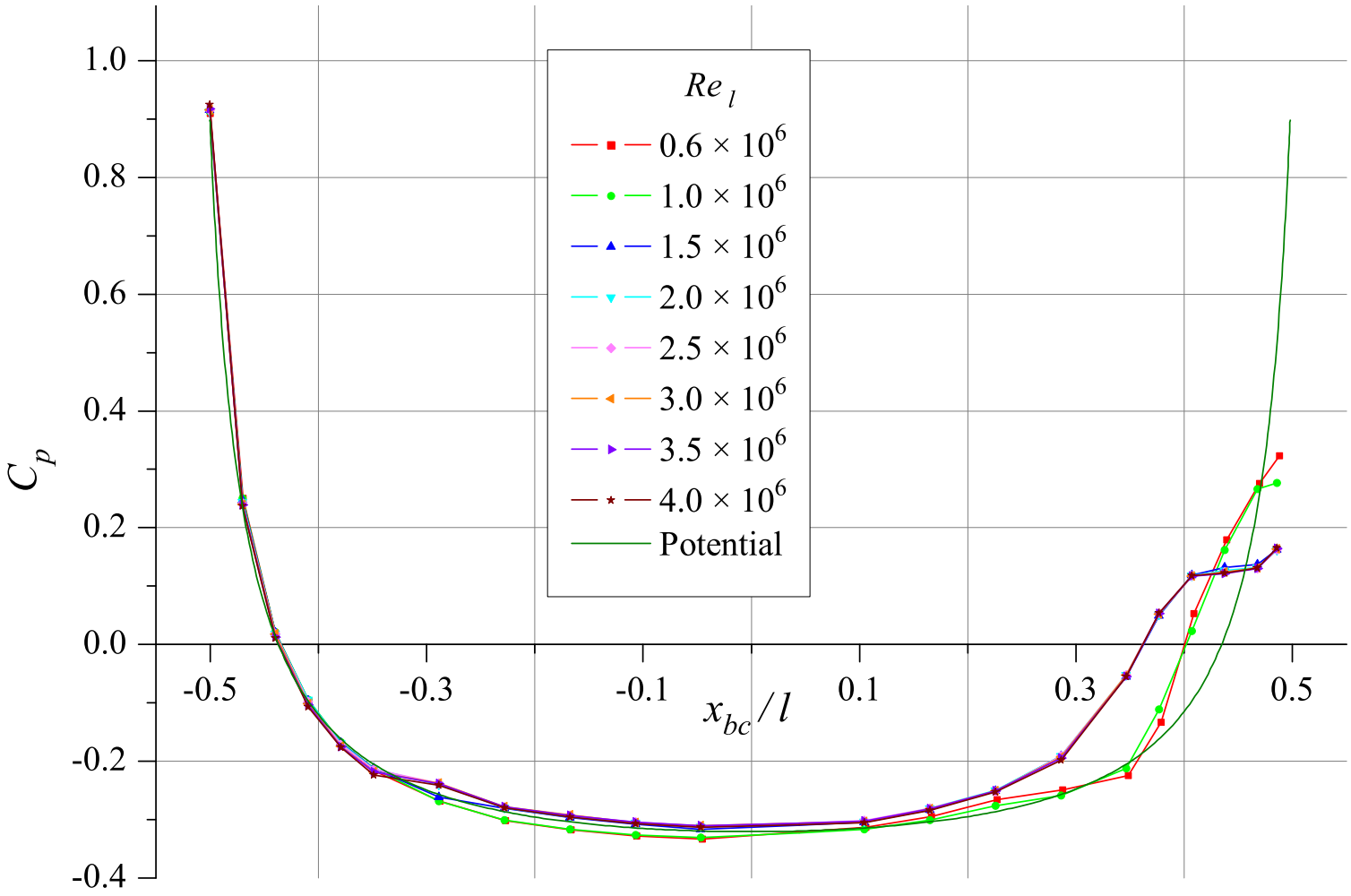

Figure C.33: Surface pressure distribution on spheroid at $\alpha = -10.2°$, $\varphi_e = -90°$, tripped at $x_{bc}/l = -0.3$

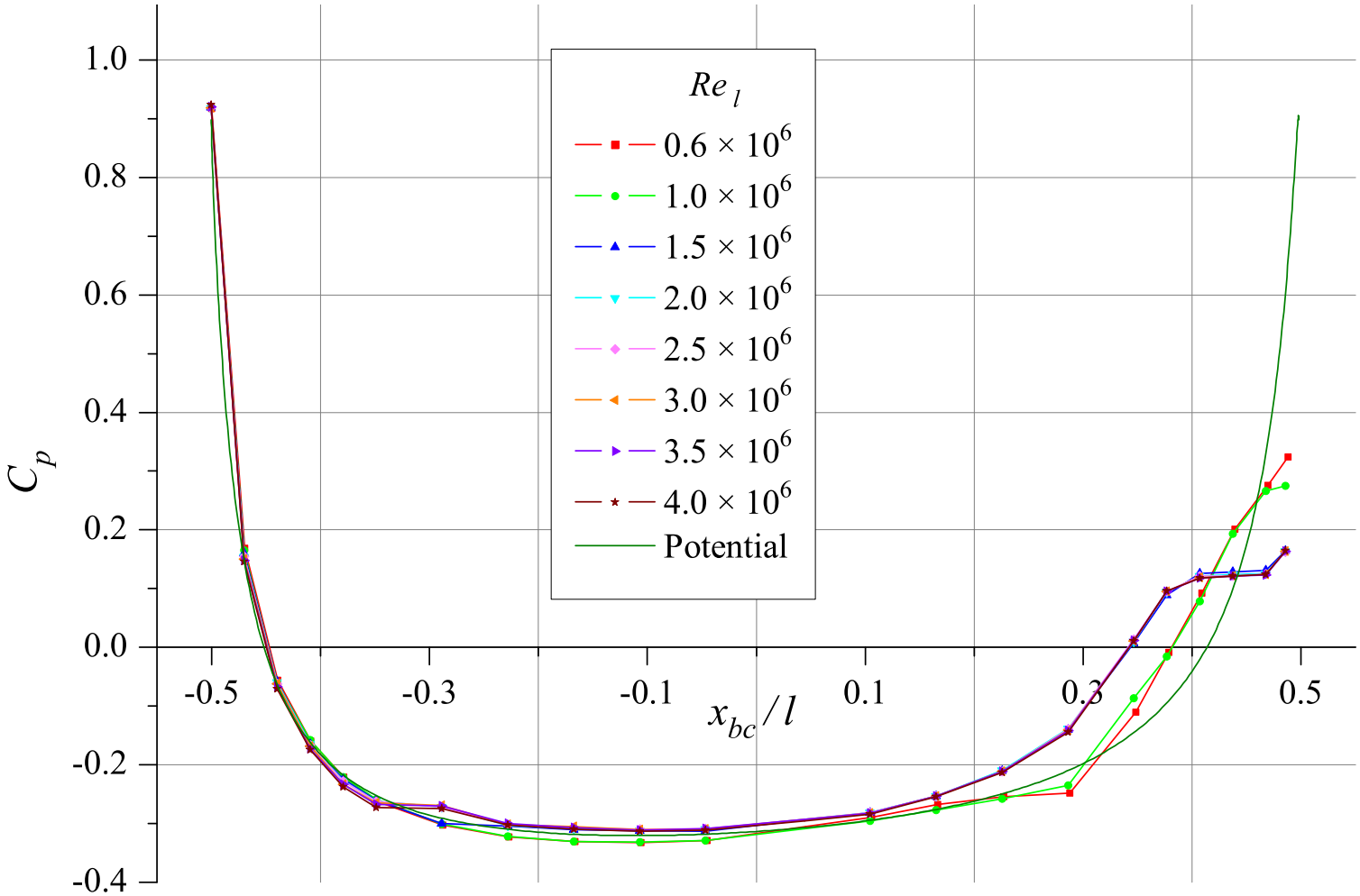

Figure C.34: Surface pressure distribution on spheroid at $\alpha = -10.2°$, $\varphi_e = -105°$, tripped at $x_{bc}/l = -0.3$

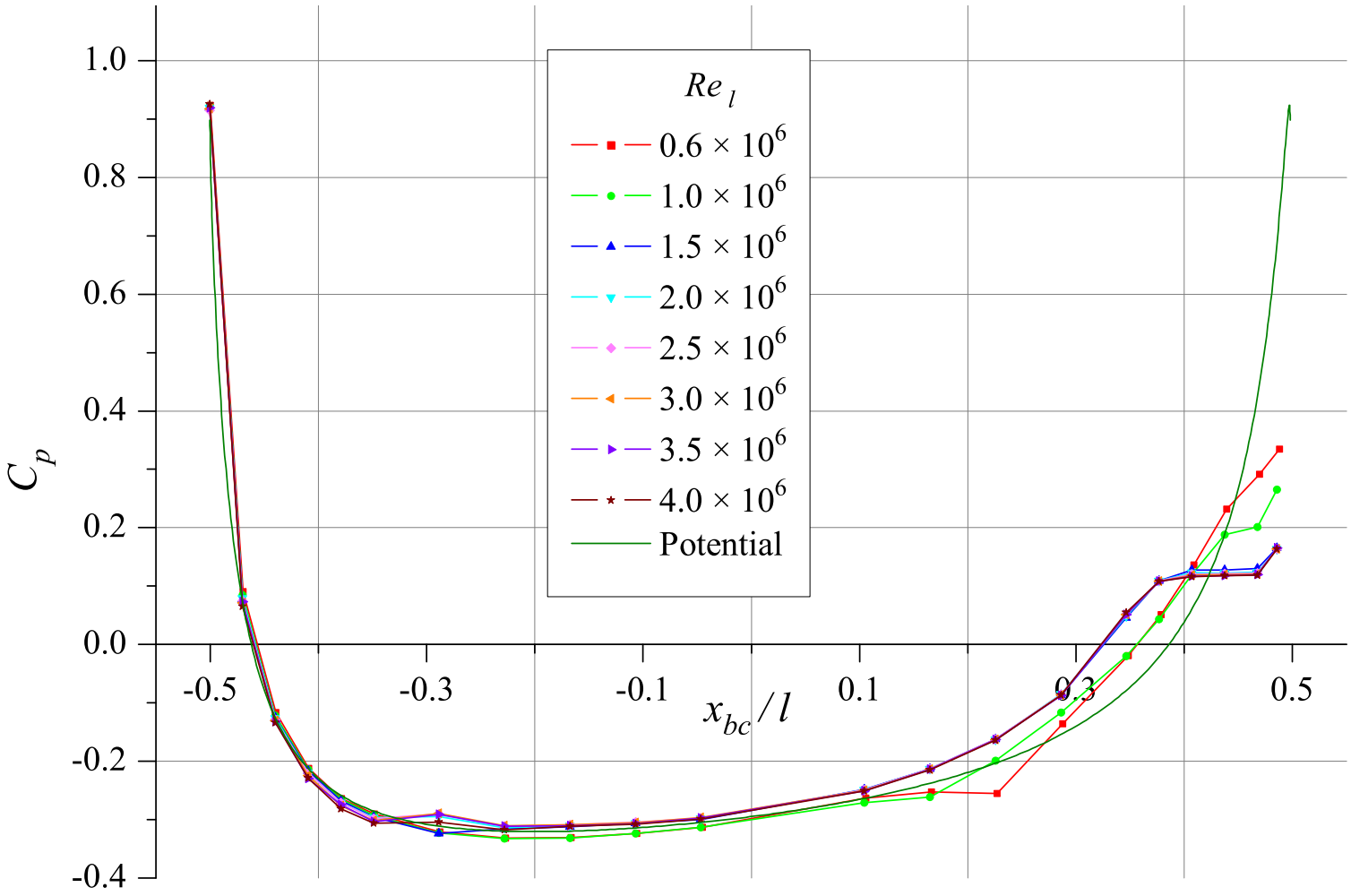

Figure C.35: Surface pressure distribution on spheroid at $\alpha = -10.2°$, $\varphi_e = -120°$, tripped at $x_{bc}/l = -0.3$

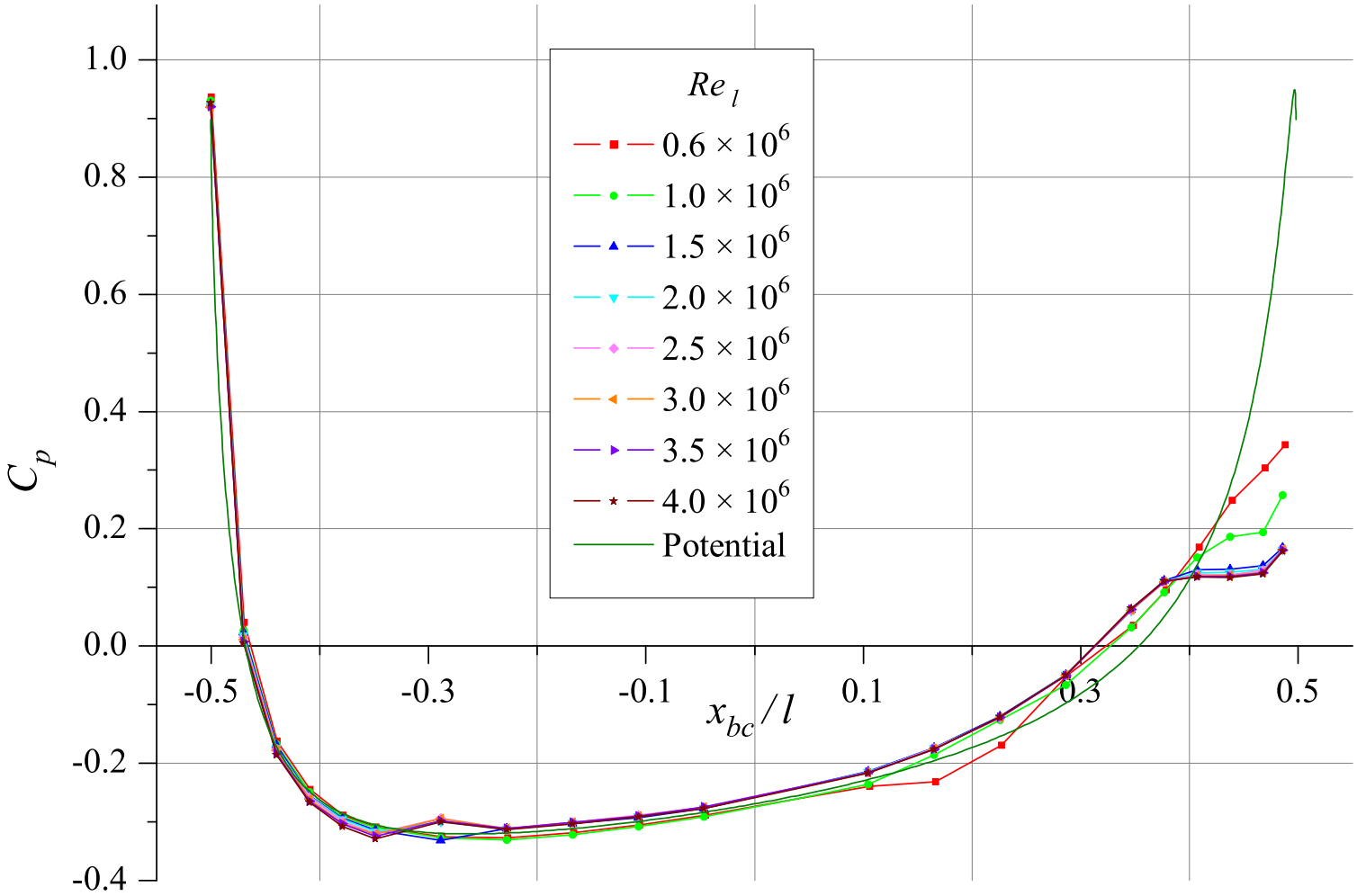

Figure C.36: Surface pressure distribution on spheroid at $\alpha = -10.2°$, $\varphi_e = -135°$, tripped at $x_{bc}/l = -0.3$

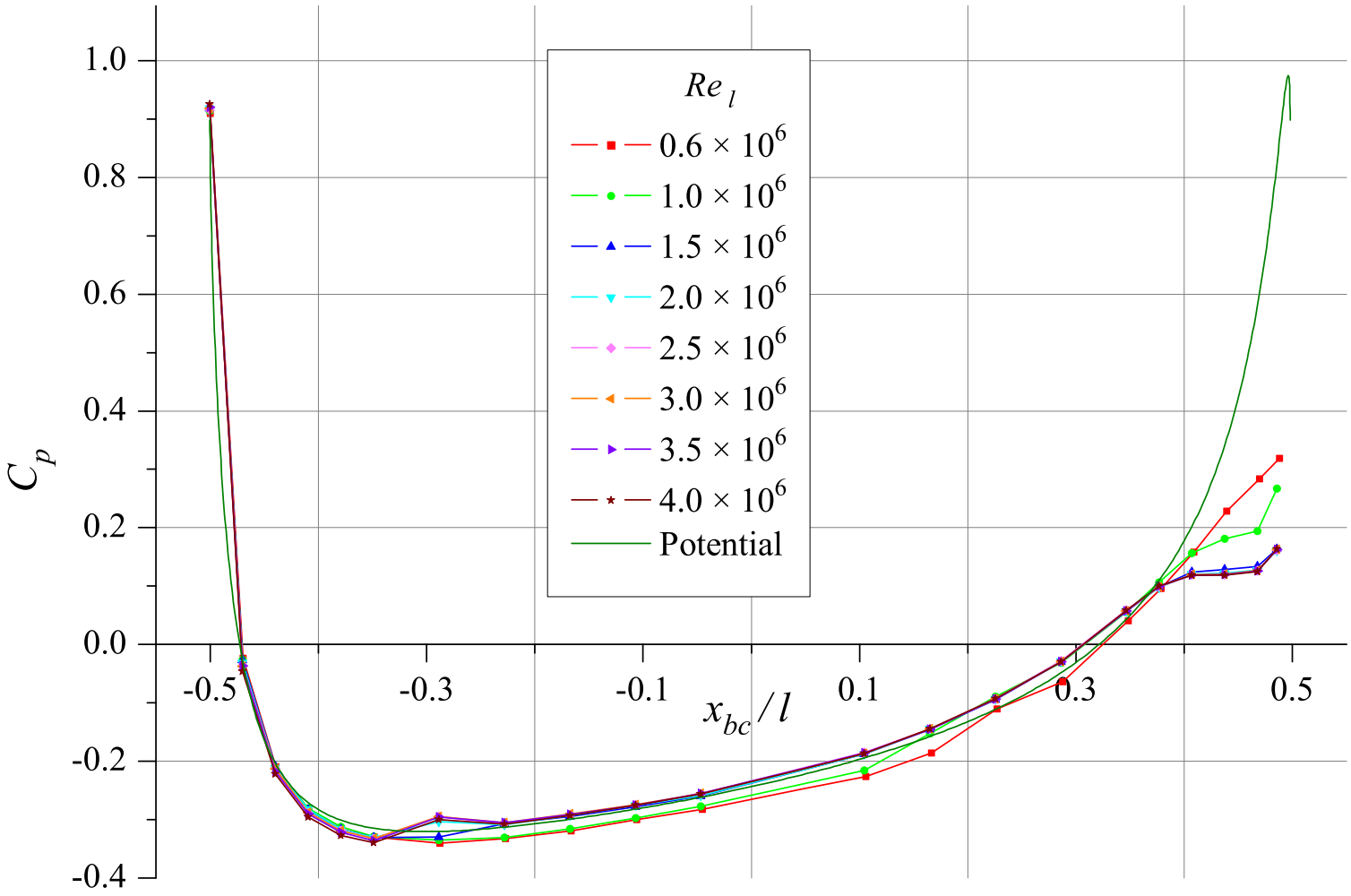

Figure C.37: Surface pressure distribution on spheroid at $\alpha = -10.2°$, $\varphi_e = -150°$, tripped at $x_{bc}/l = -0.3$

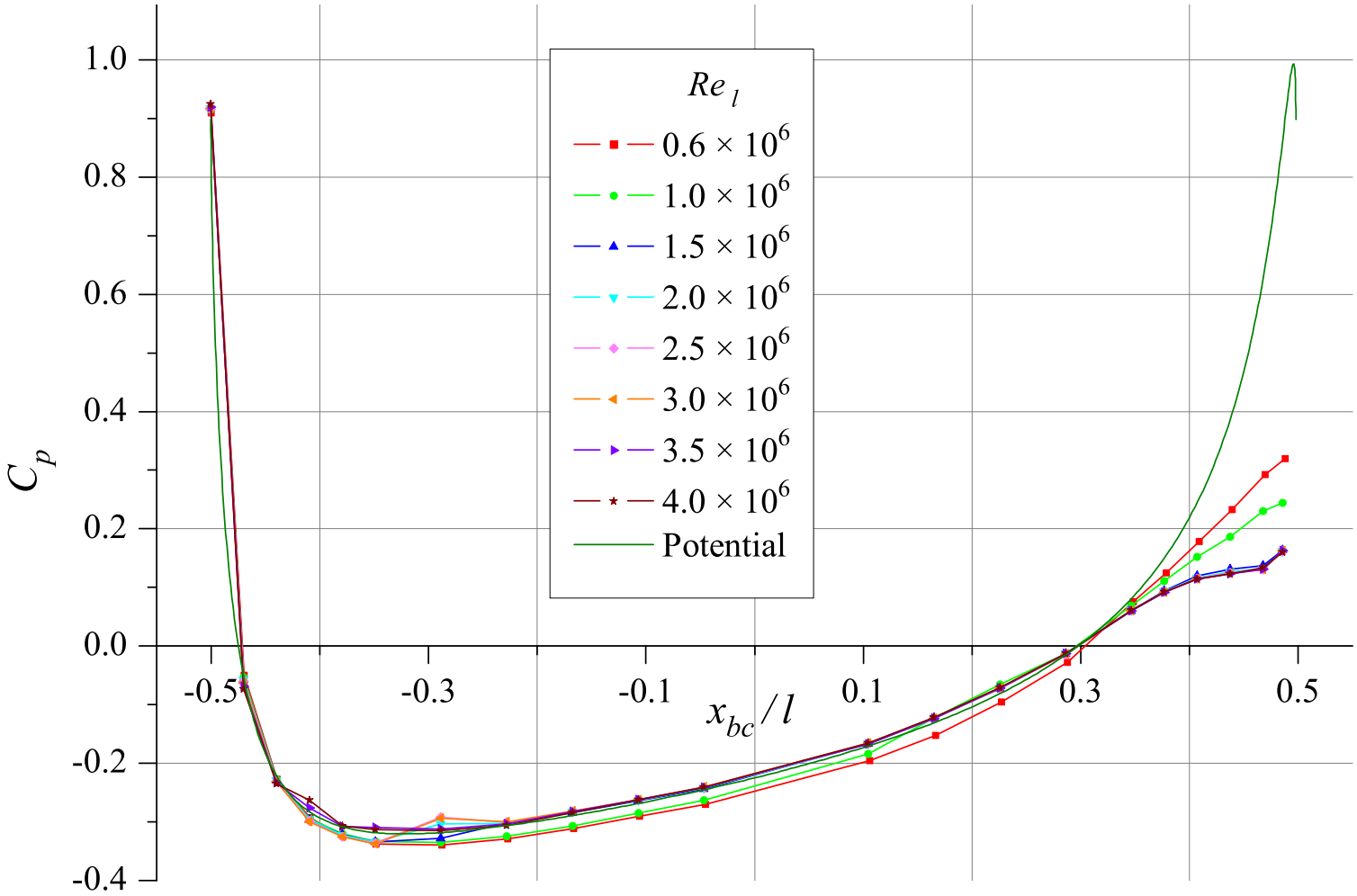

Figure C.38: Surface pressure distribution on spheroid at $\alpha = -10.2°$, $\varphi_e = -165°$, tripped at $x_{bc}/l = -0.3$

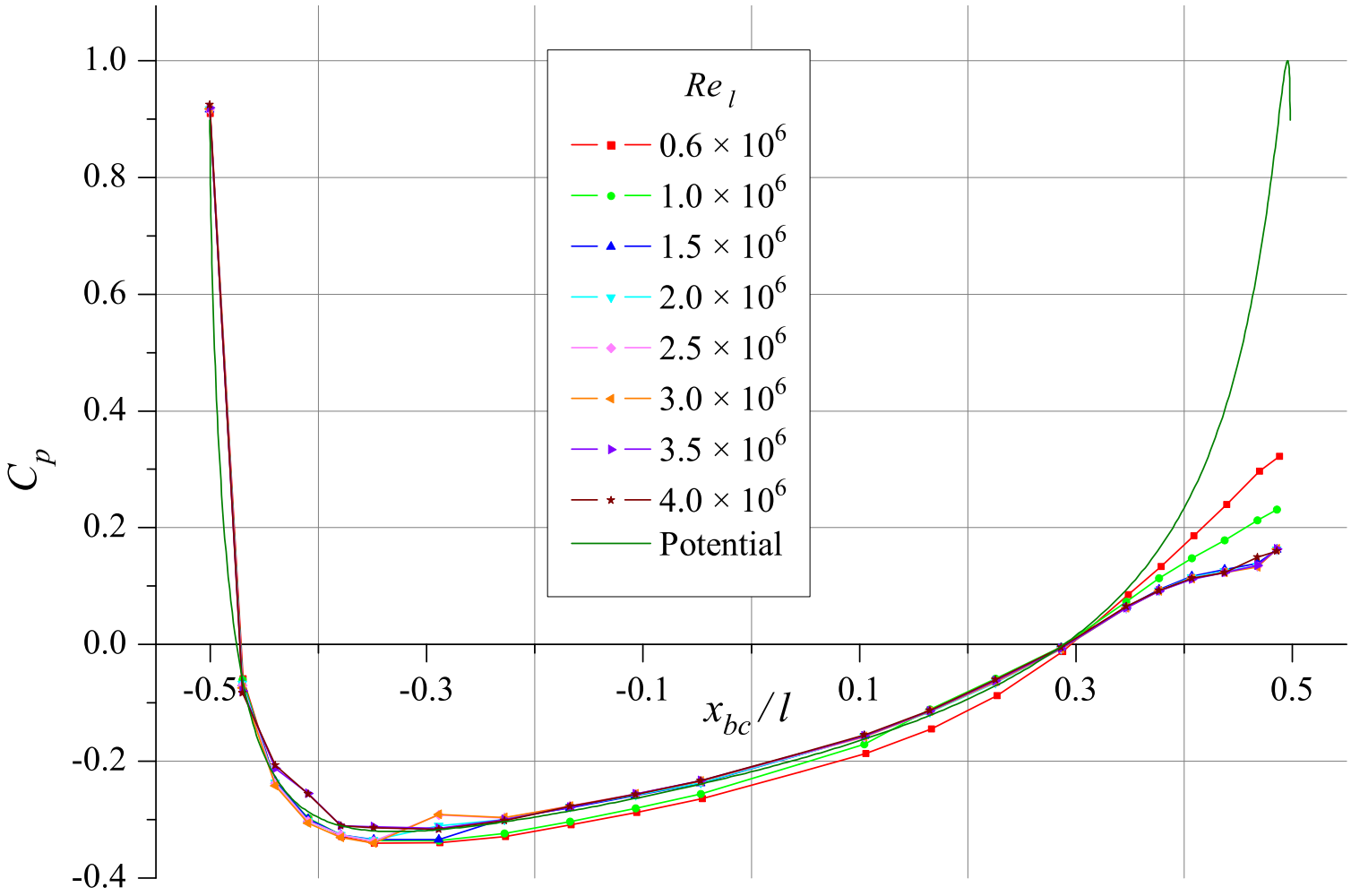

Figure C.39: Surface pressure distribution on spheroid at $\alpha = -10.2°$, $\varphi_e = -180°$, tripped at $x_{bc}/l = -0.3$

Appendix D

Ellipsoid Surface Pressure Measurements: Constant Azimuth Plots

D.1 Ellipsoid Surface Pressure at $\alpha = -0.2°$

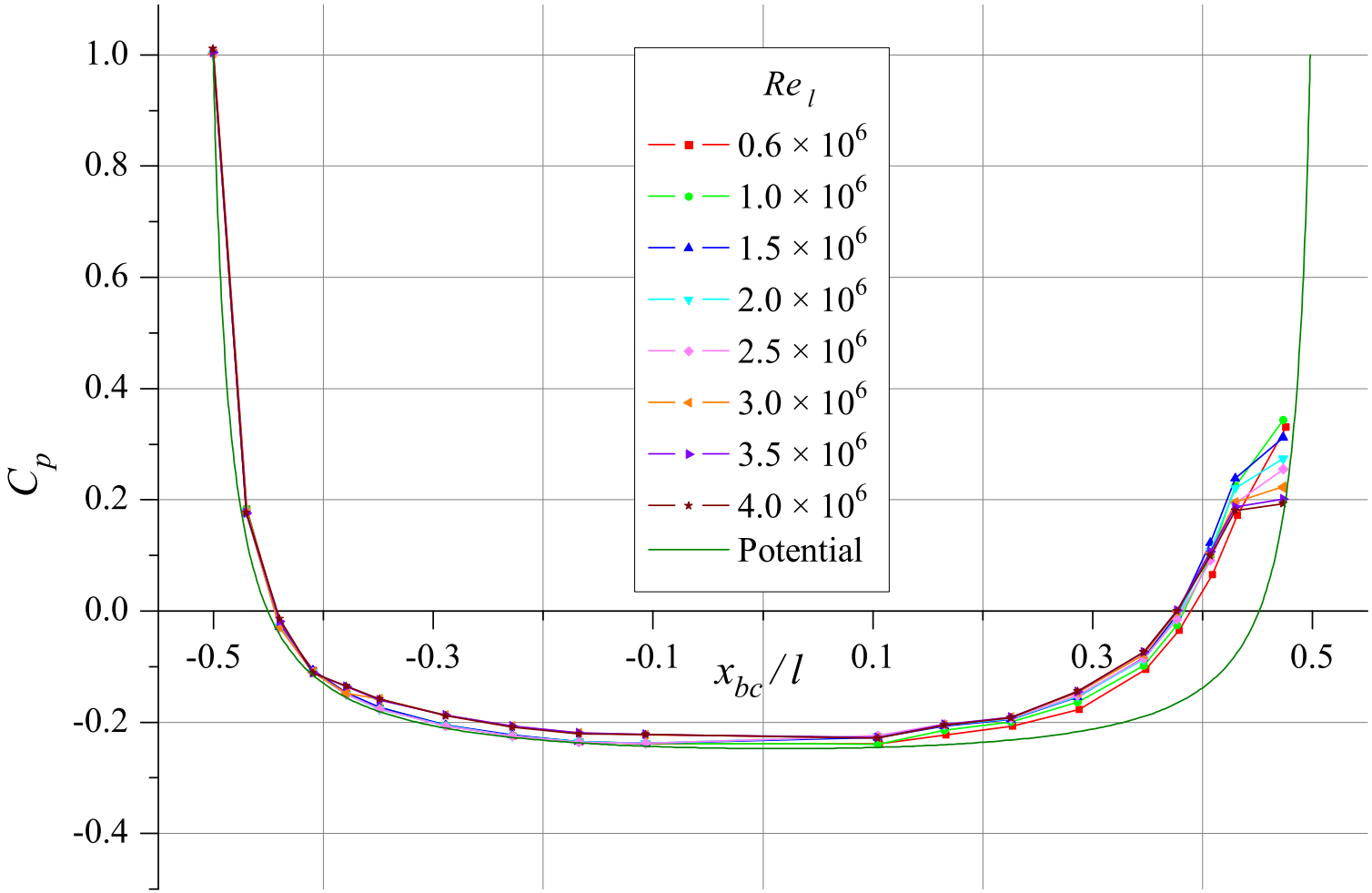

Figure D.1: Surface pressure distribution on ellipsoid at $\alpha = -0.2°$, $\varphi_e = 0°$

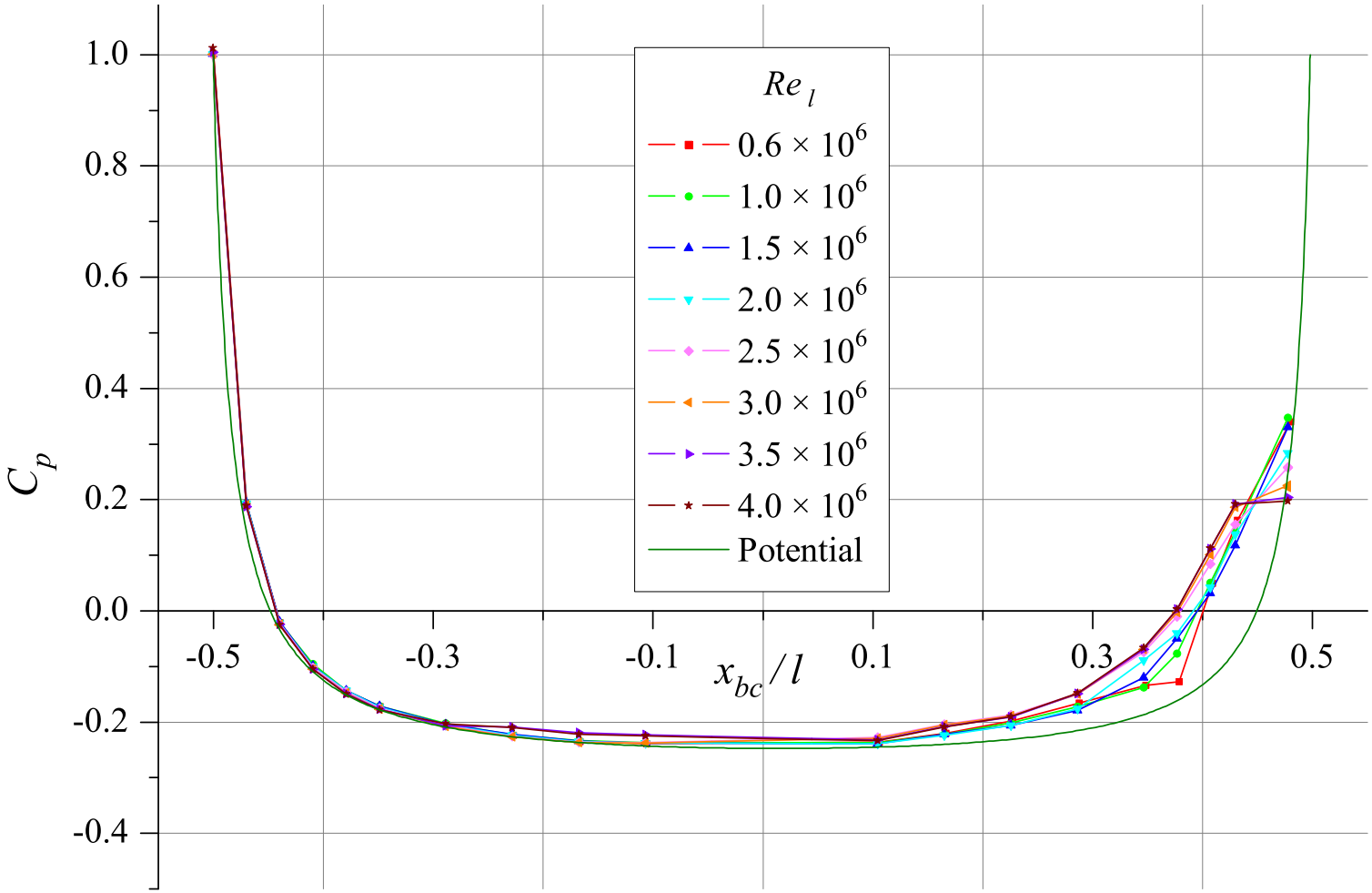

Figure D.2: Surface pressure distribution on ellipsoid at $\alpha = -0.2°$, $\varphi_e = -15°$

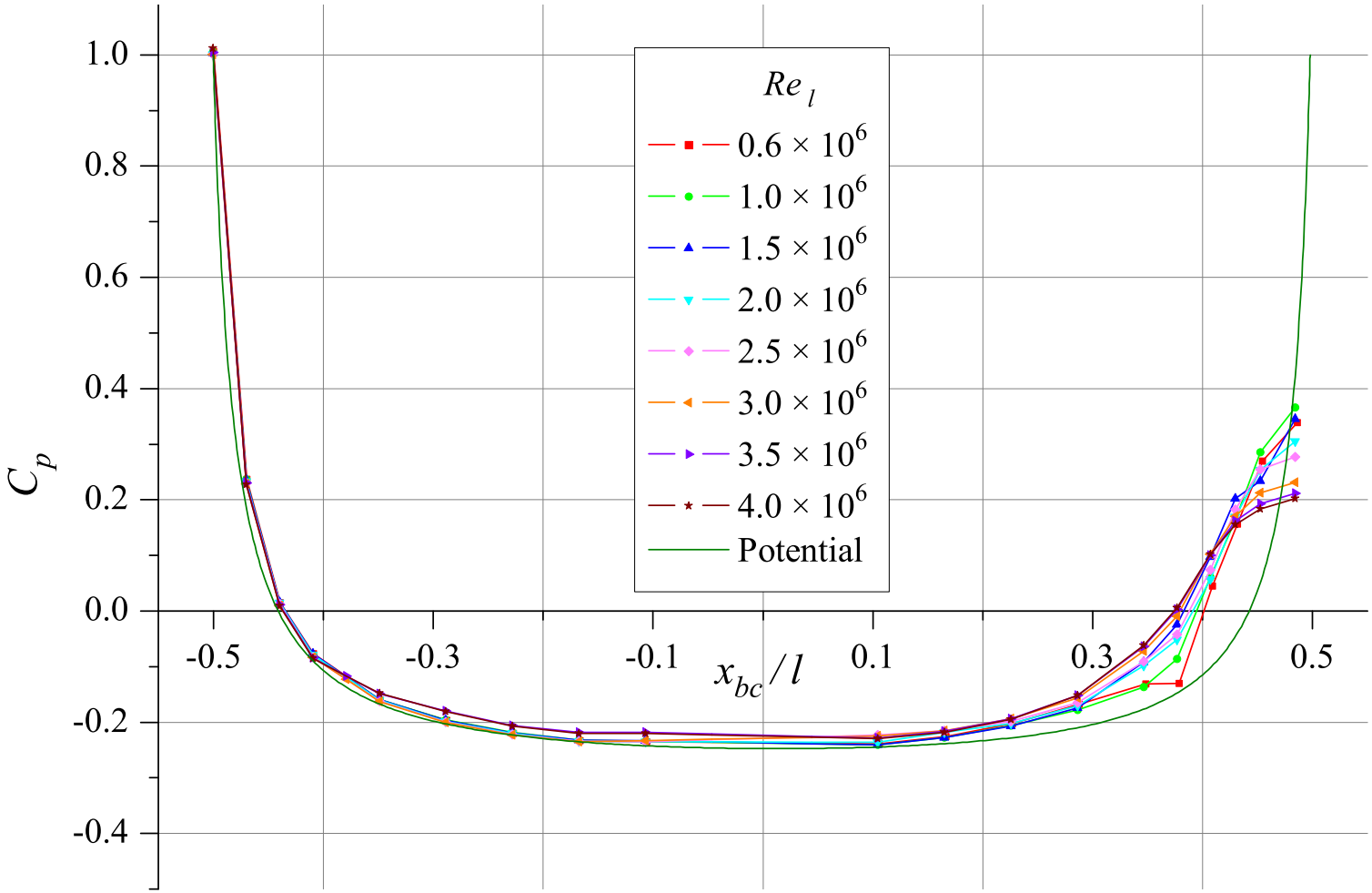

Figure D.3: Surface pressure distribution on ellipsoid at $\alpha = -0.2°$, $\varphi_e = -30°$

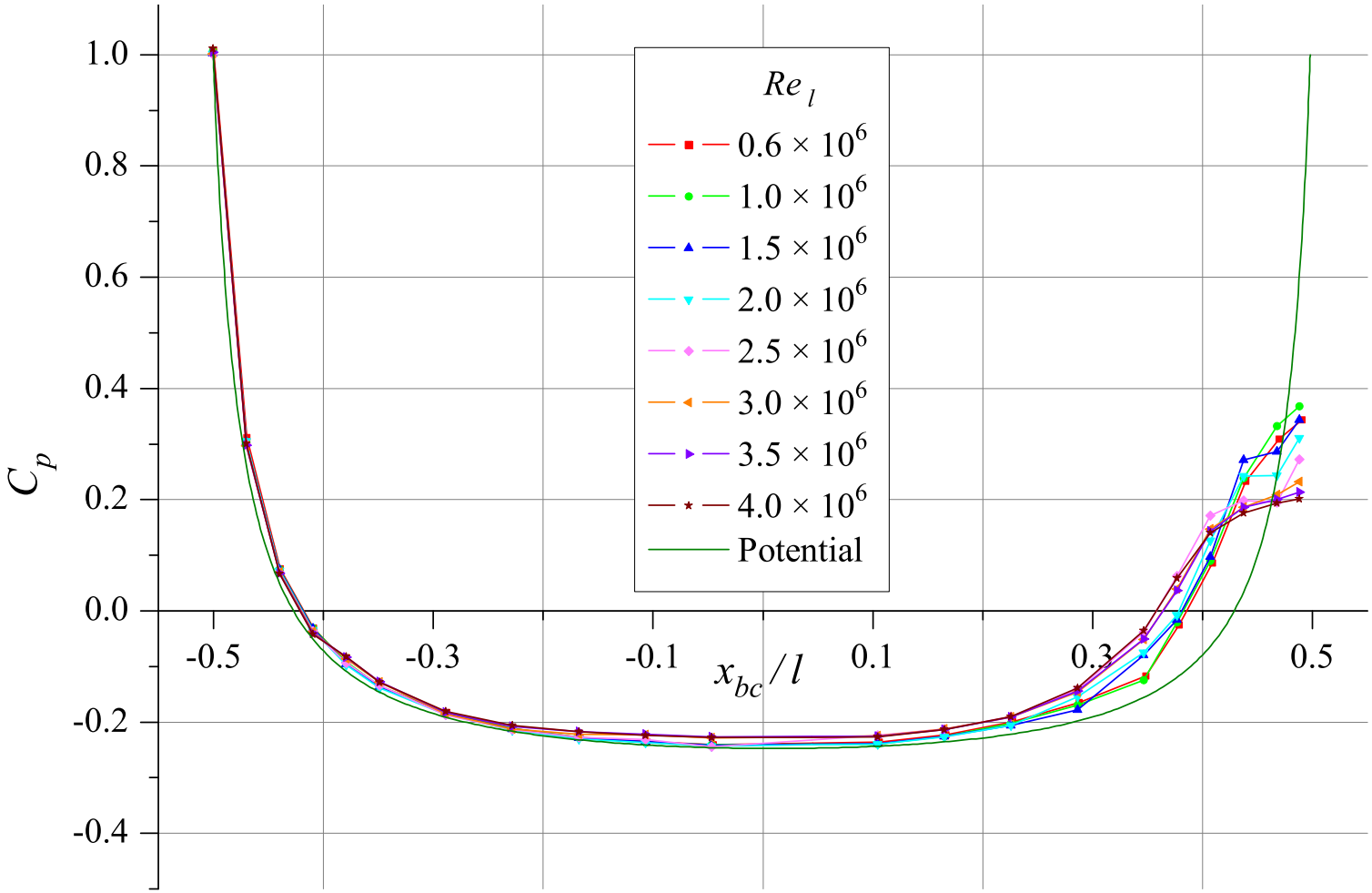

Figure D.4: Surface pressure distribution on ellipsoid at $\alpha = -0.2°$, $\varphi_e = -45°$

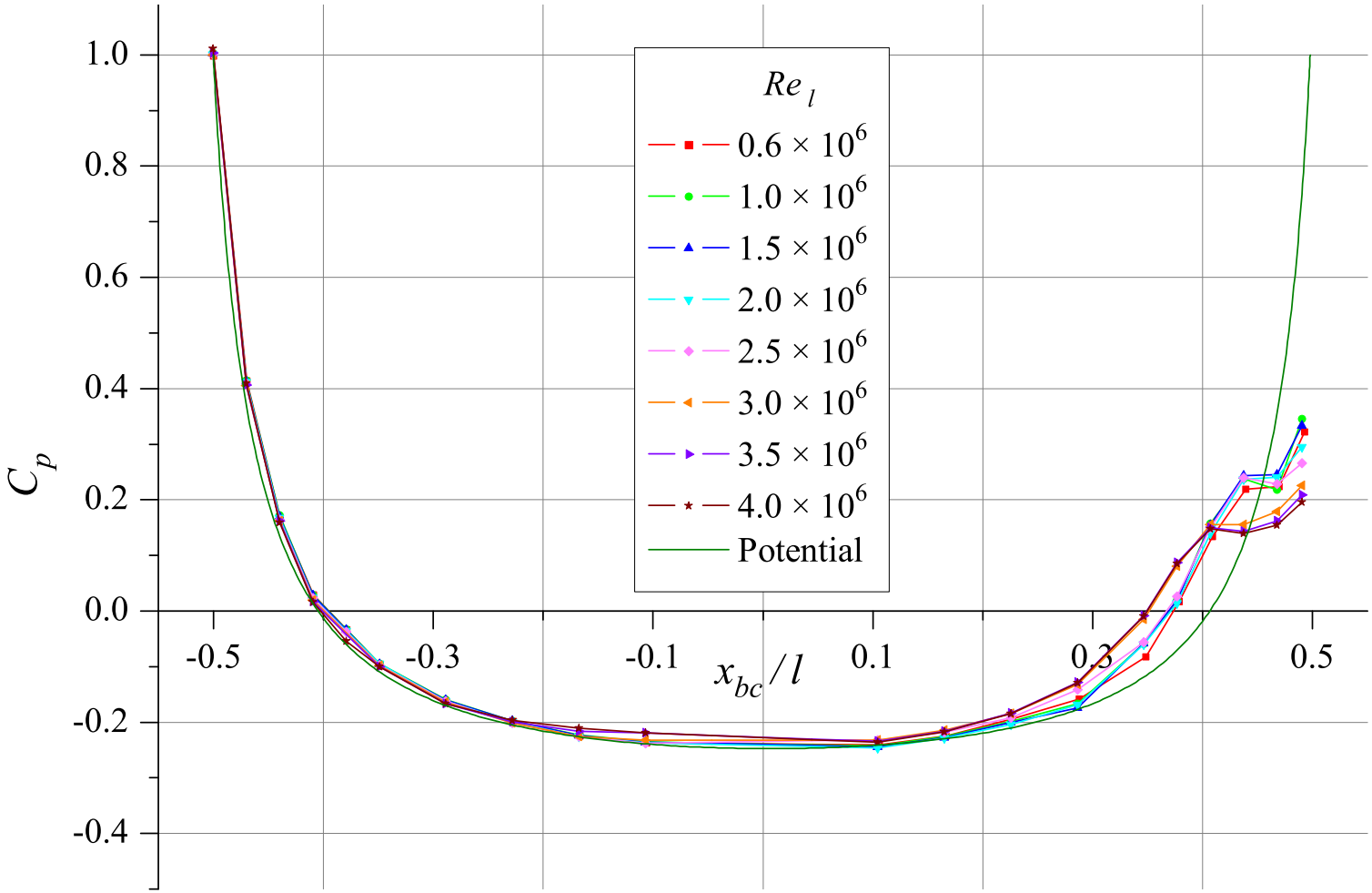

Figure D.5: Surface pressure distribution on ellipsoid at $\alpha = -0.2°$, $\varphi_e = -60°$

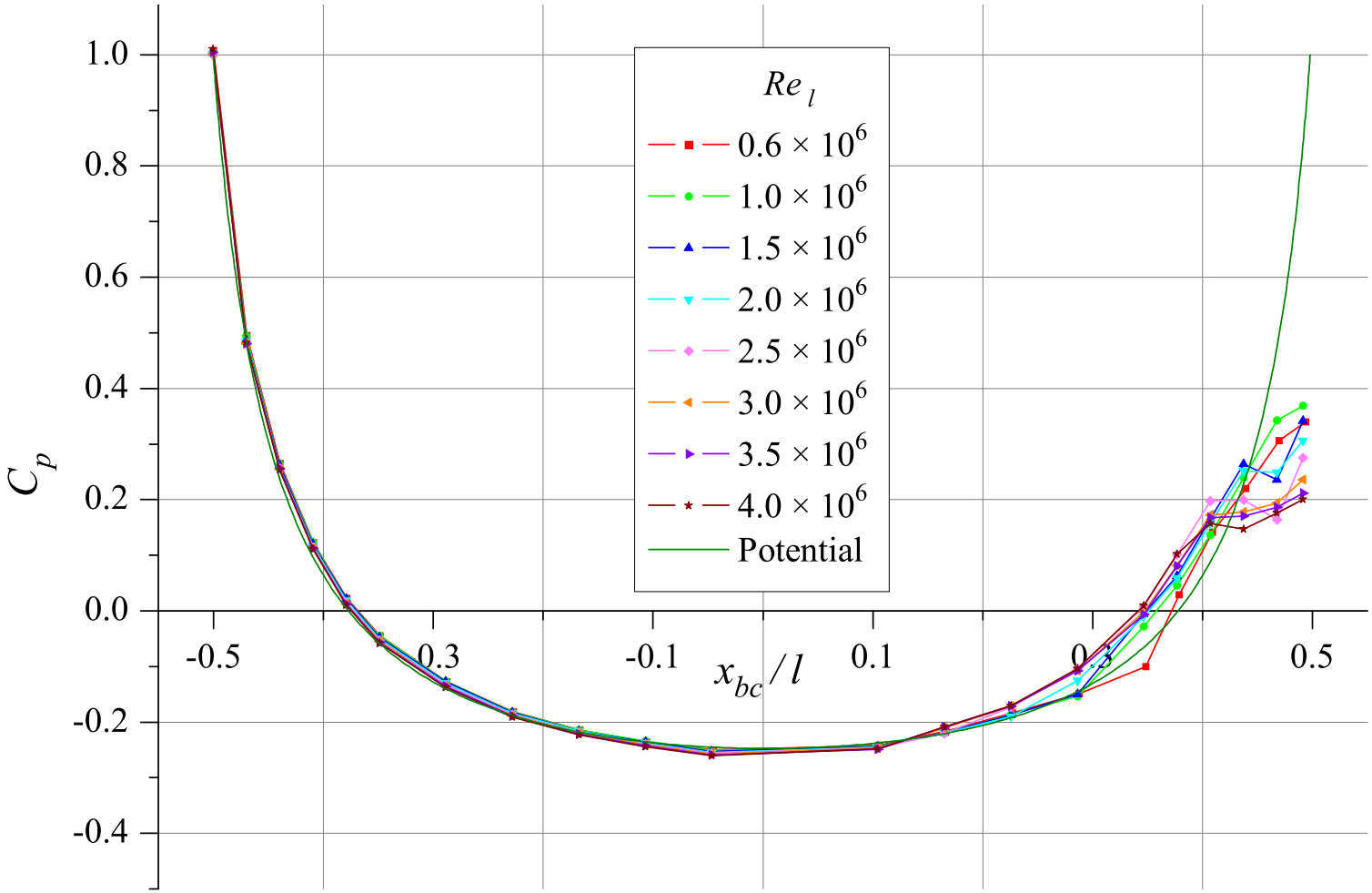

Figure D.6: Surface pressure distribution on ellipsoid at $\alpha = -0.2°$, $\varphi_e = -75°$

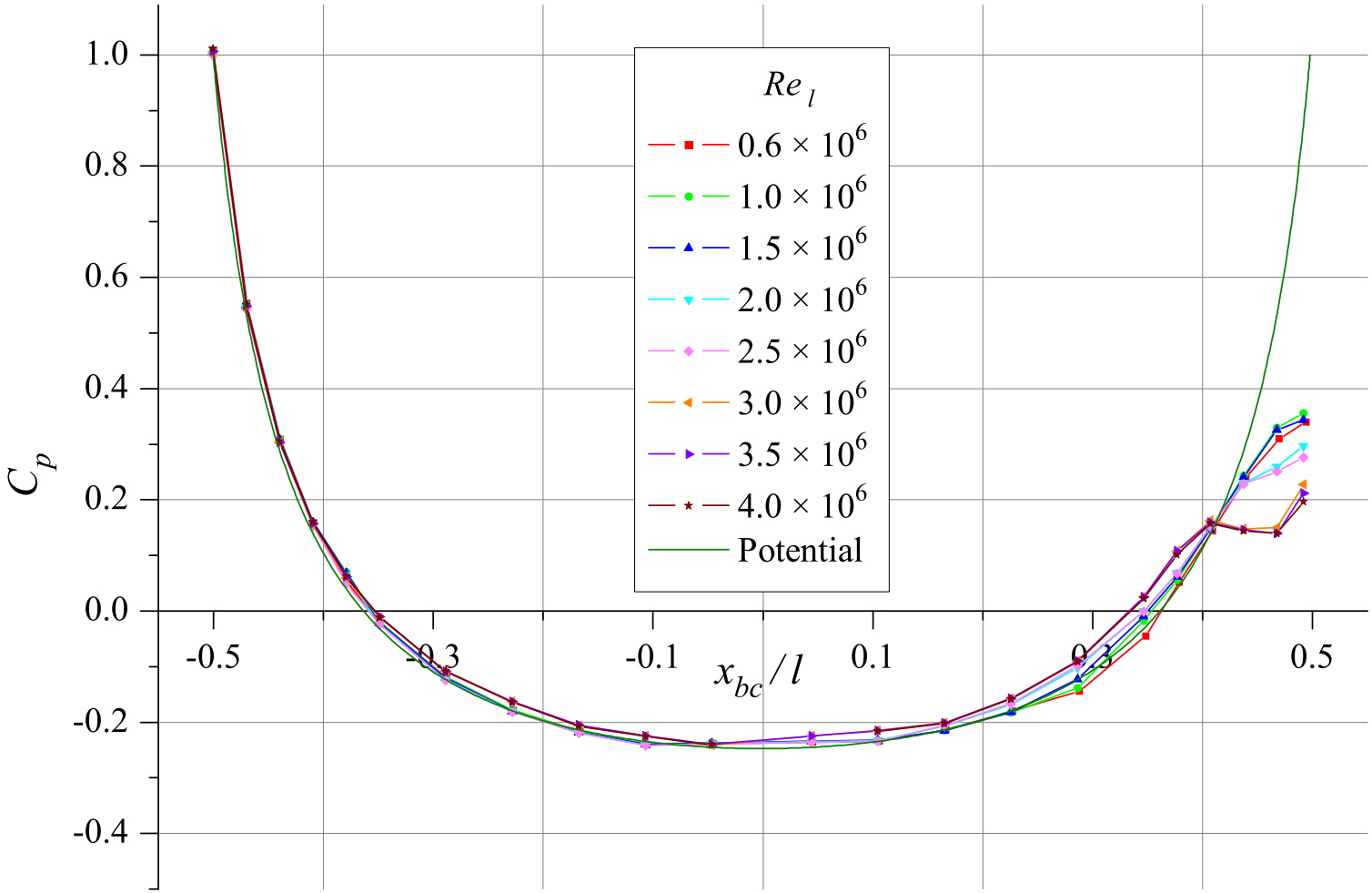

Figure D.7: Surface pressure distribution on ellipsoid at $\alpha = -0.2°$, $\varphi_e = -90°$

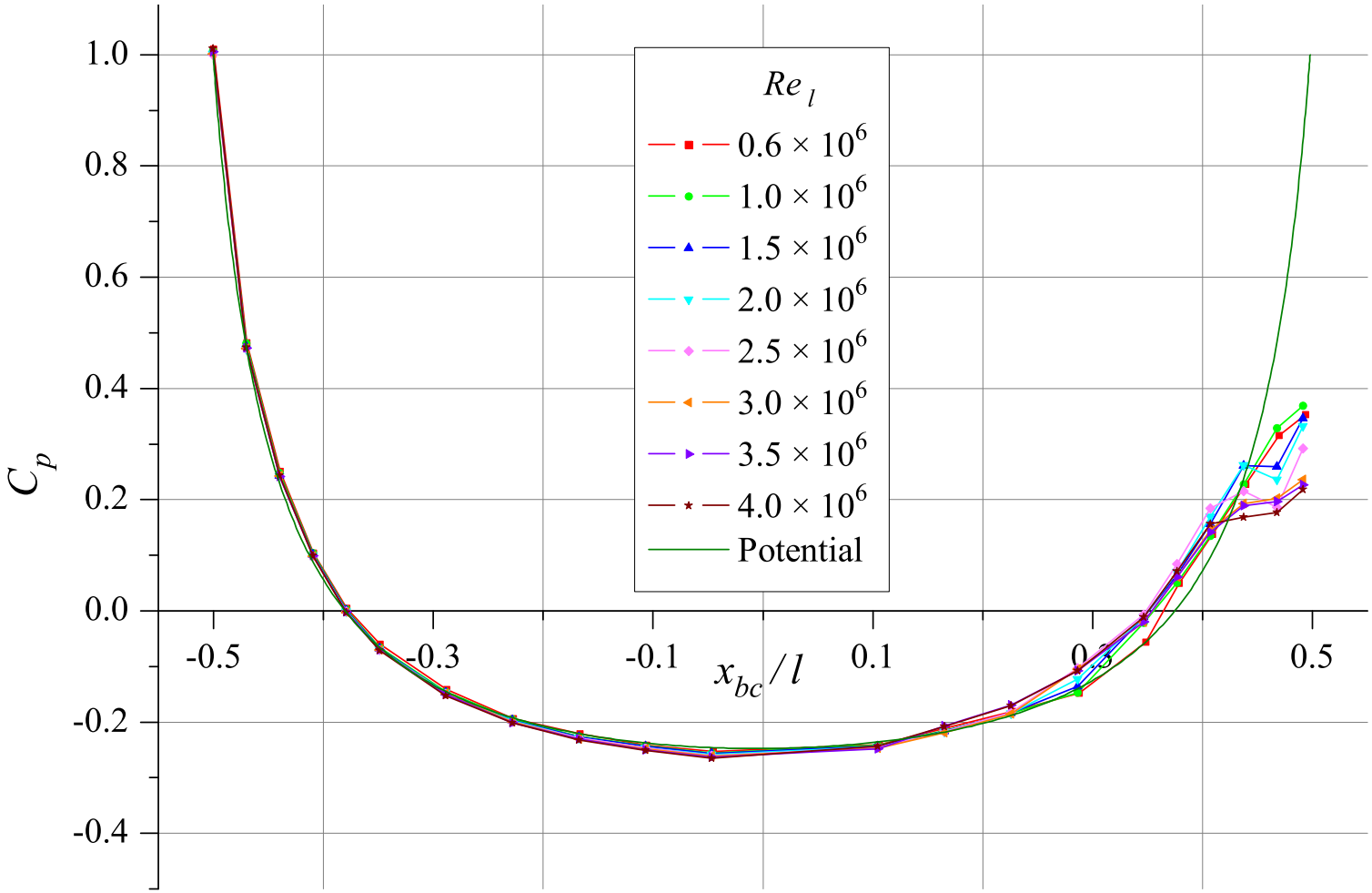

Figure D.8: Surface pressure distribution on ellipsoid at $\alpha = -0.2°$, $\varphi_e = -105°$

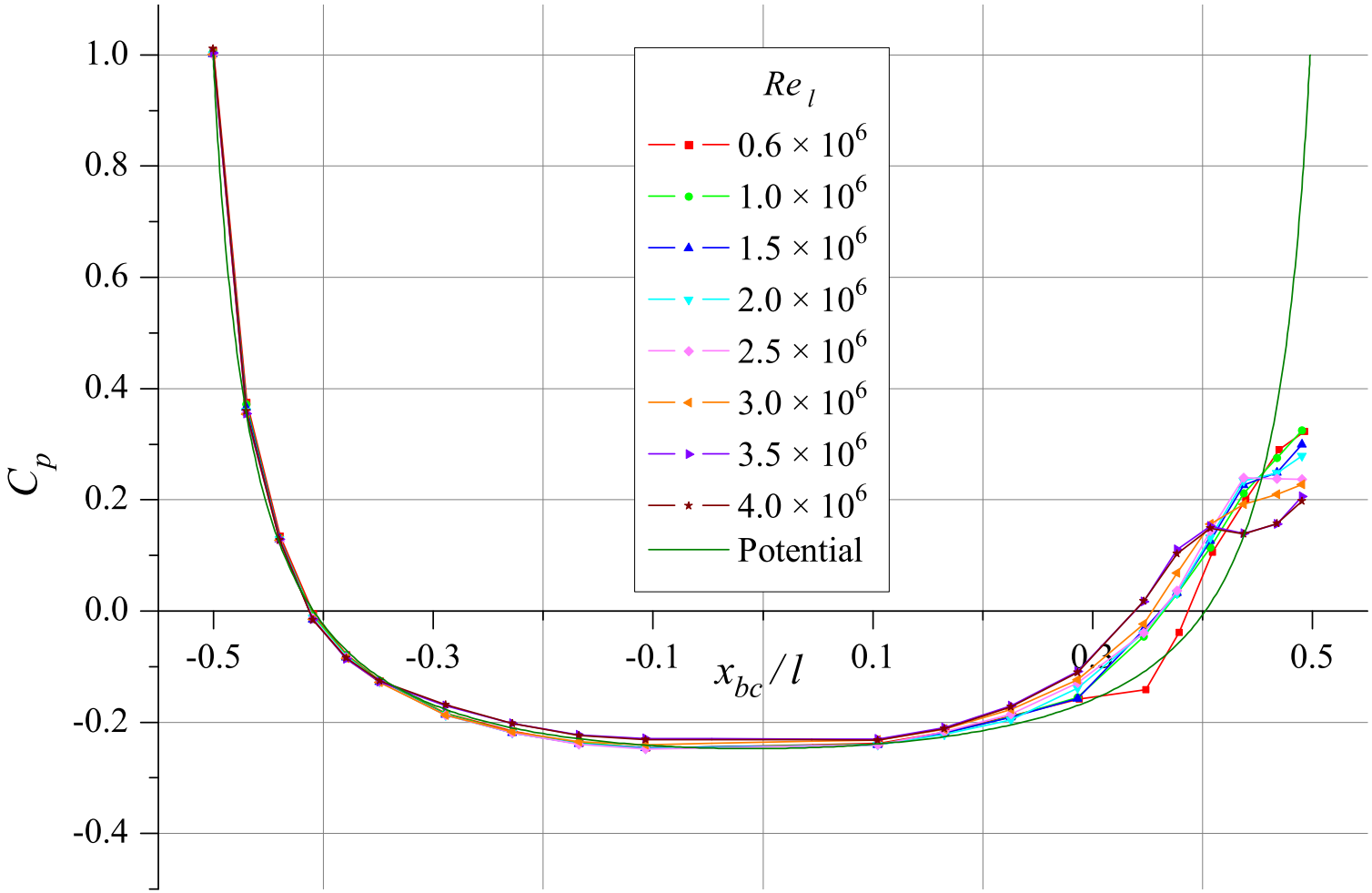

Figure D.9: Surface pressure distribution on ellipsoid at $\alpha = -0.2°$, $\varphi_e = -120°$

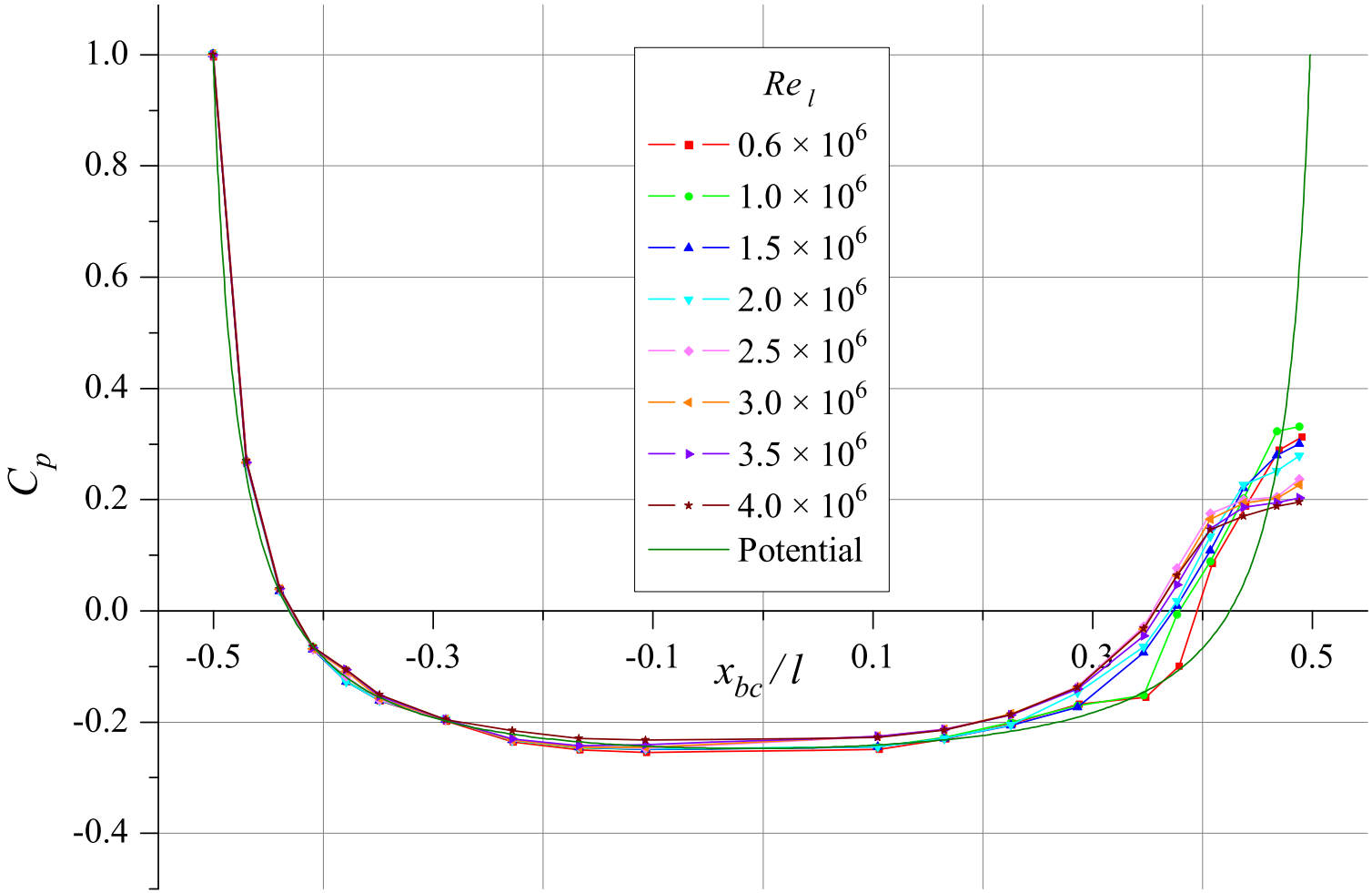

Figure D.10: Surface pressure distribution on ellipsoid at $\alpha = -0.2°$, $\varphi_e = -135°$

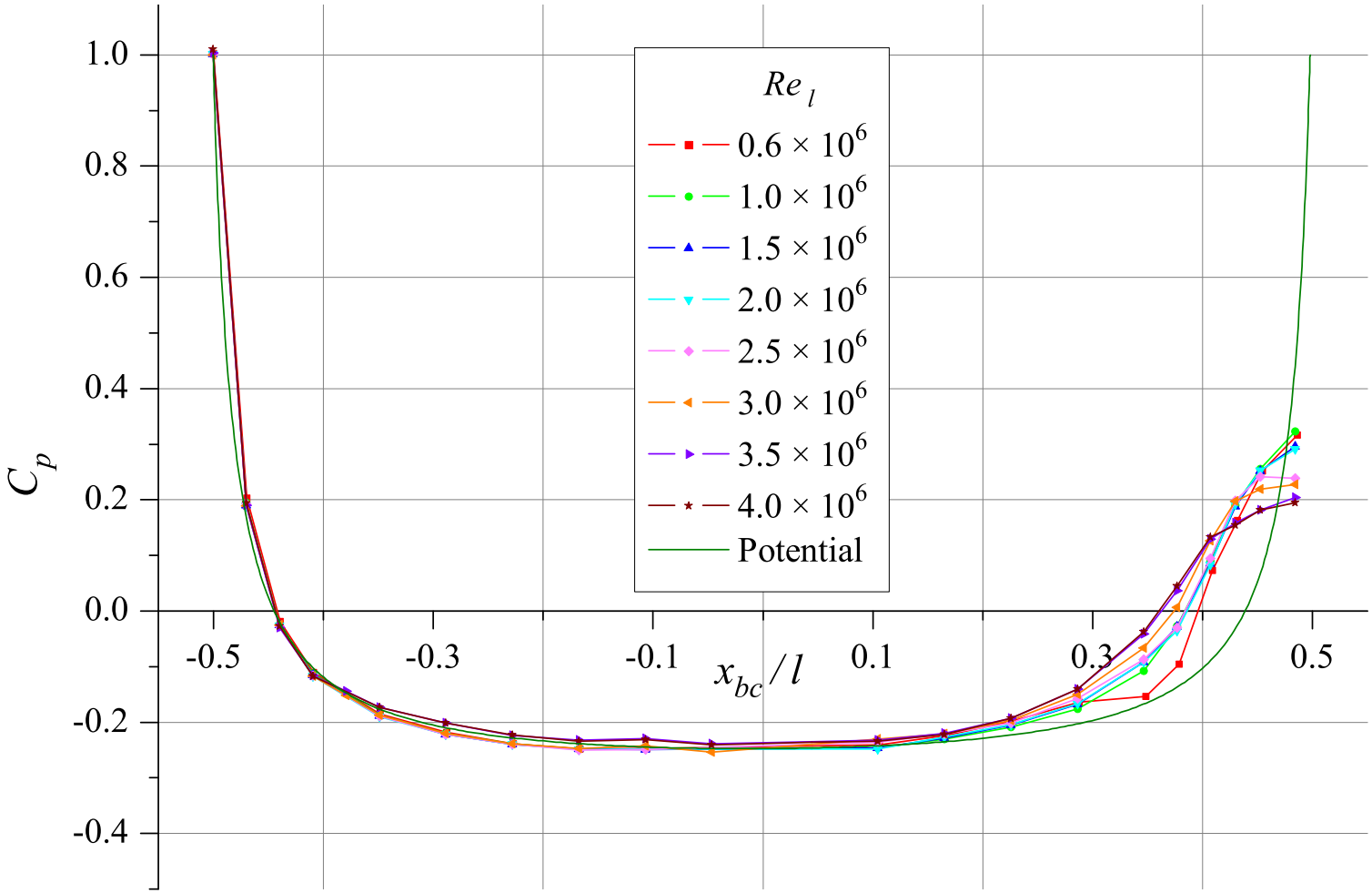

Figure D.11: Surface pressure distribution on ellipsoid at $\alpha = -0.2°$, $\varphi_e = -150°$

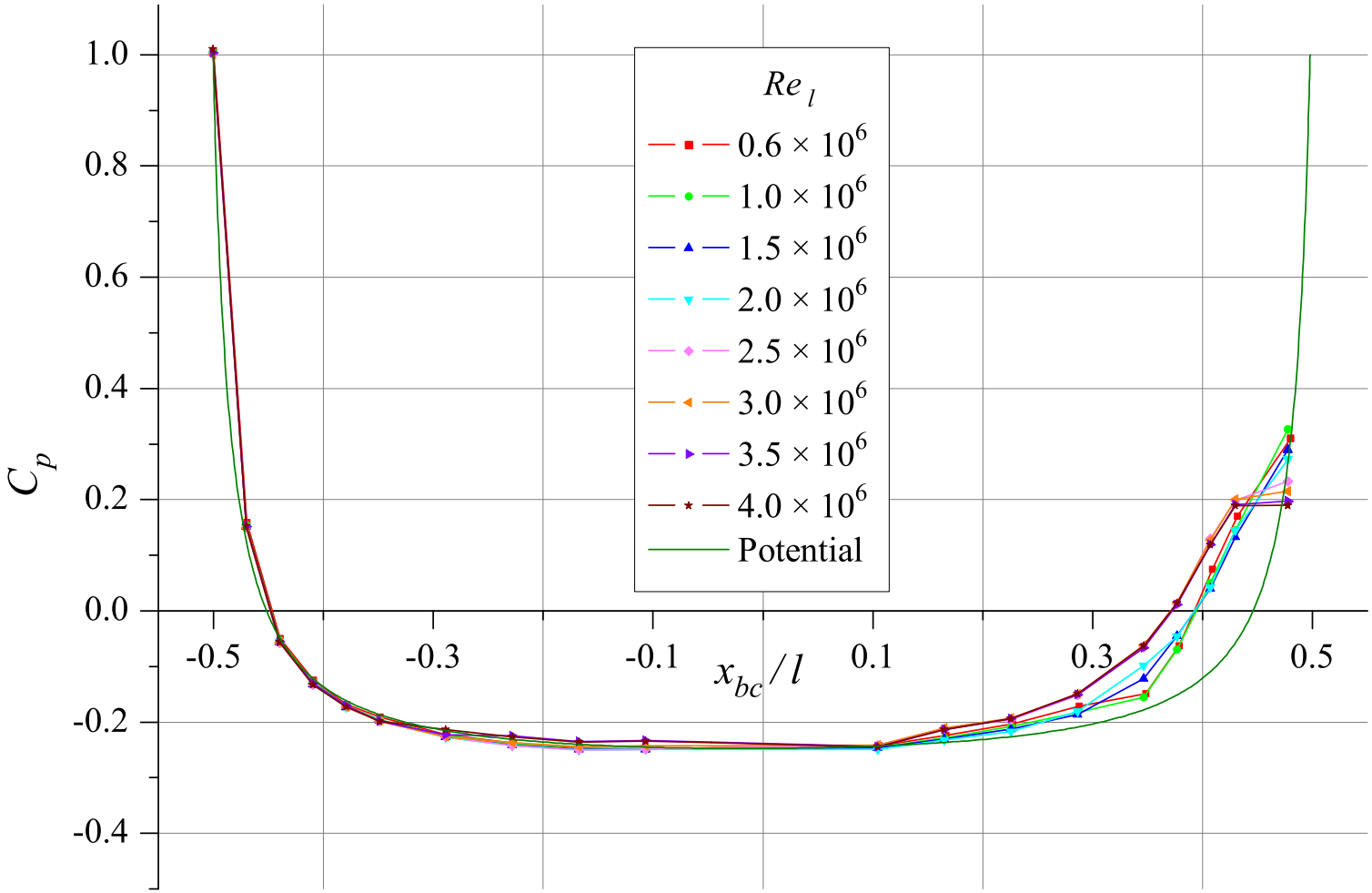

Figure D.12: Surface pressure distribution on ellipsoid at $\alpha = -0.2°$, $\varphi_e = -165°$

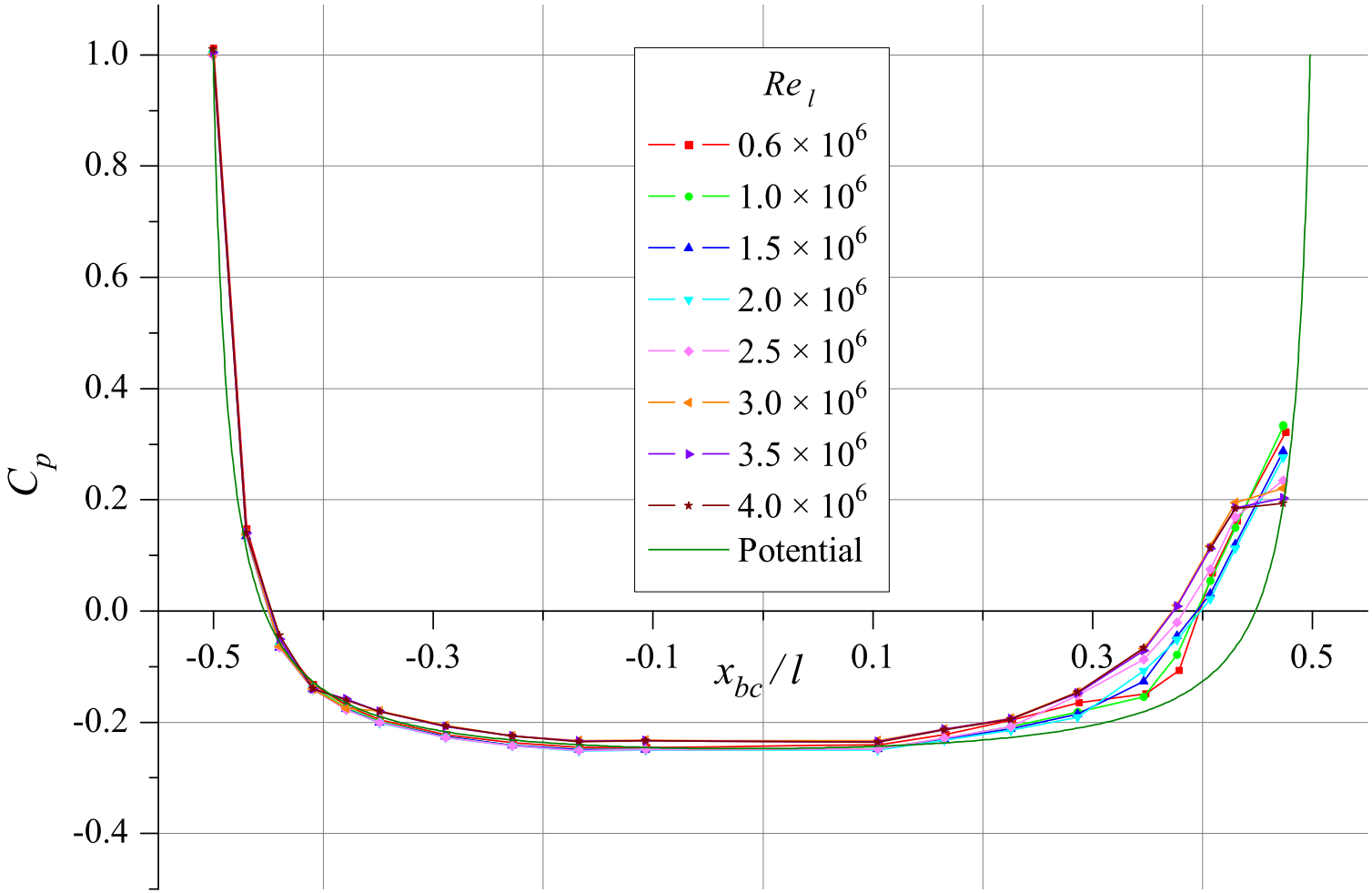

Figure D.13: Surface pressure distribution on ellipsoid at $\alpha = -0.2°$, $\varphi_e = -180°$

D.2 Ellipsoid Surface Pressure at $\alpha = -6.2°$

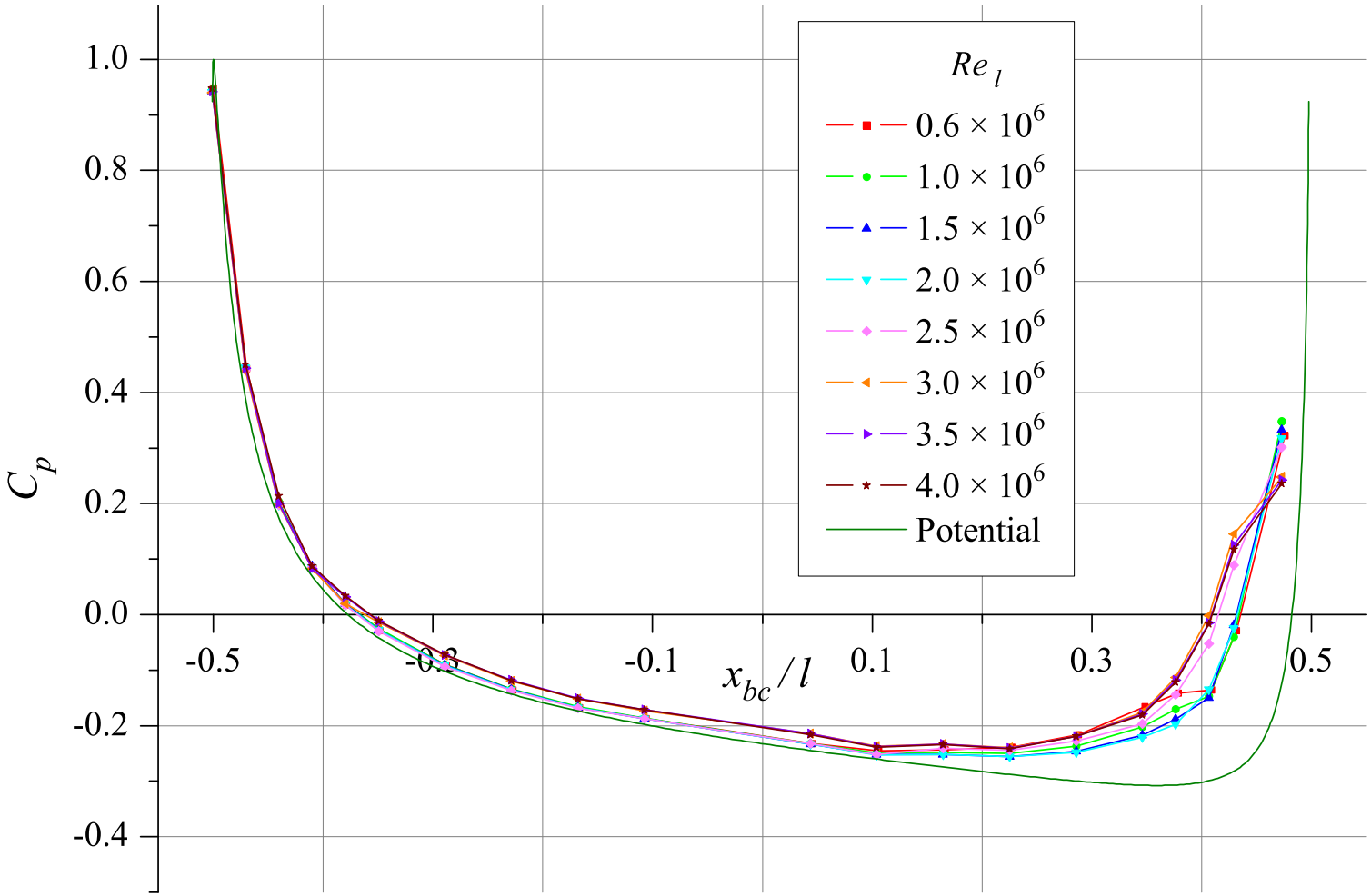

Figure D.14: Surface pressure distribution on ellipsoid at $\alpha = -6.2°$, $\varphi_e = 0°$

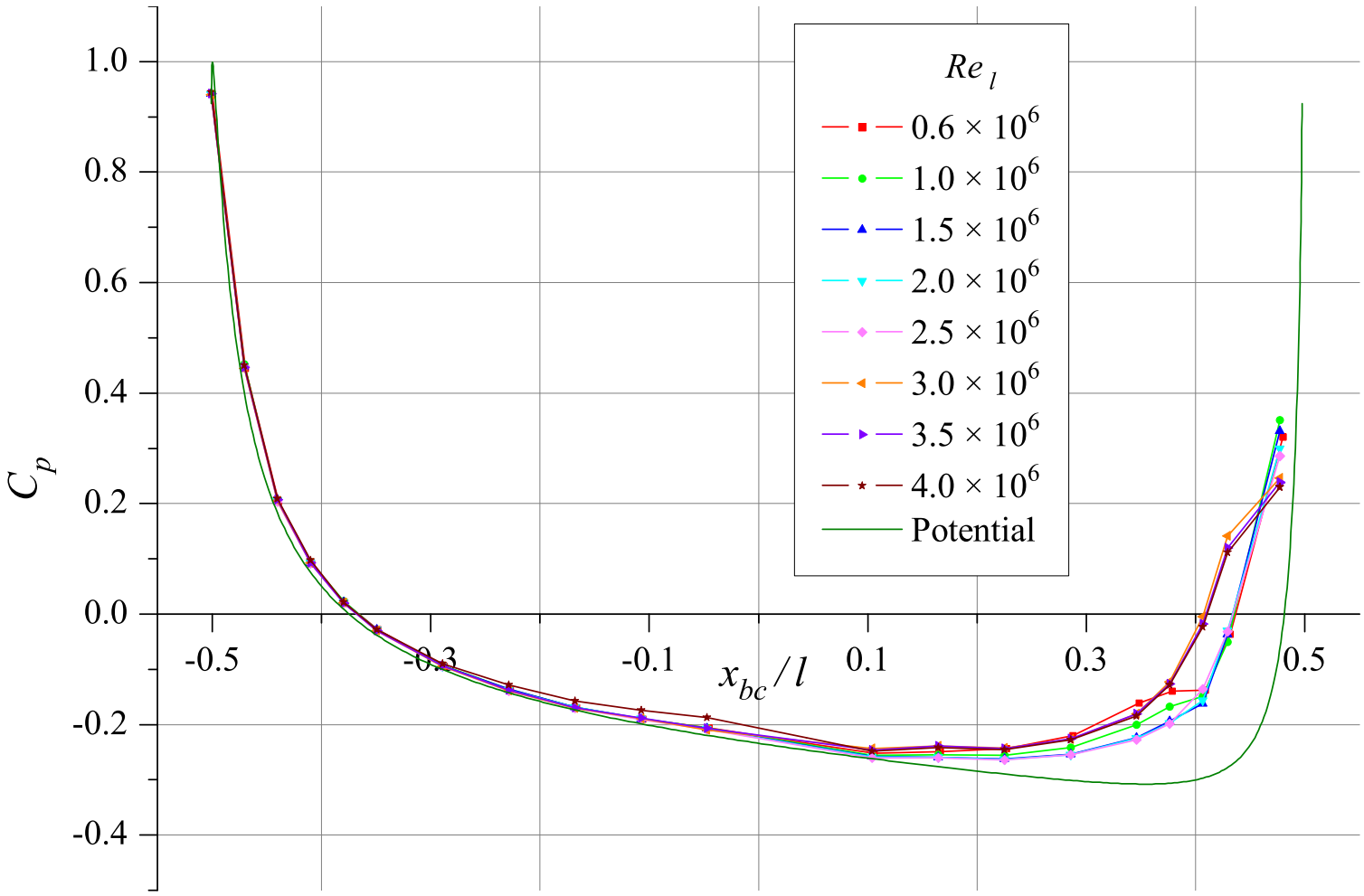

Figure D.15: Surface pressure distribution on ellipsoid at $\alpha = -6.2°$, $\varphi_e = -15°$

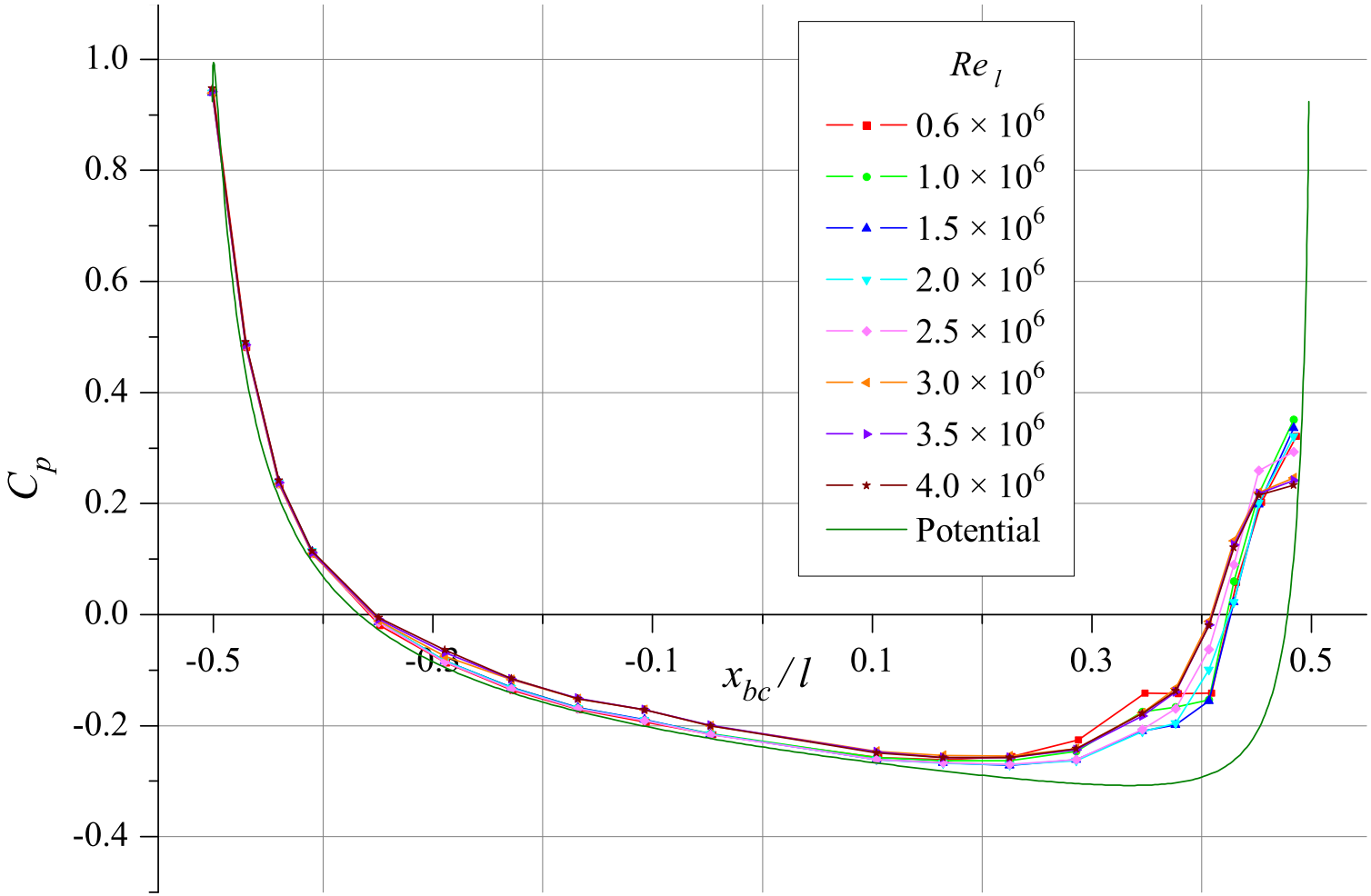

Figure D.16: Surface pressure distribution on ellipsoid at $\alpha = -6.2°$, $\varphi_e = -30°$

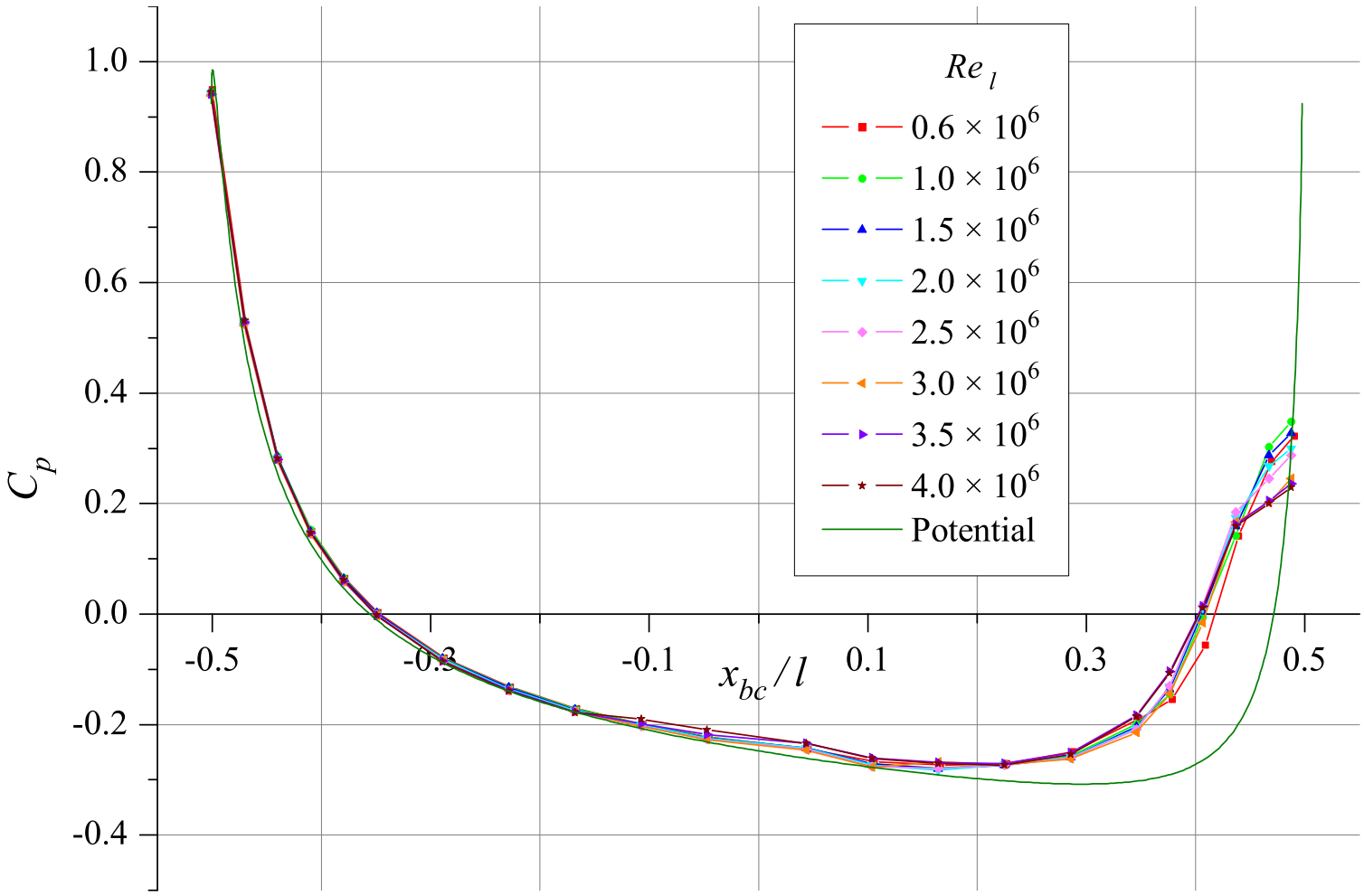

Figure D.17: Surface pressure distribution on ellipsoid at $\alpha = -6.2°$, $\varphi_e = -45°$

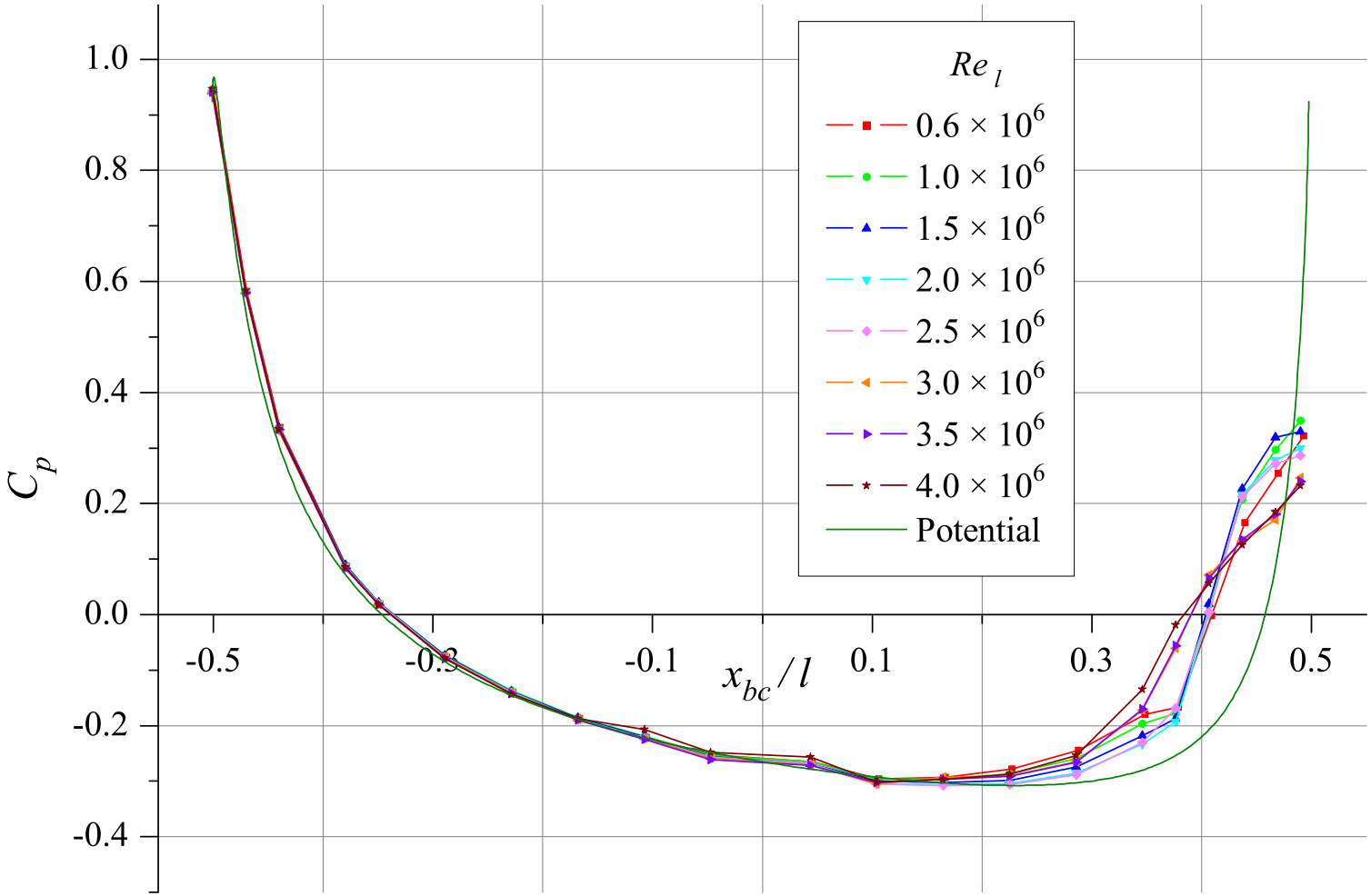

Figure D.18: Surface pressure distribution on ellipsoid at $\alpha = -6.2°$, $\varphi_e = -60°$

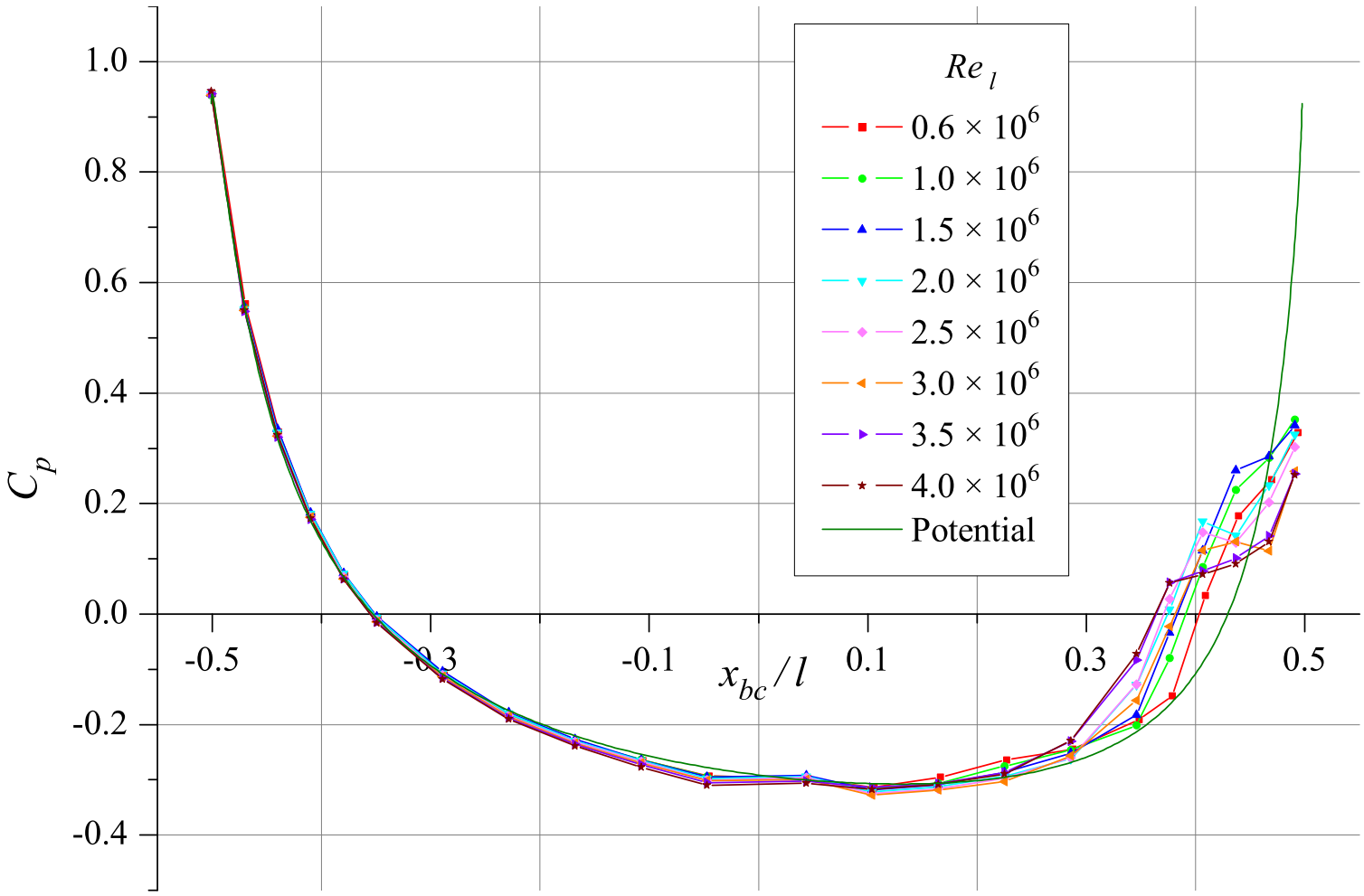

Figure D.19: Surface pressure distribution on ellipsoid at $\alpha = -6.2°$, $\varphi_e = -75°$

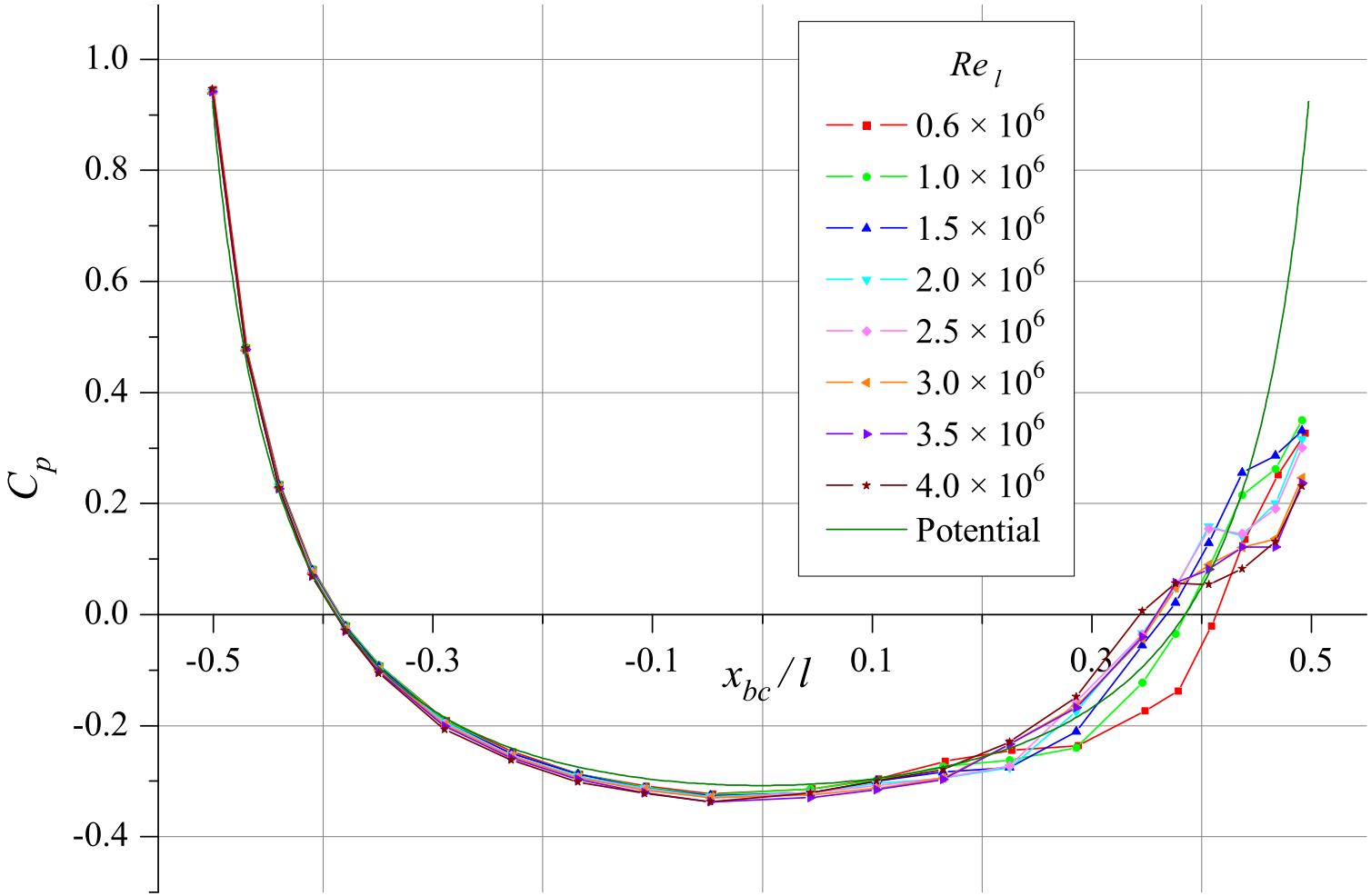

Figure D.20: Surface pressure distribution on ellipsoid at $\alpha = -6.2°$, $\varphi_e = -90°$

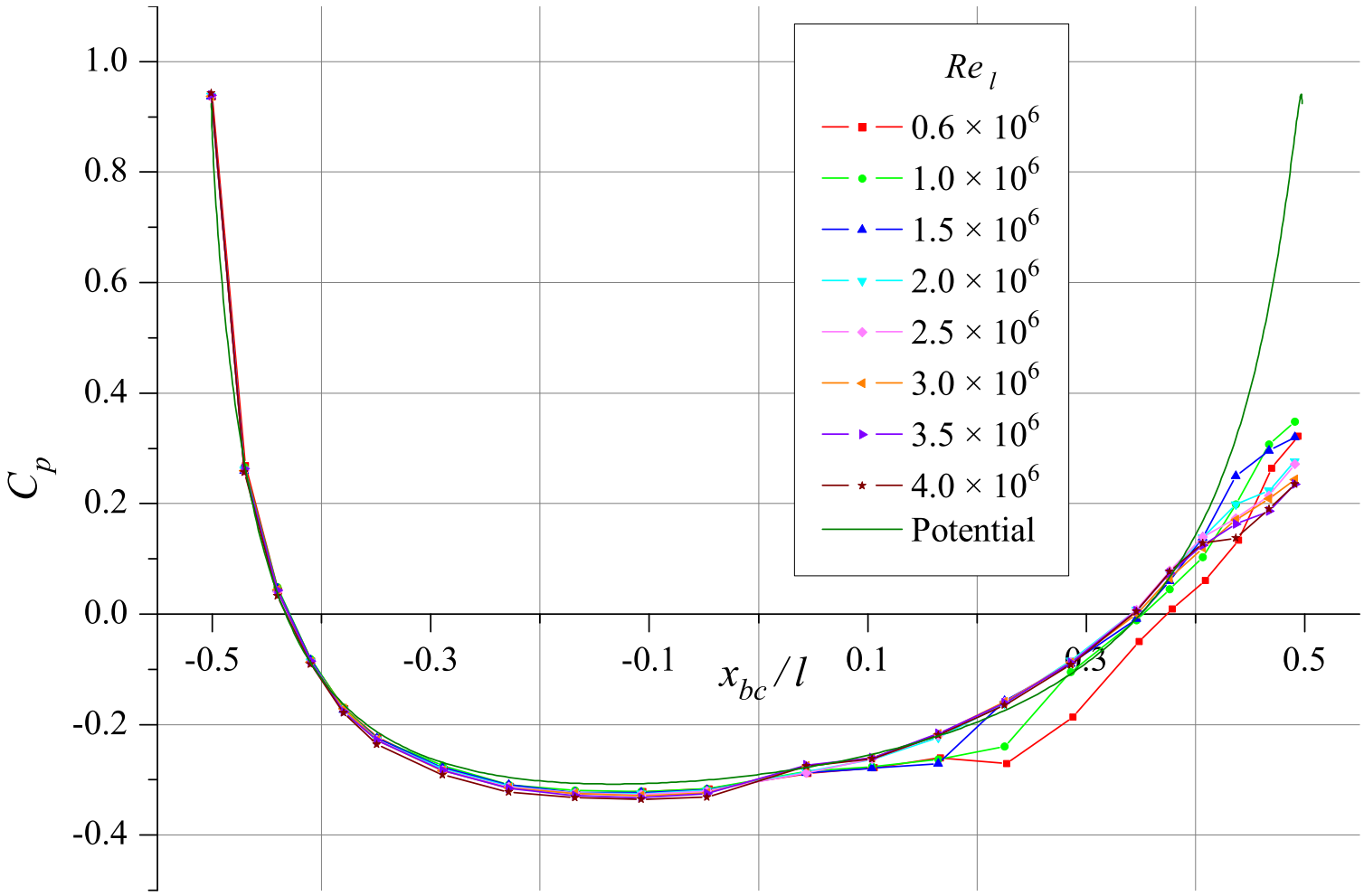

Figure D.21: Surface pressure distribution on ellipsoid at $\alpha = -6.2°$, $\varphi_e = -105°$

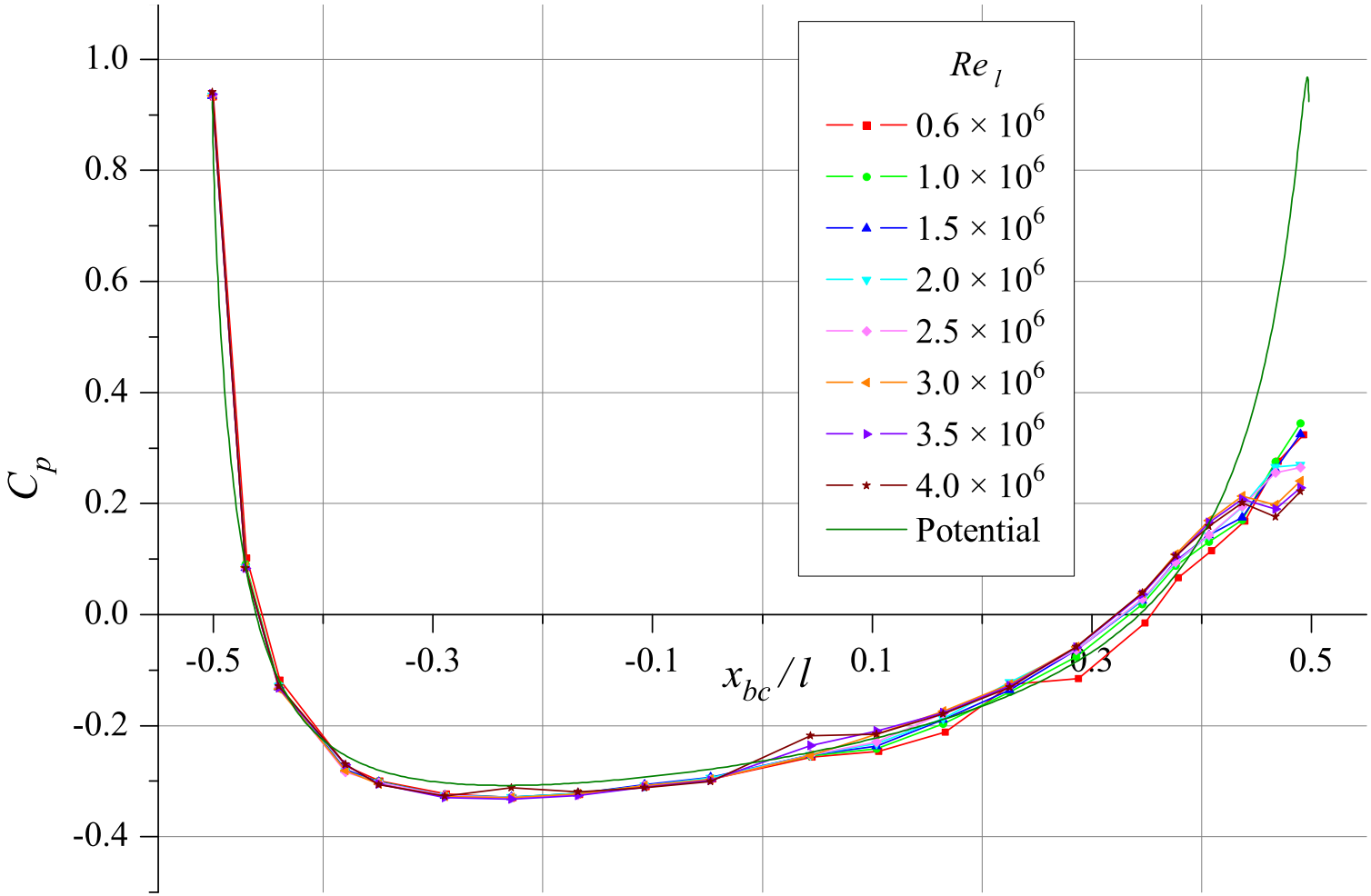

Figure D.22: Surface pressure distribution on ellipsoid at $\alpha = -6.2°$, $\varphi_e = -120°$

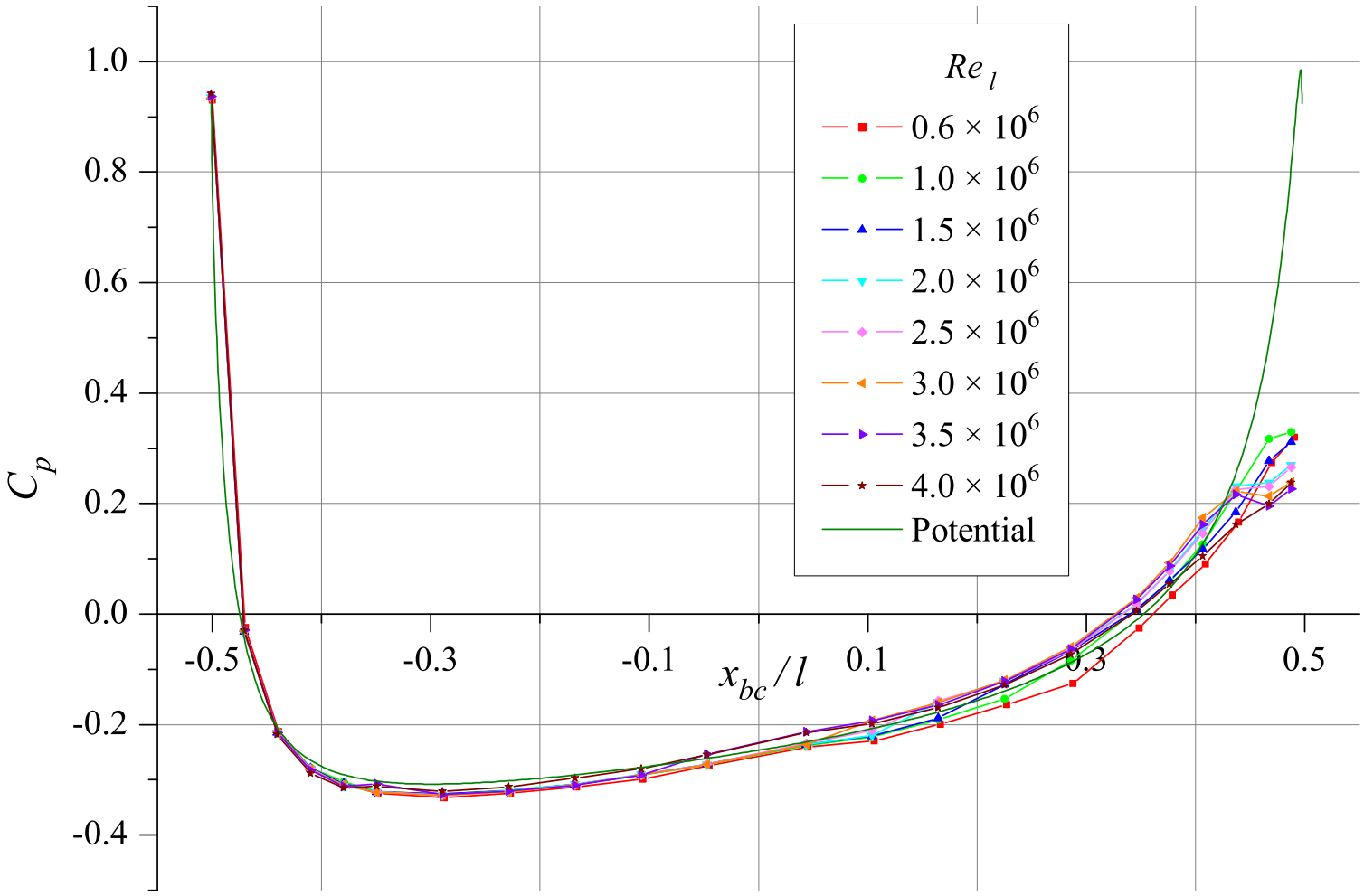

Figure D.23: Surface pressure distribution on ellipsoid at $\alpha = -6.2°$, $\varphi_e = -135°$

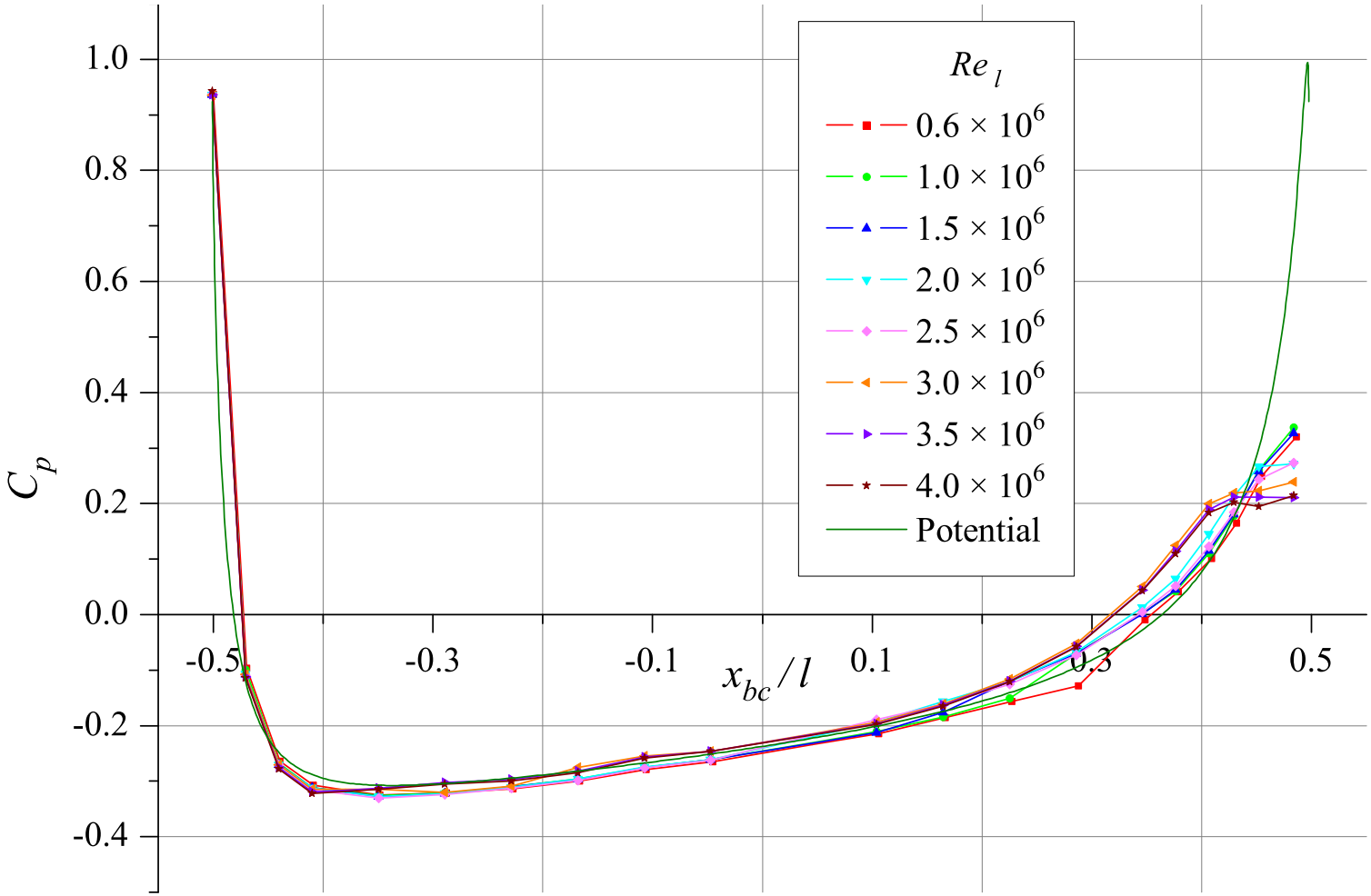

Figure D.24: Surface pressure distribution on ellipsoid at $\alpha = -6.2°$, $\varphi_e = -150°$

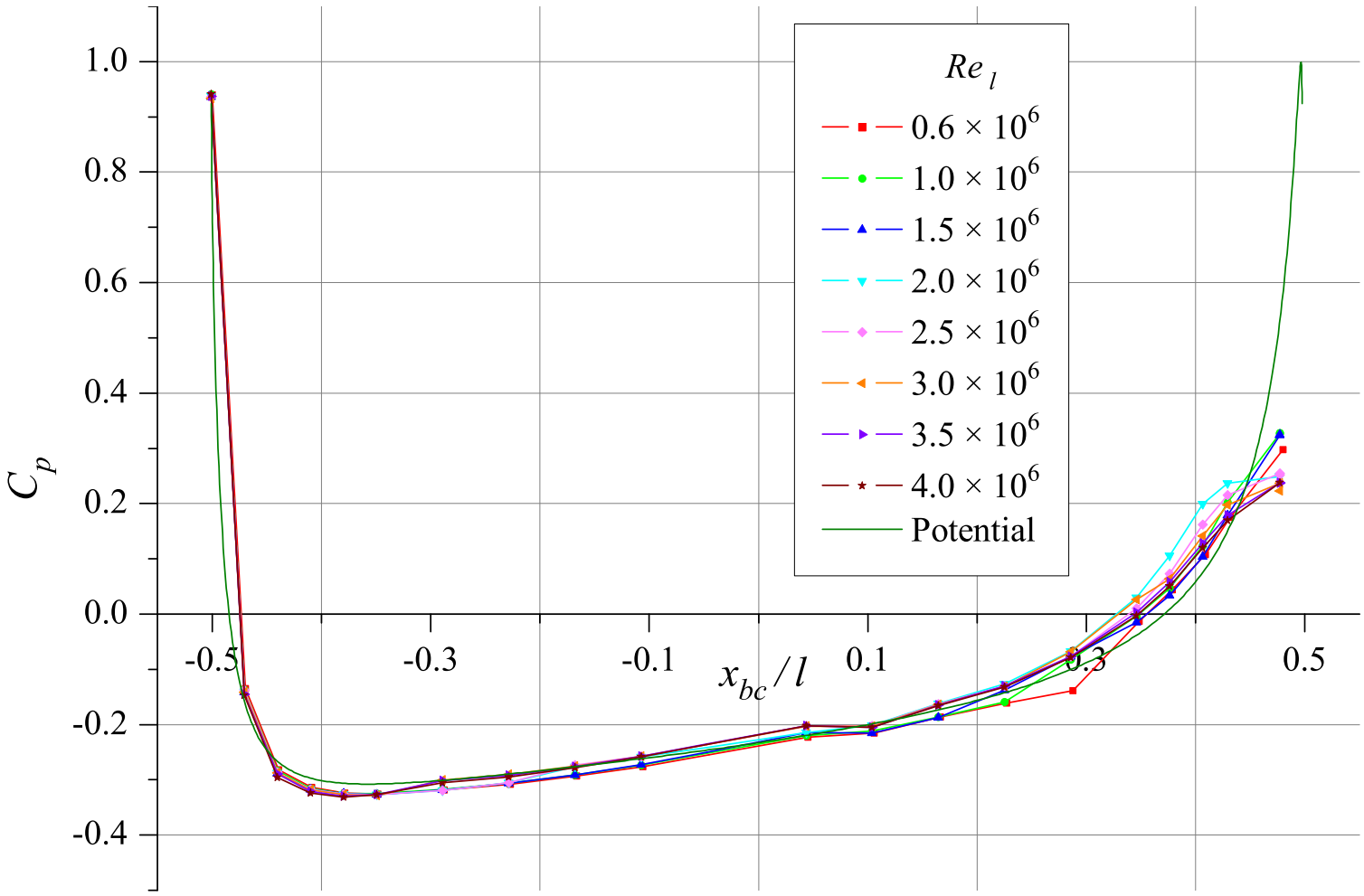

Figure D.25: Surface pressure distribution on ellipsoid at $\alpha = -6.2°$, $\varphi_e = -165°$

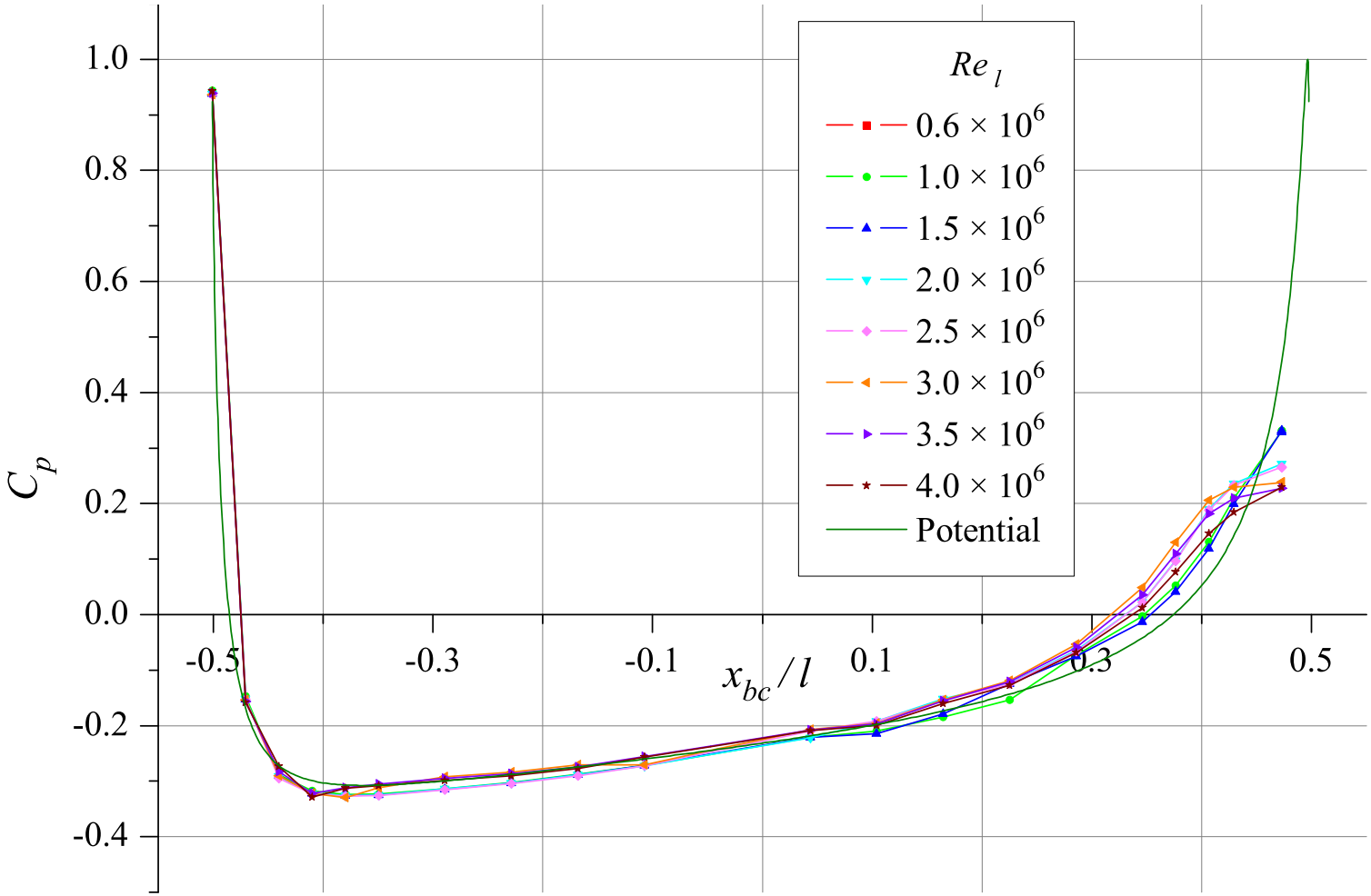

Figure D.26: Surface pressure distribution on ellipsoid at $\alpha = -6.2°$, $\varphi_e = -180°$

D.3 Ellipsoid Surface Pressure at $\alpha = -10.2°$

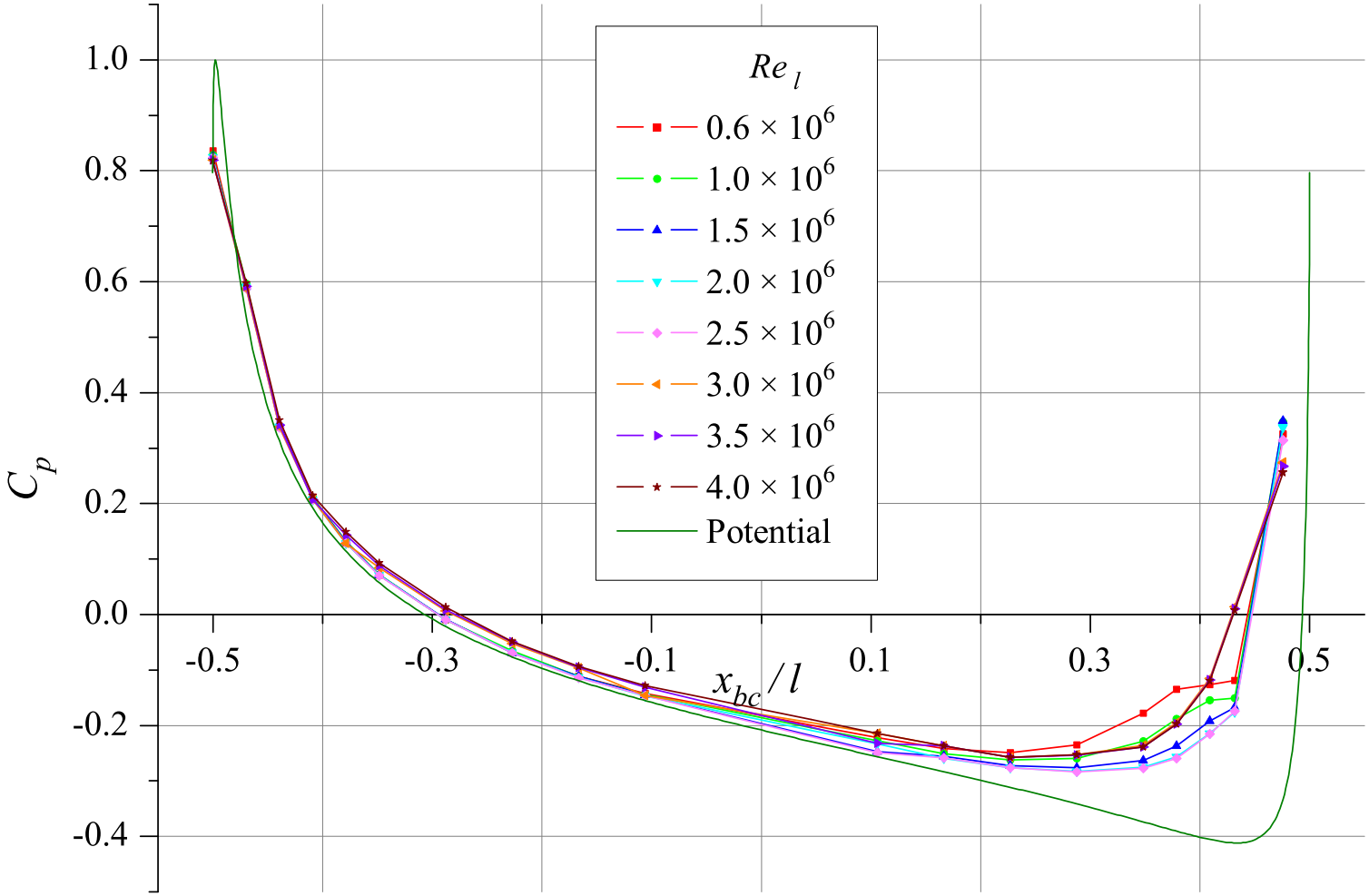

Figure D.27: Surface pressure distribution on ellipsoid at $\alpha = -10.2°$, $\varphi_e = 0°$

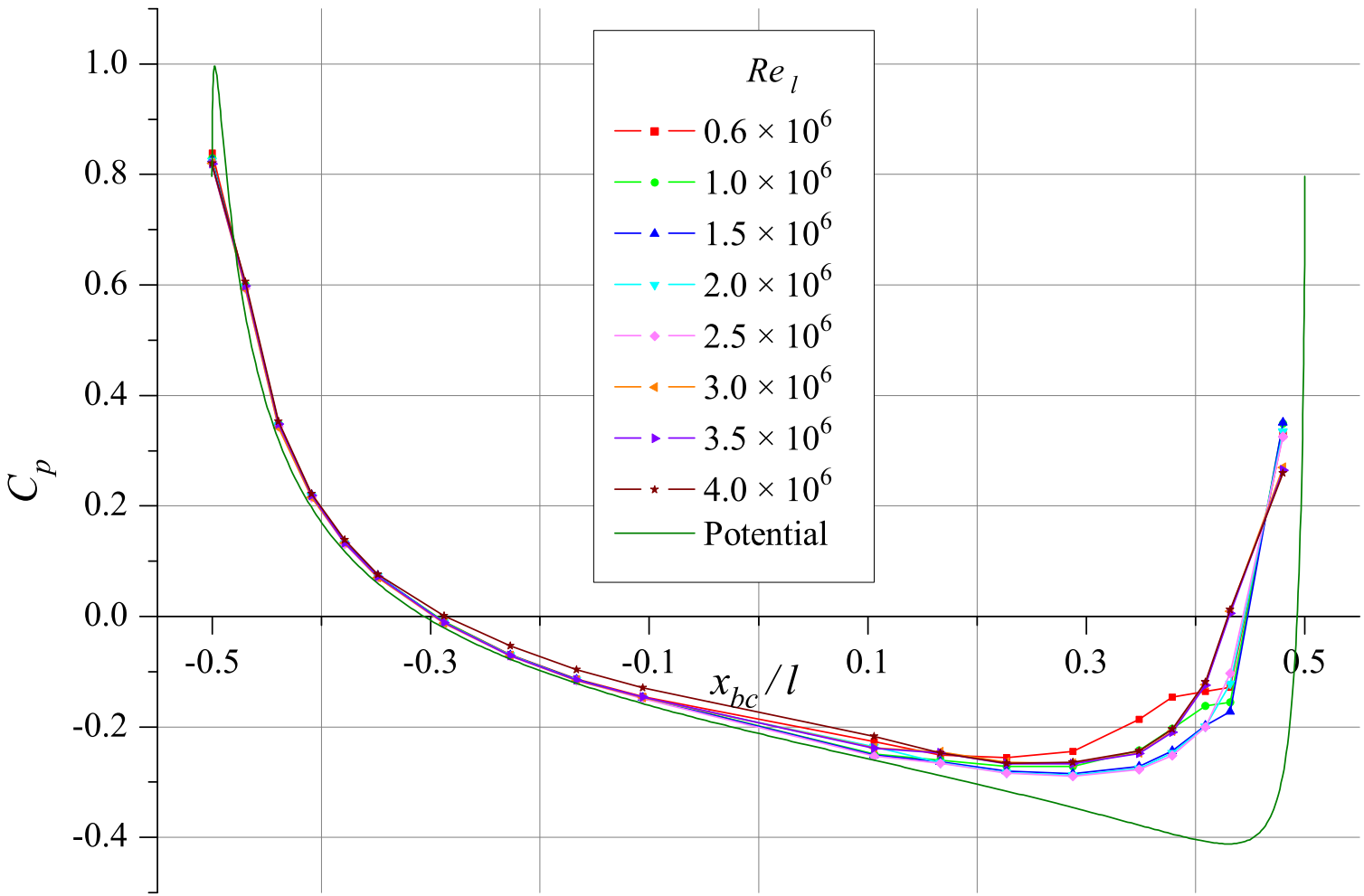

Figure D.28: Surface pressure distribution on ellipsoid at $\alpha = -10.2°$, $\varphi_e = -15°$

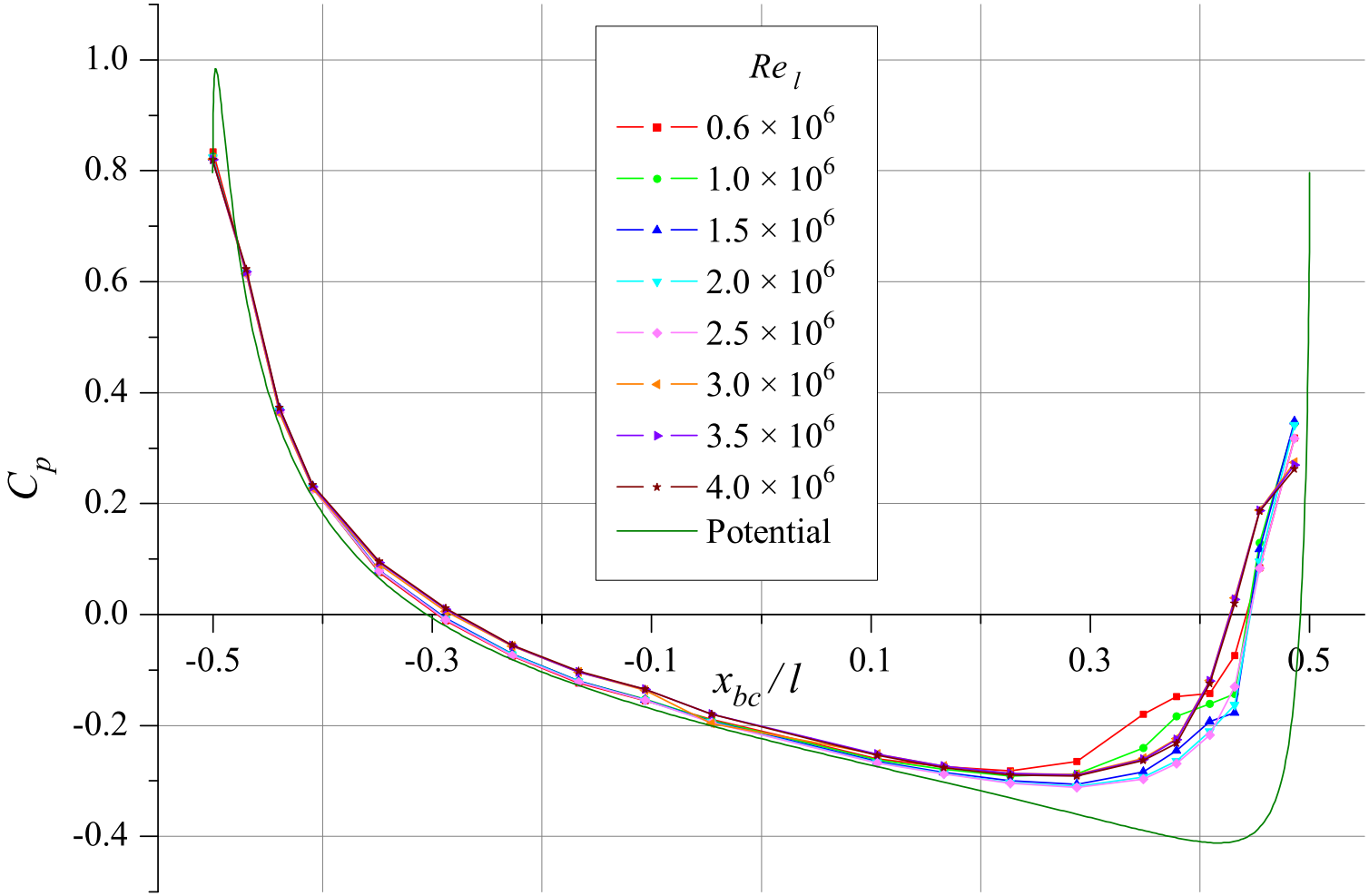

Figure D.29: Surface pressure distribution on ellipsoid at $\alpha = -10.2°$, $\varphi_e = -30°$

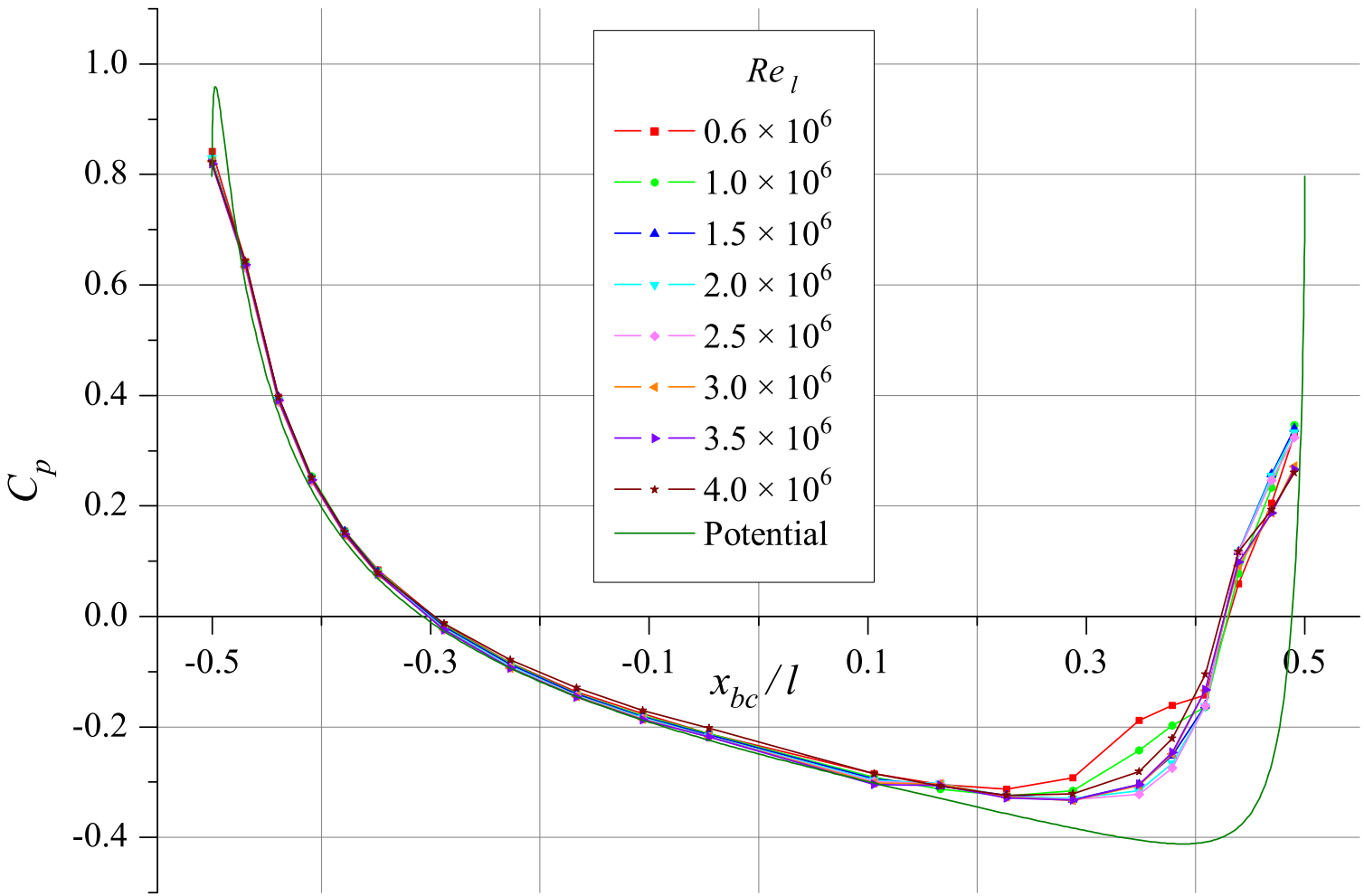

Figure D.30: Surface pressure distribution on ellipsoid at $\alpha = -10.2°$, $\varphi_e = -45°$

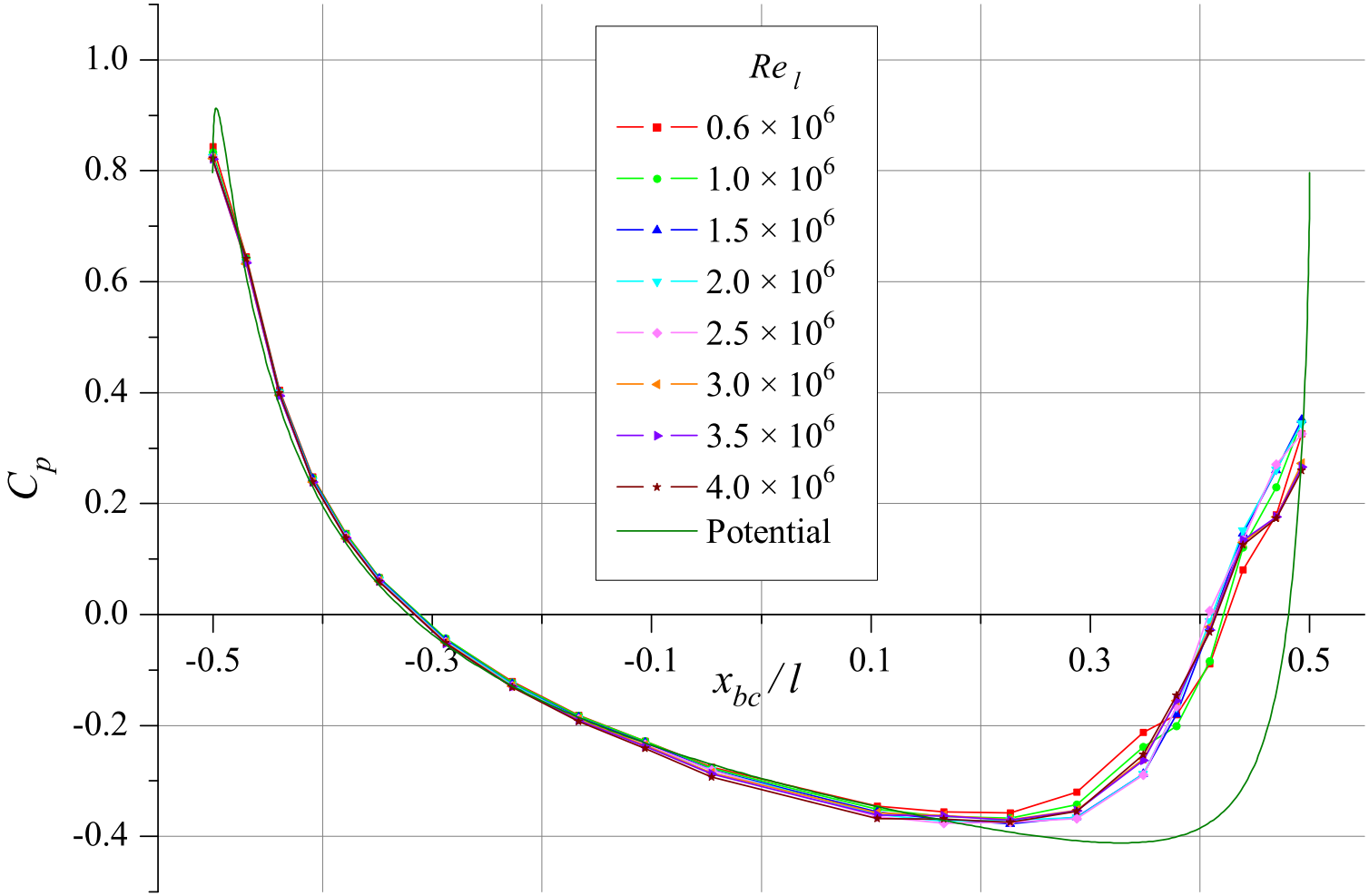

Figure D.31: Surface pressure distribution on ellipsoid at $\alpha = -10.2°$, $\varphi_e = -60°$

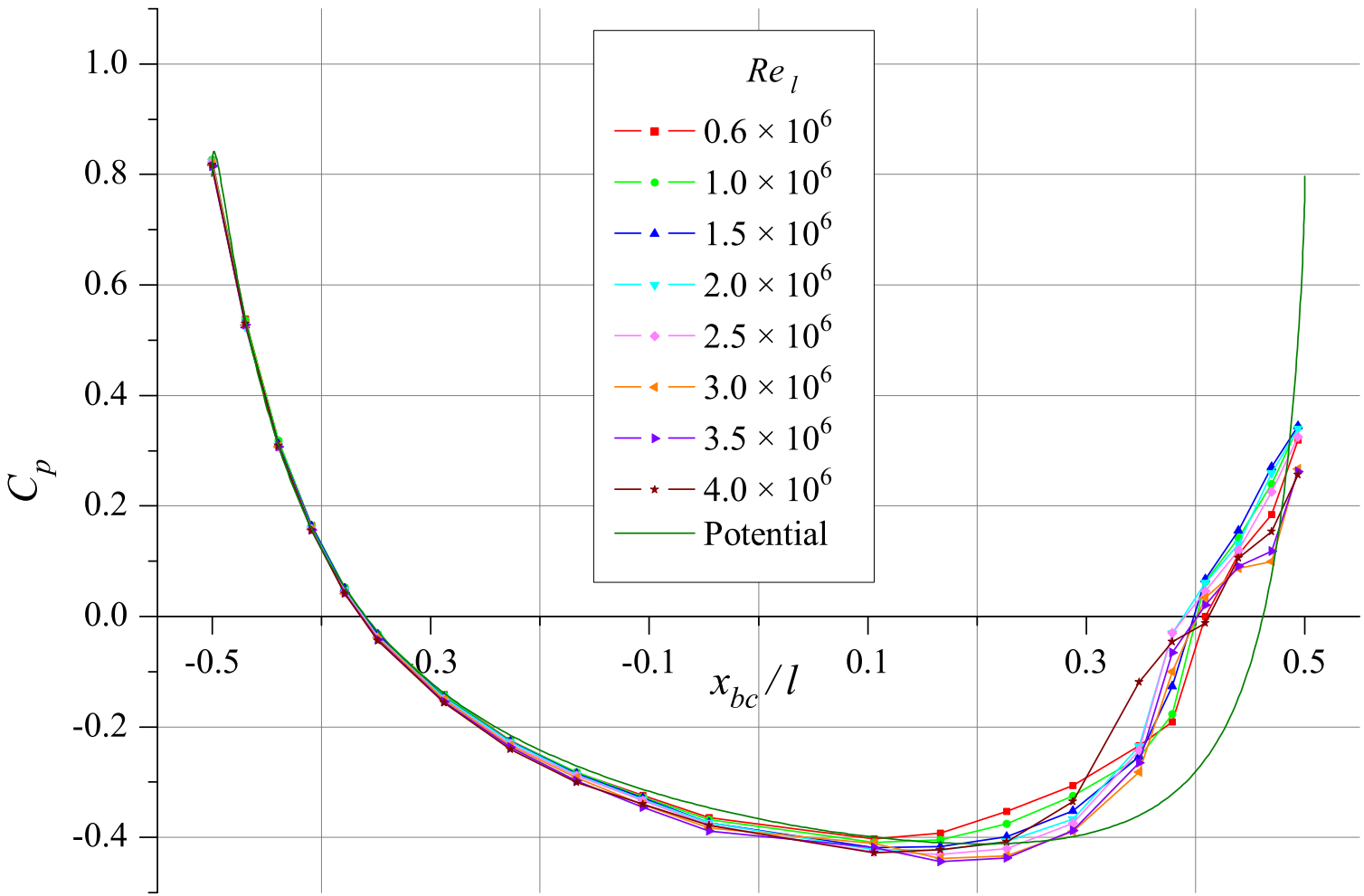

Figure D.32: Surface pressure distribution on ellipsoid at $\alpha = -10.2°$, $\varphi_e = -75°$

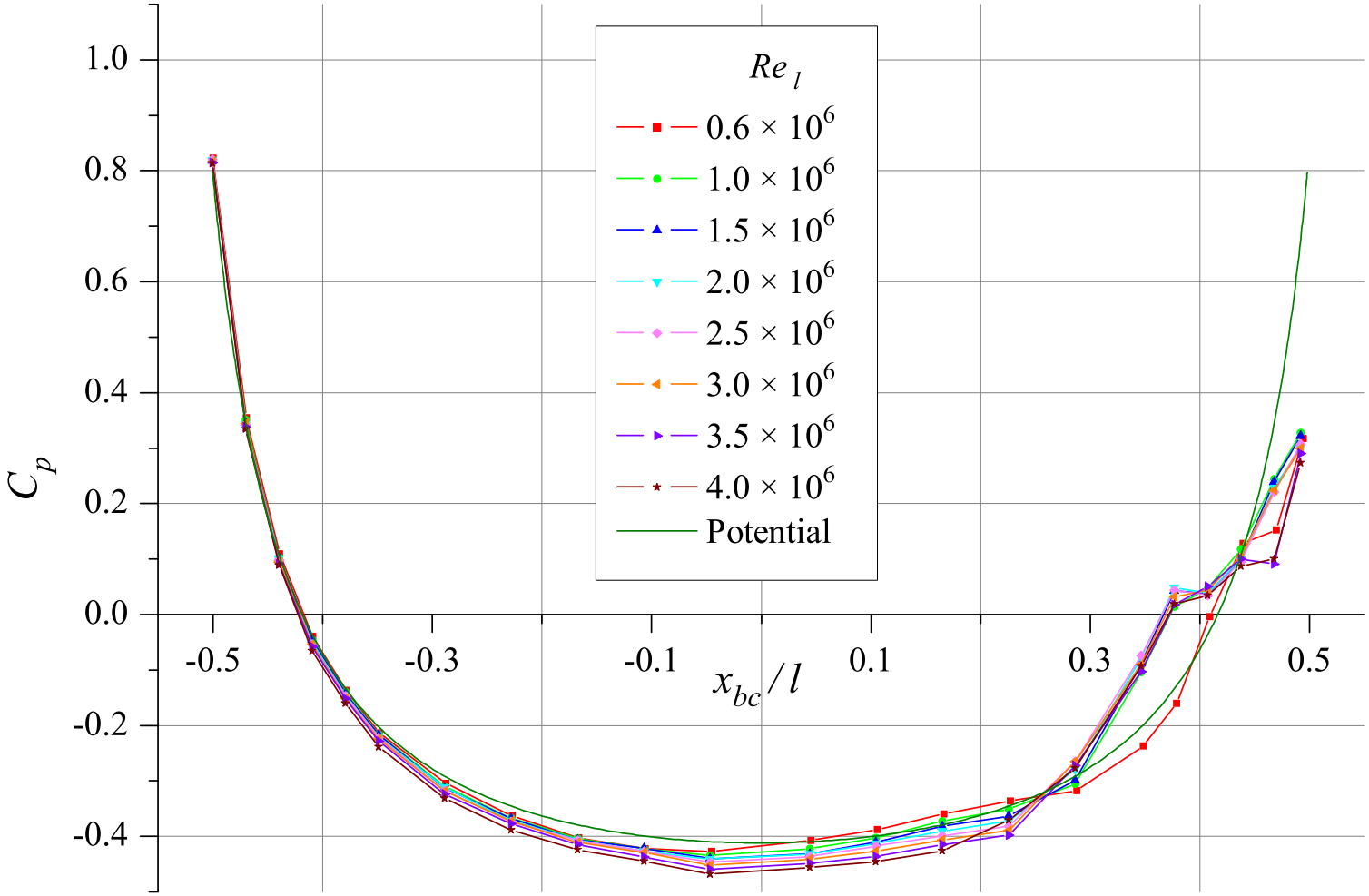

Figure D.33: Surface pressure distribution on ellipsoid at $\alpha = -10.2°$, $\varphi_e = -90°$

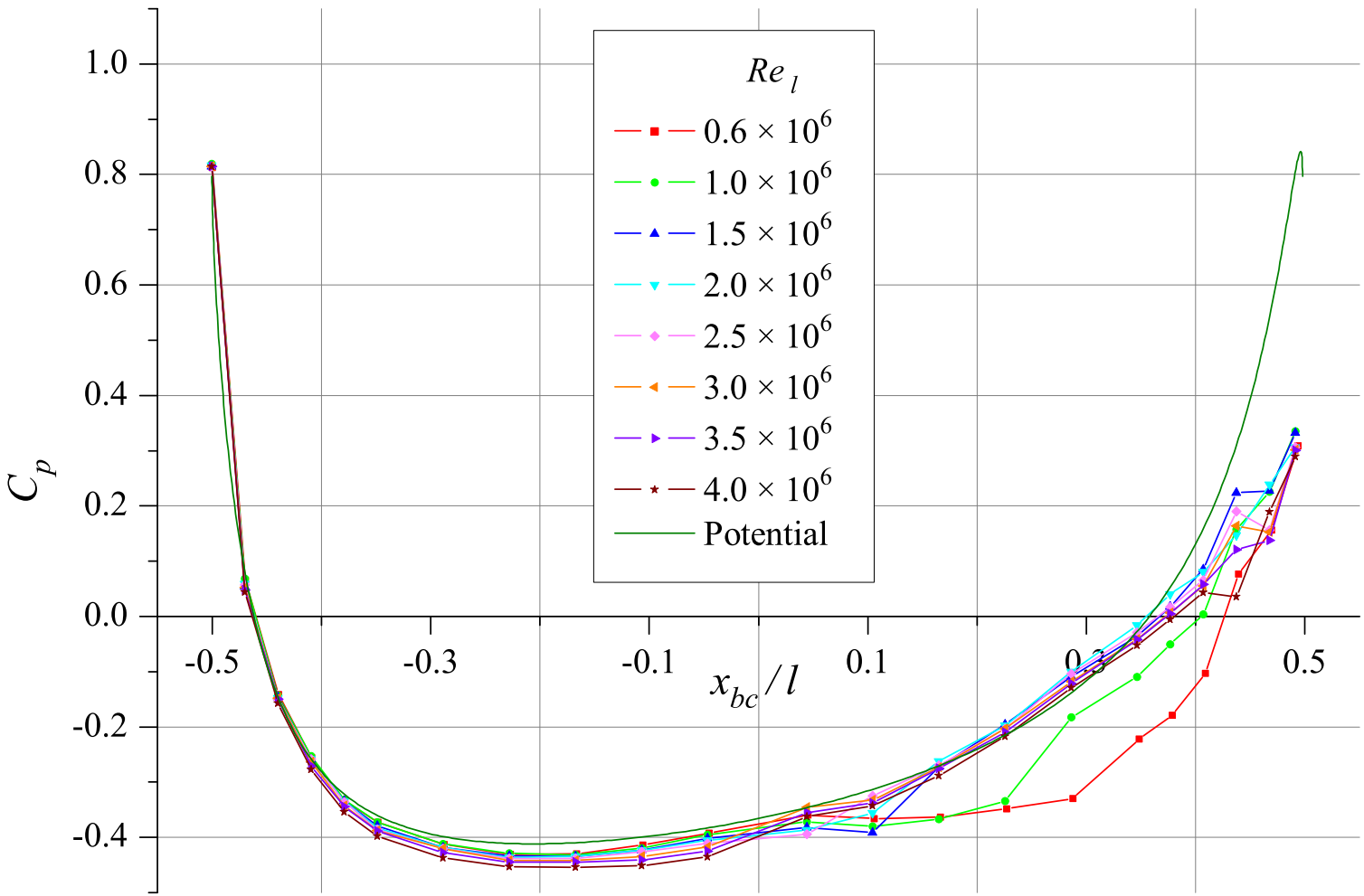

Figure D.34: Surface pressure distribution on ellipsoid at $\alpha = -10.2°$, $\varphi_e = -105°$

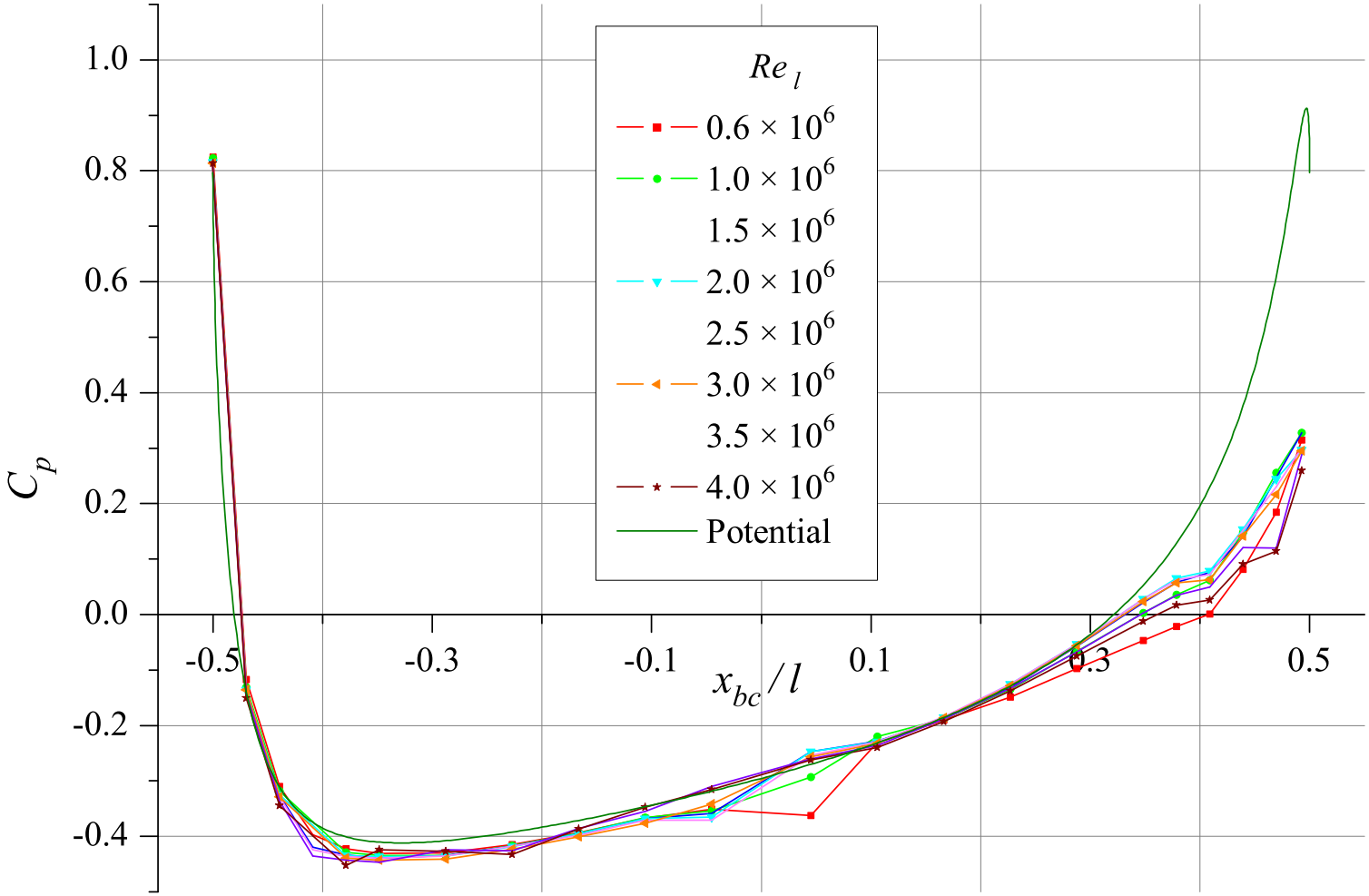

Figure D.35: Surface pressure distribution on ellipsoid at $\alpha = -10.2°$, $\varphi_e = -120°$

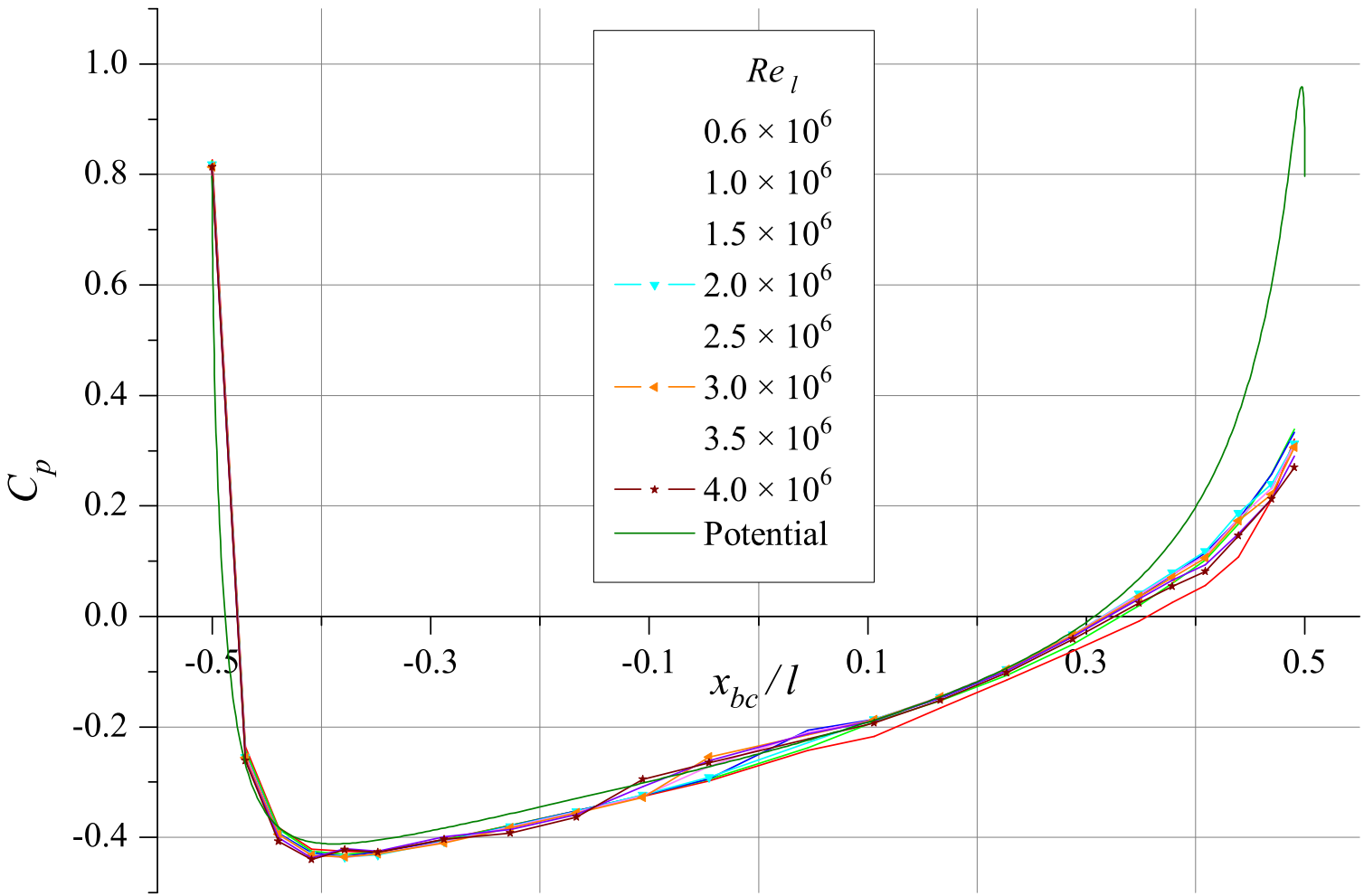

Figure D.36: Surface pressure distribution on ellipsoid at $\alpha = -10.2°$, $\varphi_e = -135°$

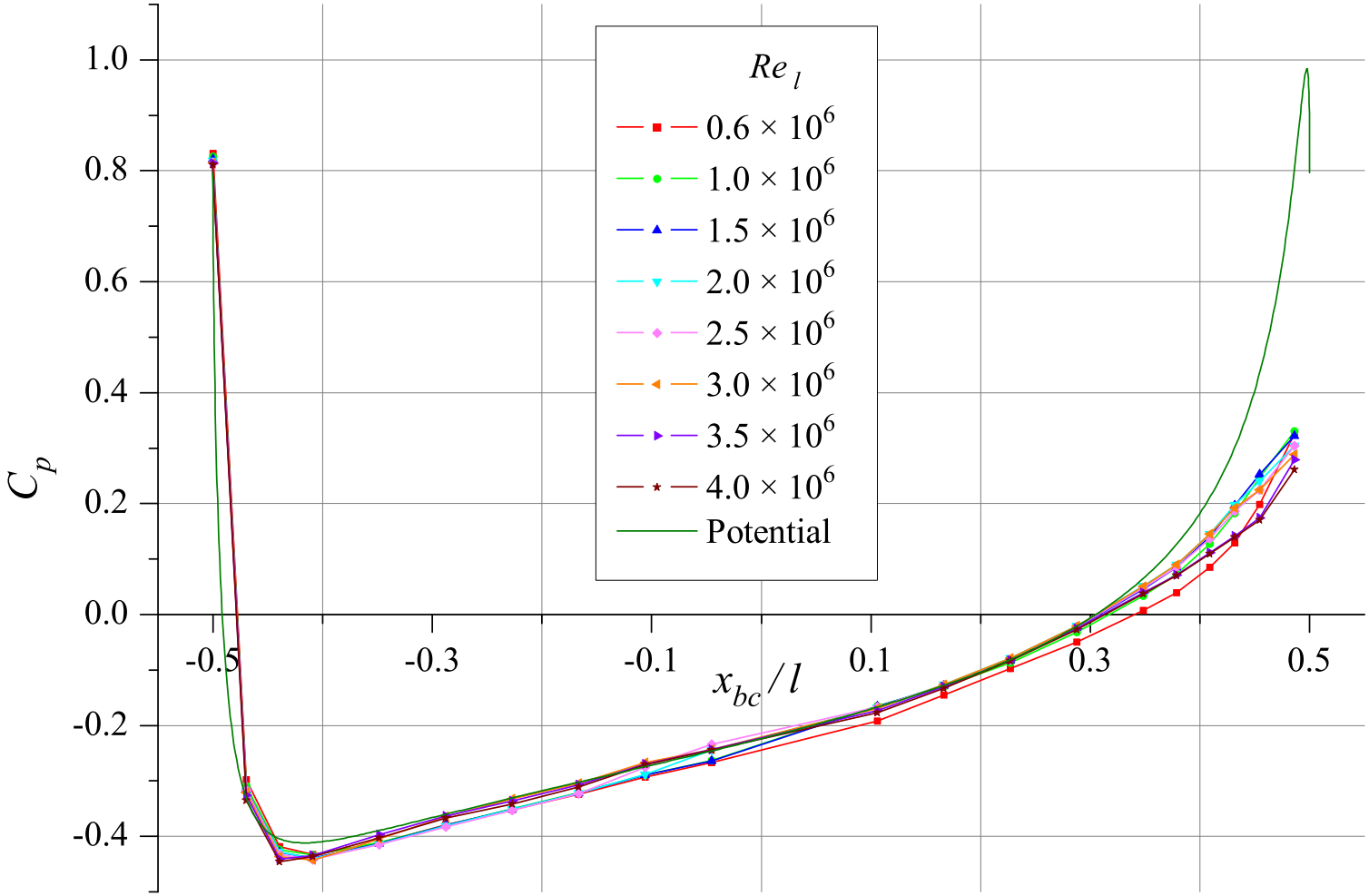

Figure D.37: Surface pressure distribution on ellipsoid at $\alpha = -10.2°$, $\varphi_e = -150°$

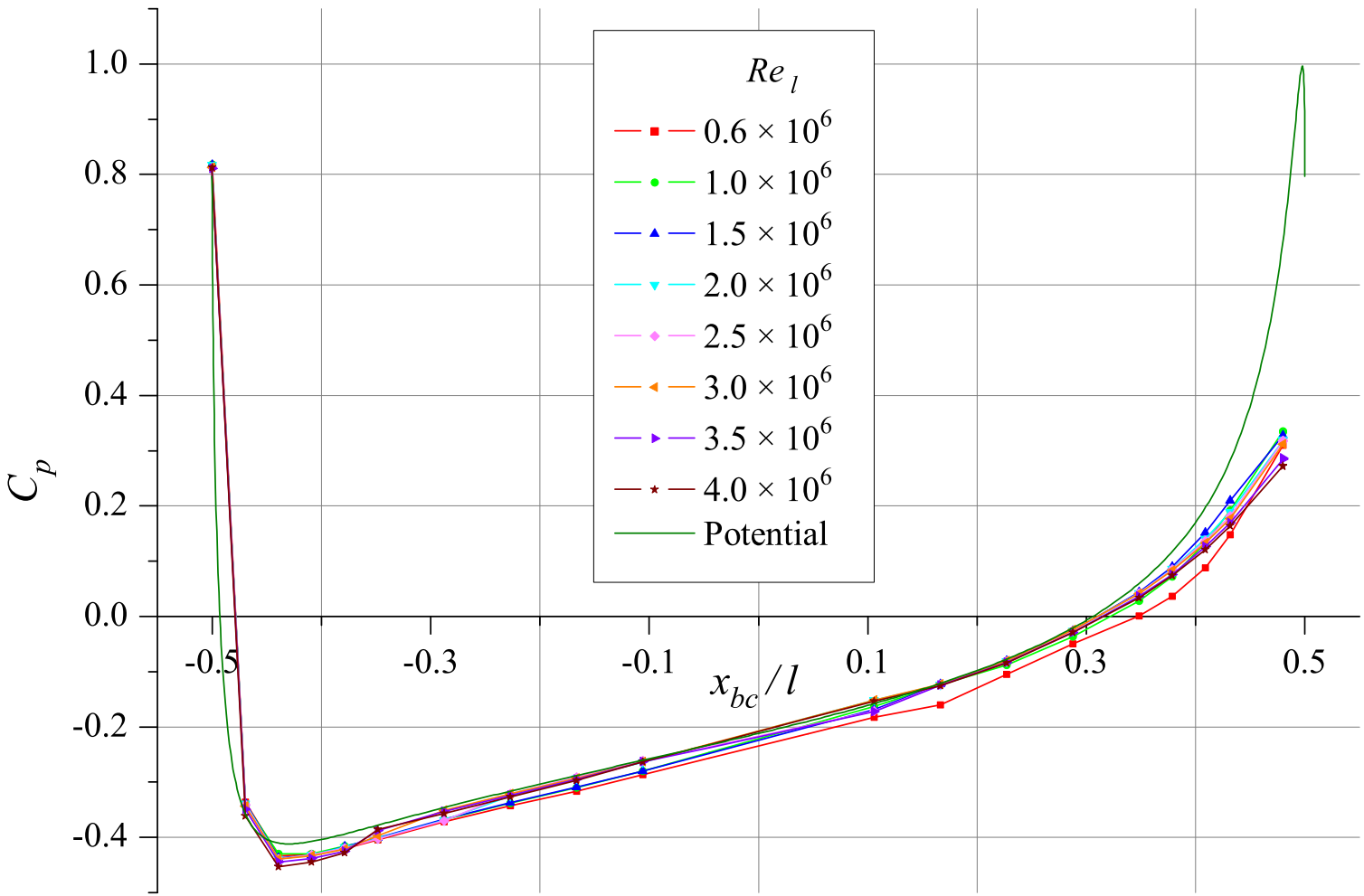

Figure D.38: Surface pressure distribution on ellipsoid at $\alpha = -10.2°$, $\varphi_e = -165°$

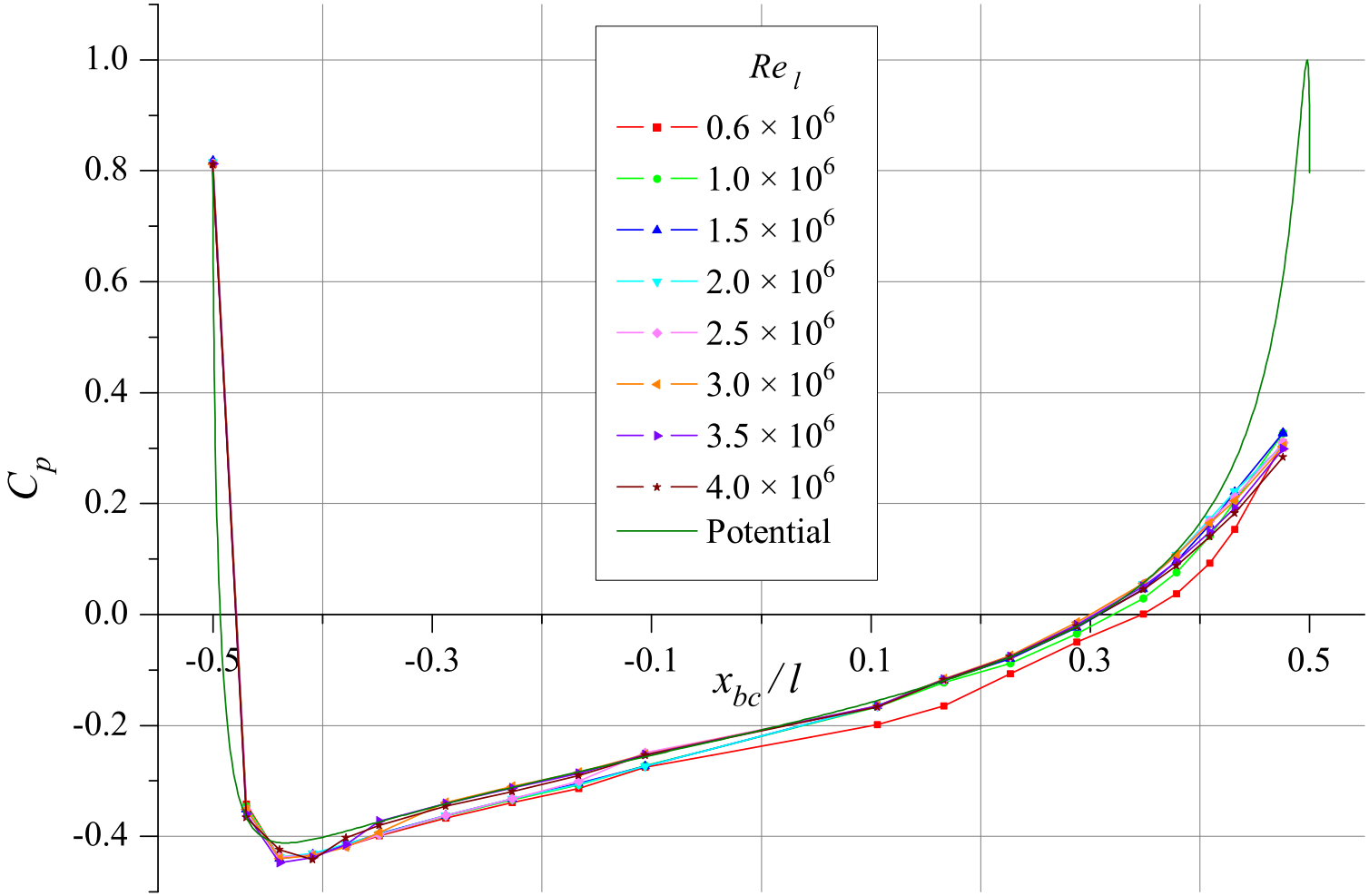

Figure D.39: Surface pressure distribution on ellipsoid at $\alpha = -10.2°$, $\varphi_e = -180°$

D.4 Ellipsoid Surface Pressure at $\alpha = -10.2°$, Tripped $x_{bc}/l = -0.3$

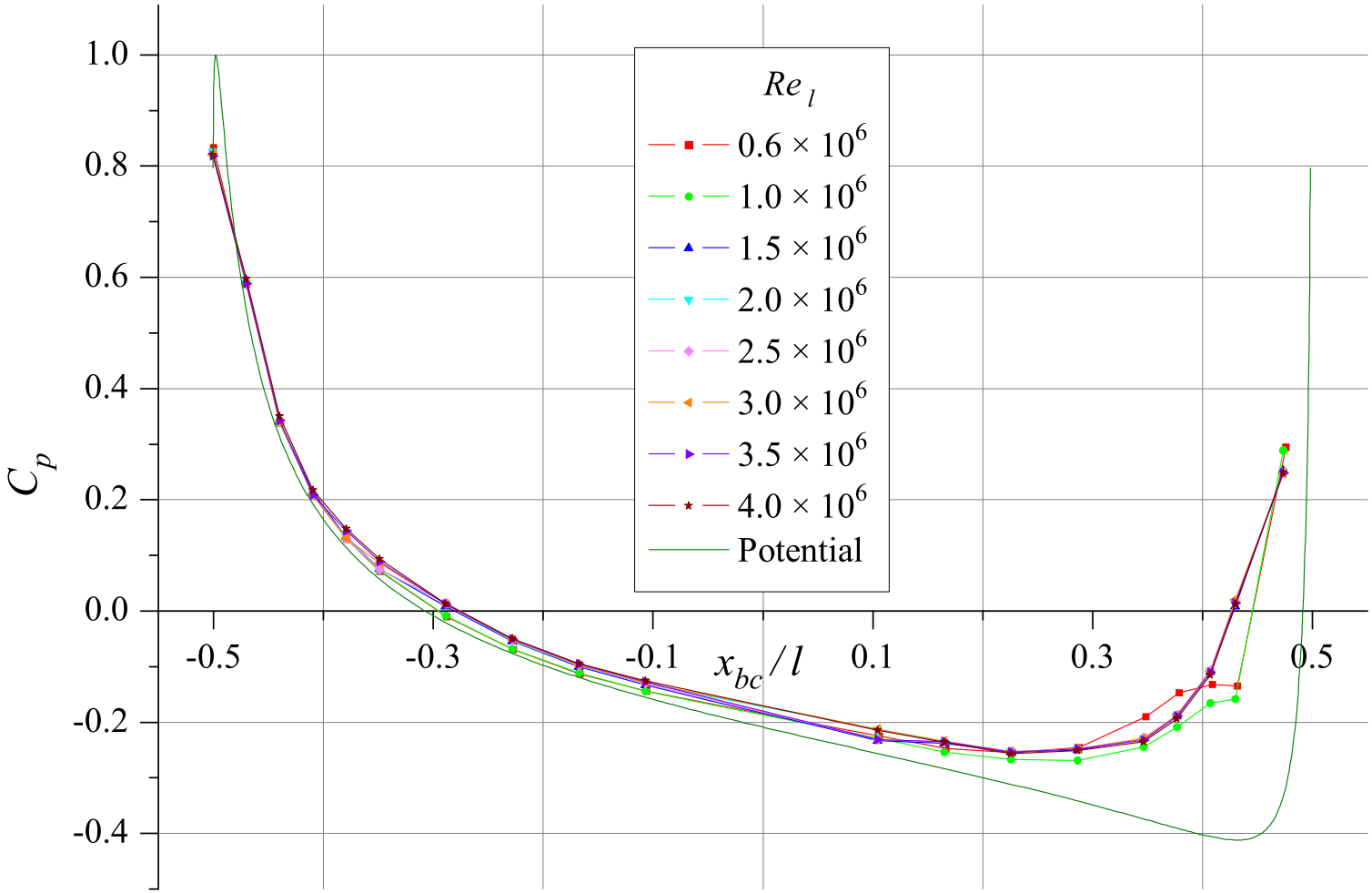

Figure D.40: Surface pressure distribution on ellipsoid at $\alpha = -10.2°$, $\varphi_e = 0°$, tripped at $x_{bc}/l = -0.3$

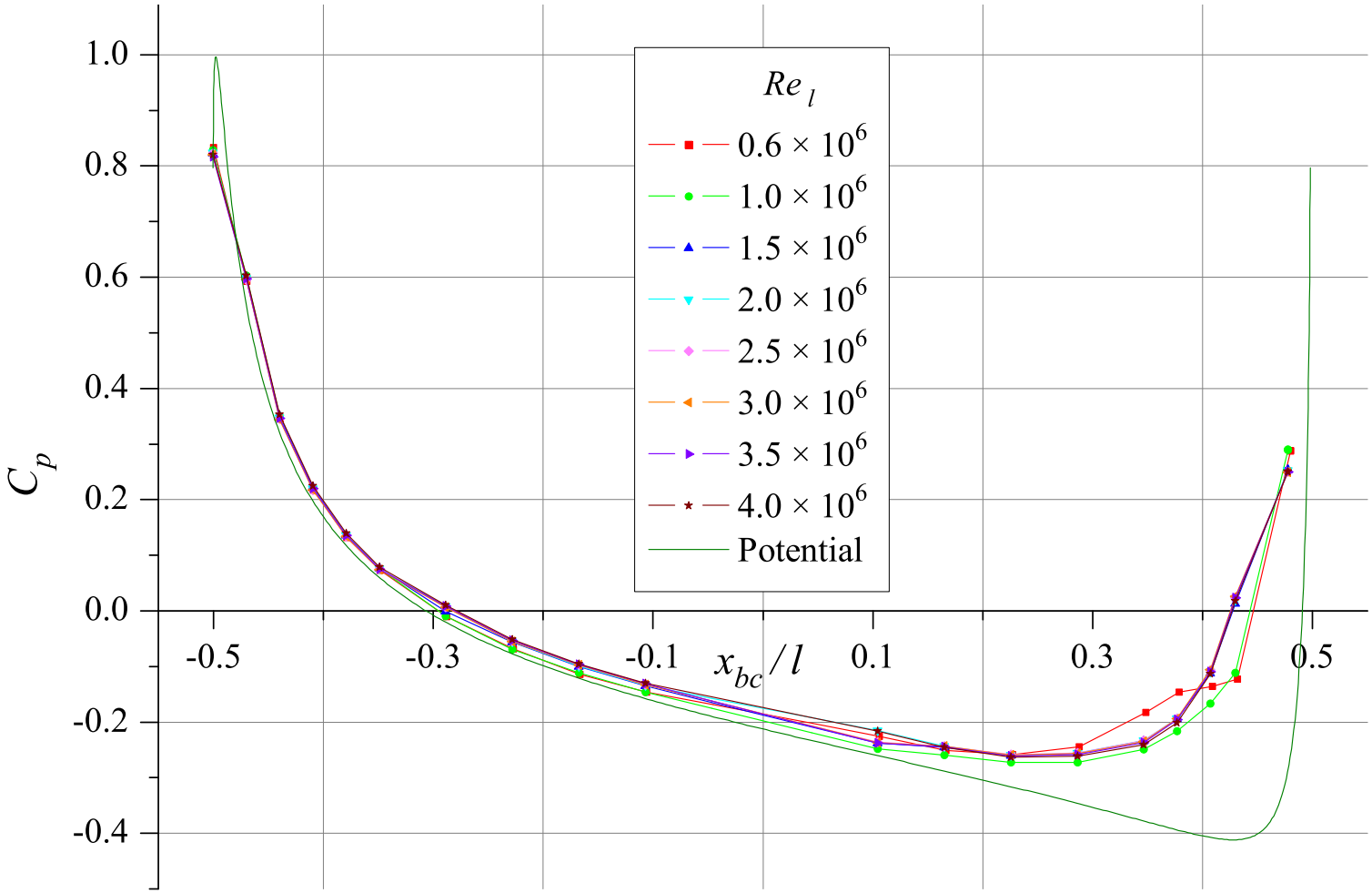

Figure D.41: Surface pressure distribution on ellipsoid at $\alpha = -10.2°$, $\varphi_e = -15°$, tripped at $x_{bc}/l = -0.3$

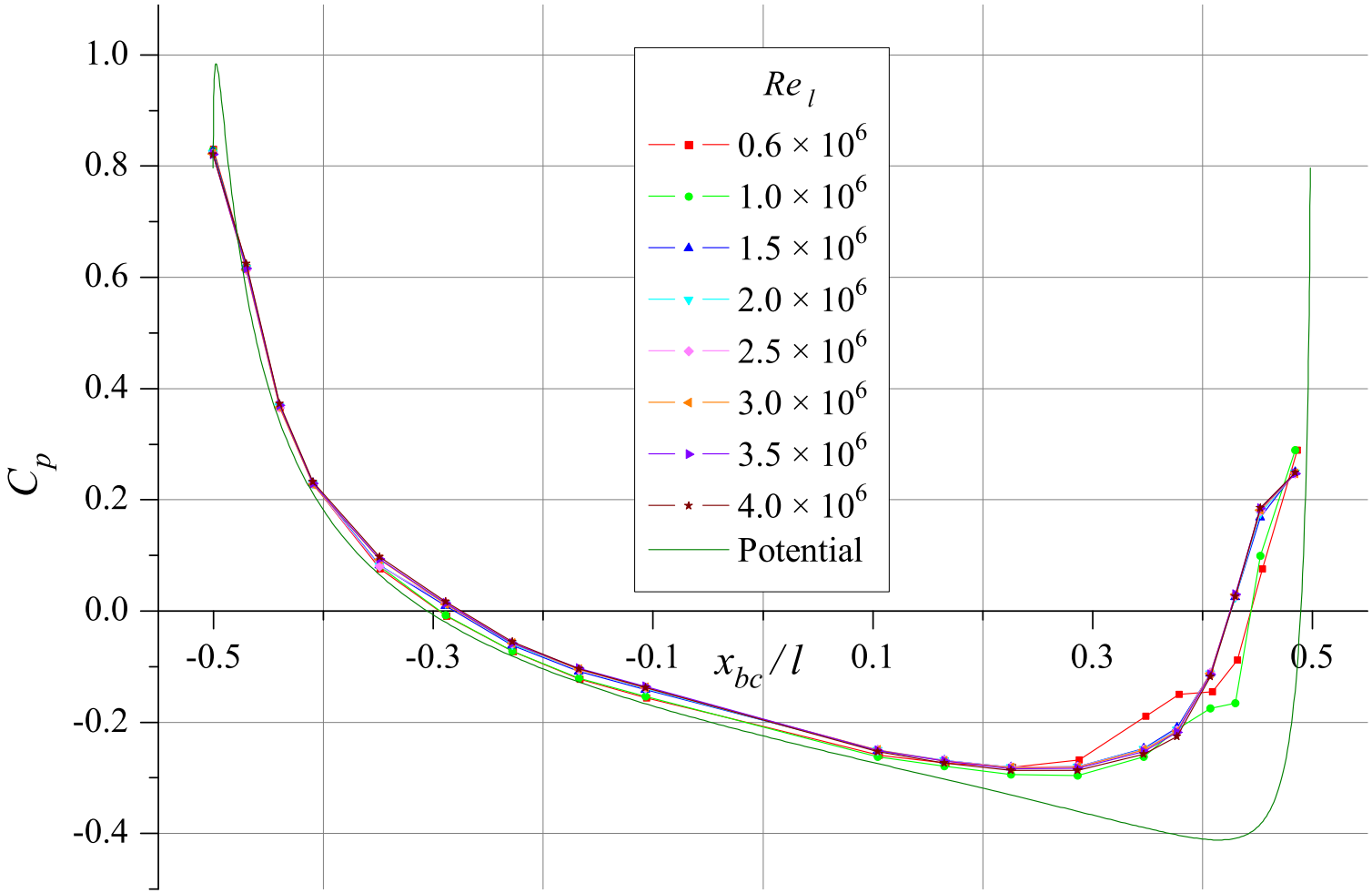

Figure D.42: Surface pressure distribution on ellipsoid at $\alpha = -10.2°$, $\varphi_e = -30°$, tripped at $x_{bc}/l = -0.3$

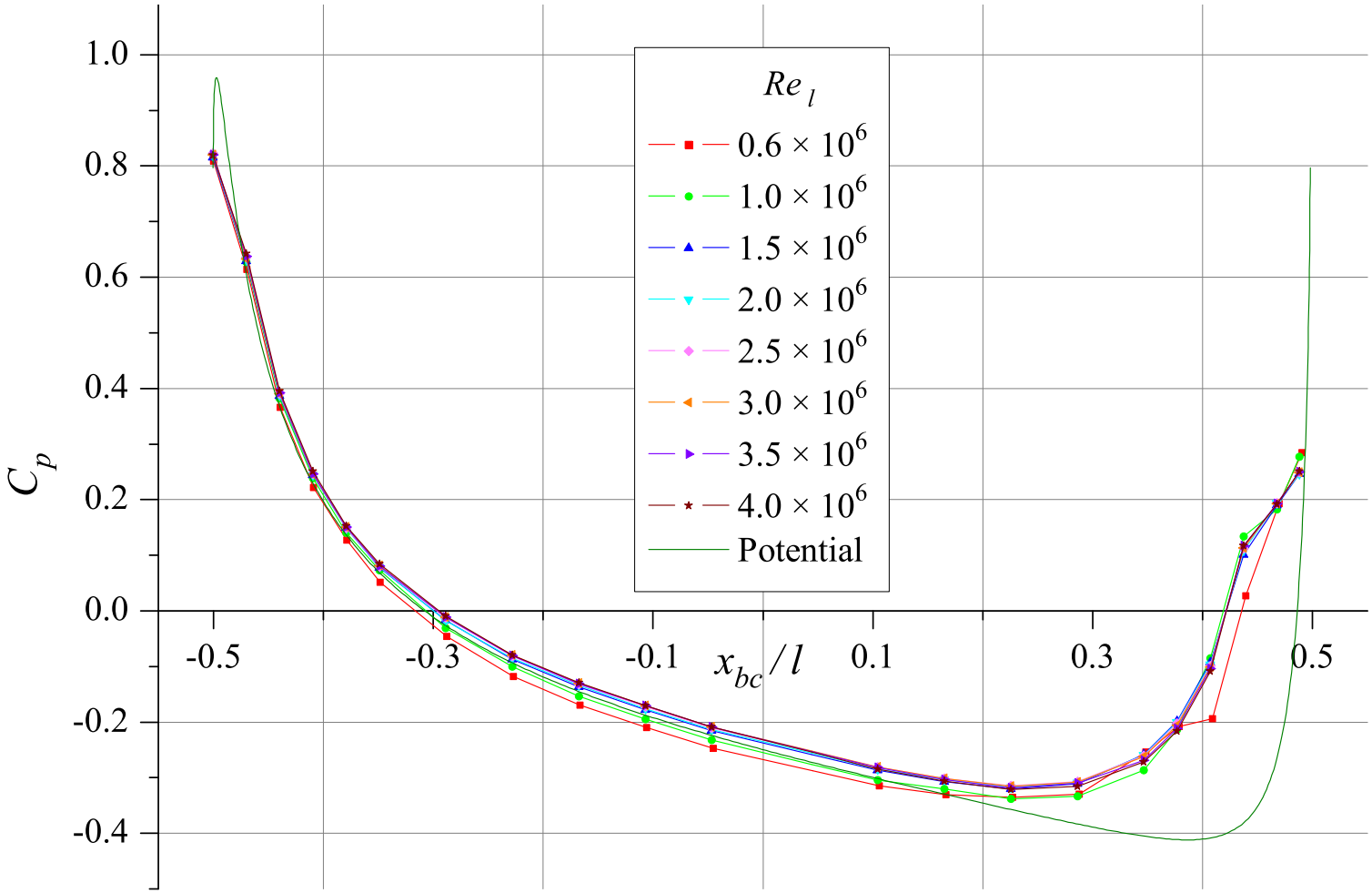

Figure D.43: Surface pressure distribution on ellipsoid at $\alpha = -10.2°$, $\varphi_e = -45°$, tripped at $x_{bc}/l = -0.3$

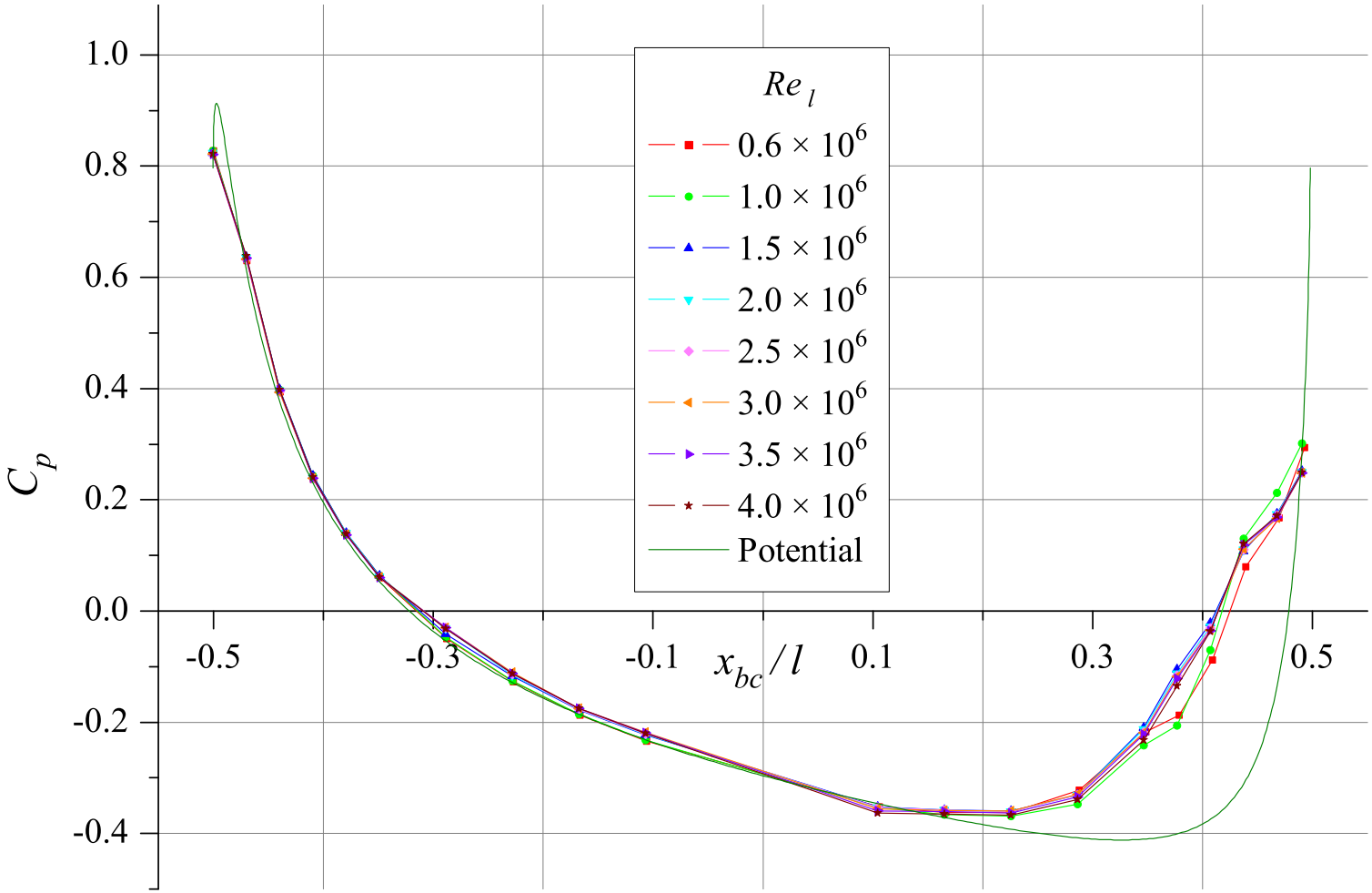

Figure D.44: Surface pressure distribution on ellipsoid at $\alpha = -10.2°$, $\varphi_e = -60°$, tripped at $x_{bc}/l = -0.3$

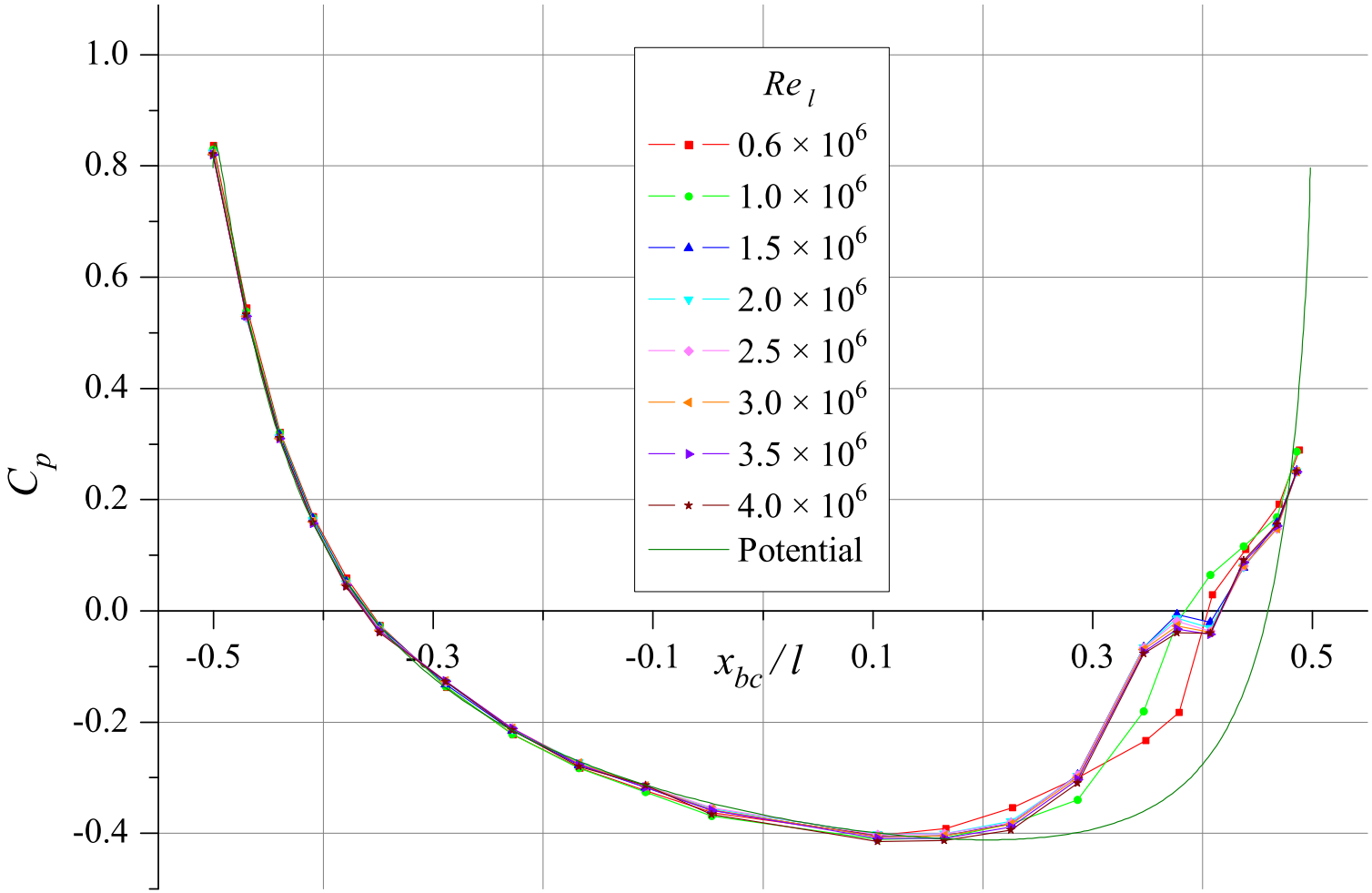

Figure D.45: Surface pressure distribution on ellipsoid at $\alpha = -10.2°$, $\varphi_e = -75°$, tripped at $x_{bc}/l = -0.3$

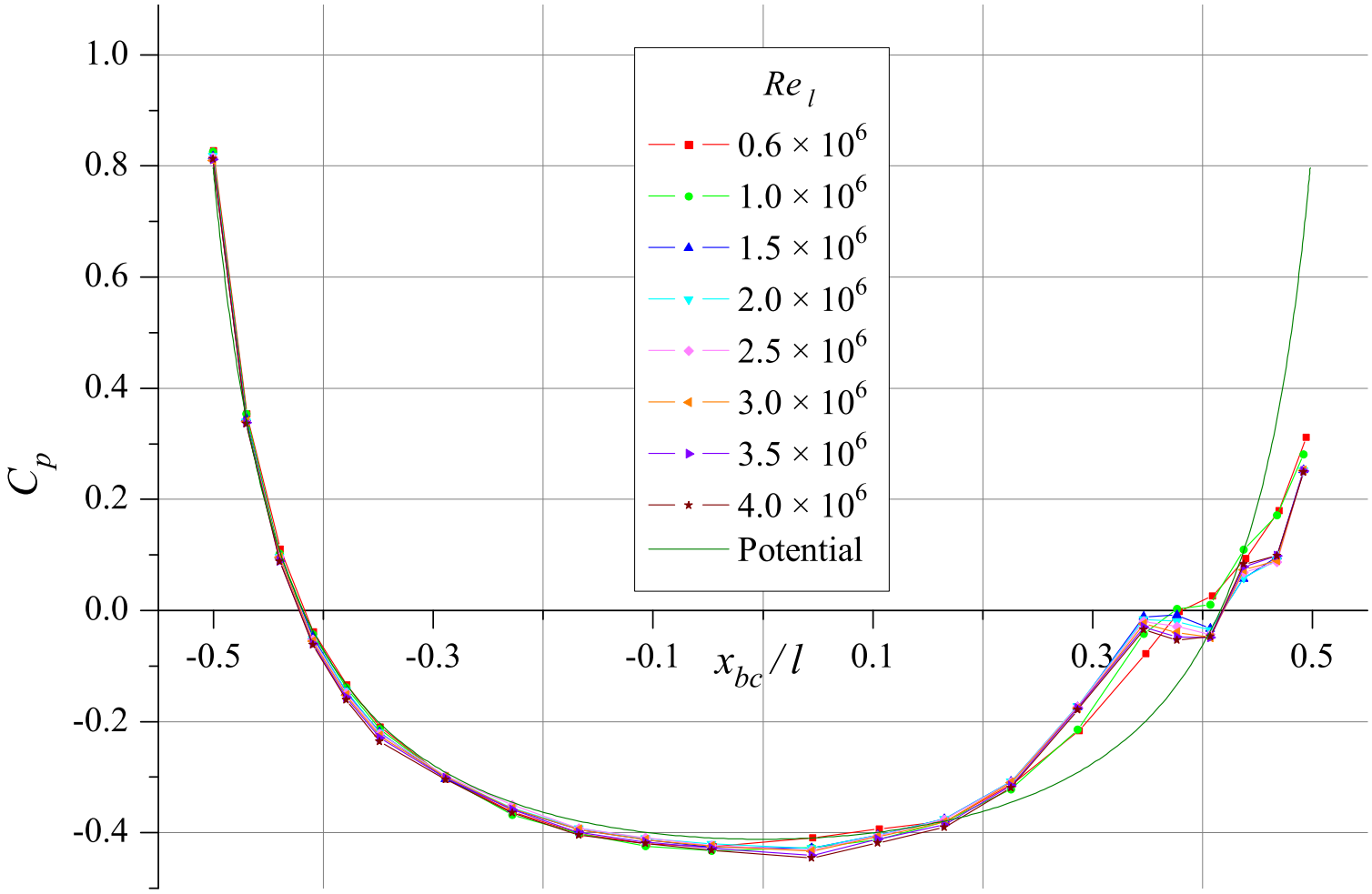

Figure D.46: Surface pressure distribution on ellipsoid at $\alpha = -10.2°$, $\varphi_e = -90°$, tripped at $x_{bc}/l = -0.3$

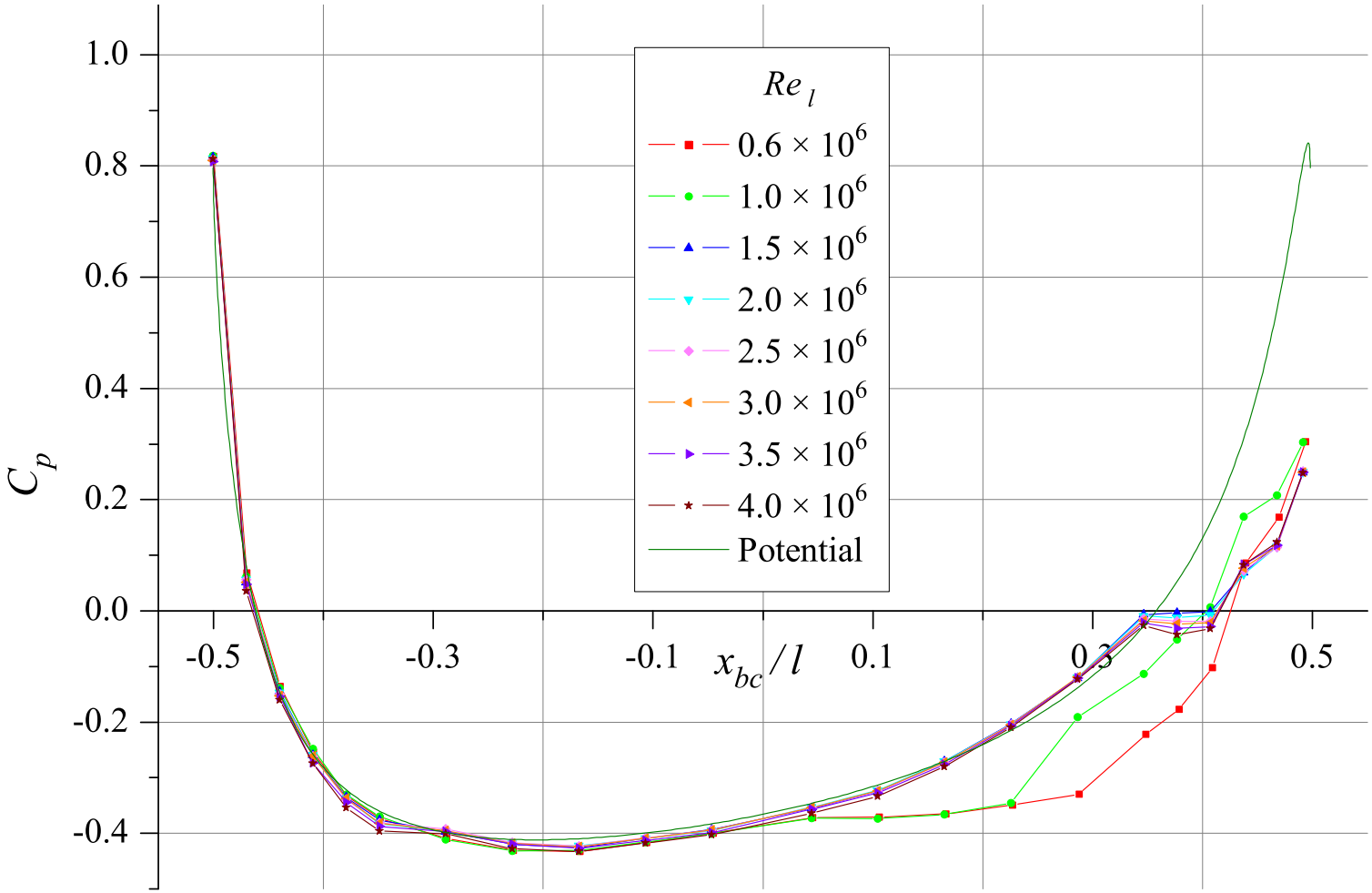

Figure D.47: Surface pressure distribution on ellipsoid at $\alpha = -10.2°$, $\varphi_e = -105°$, tripped at $x_{bc}/l = -0.3$

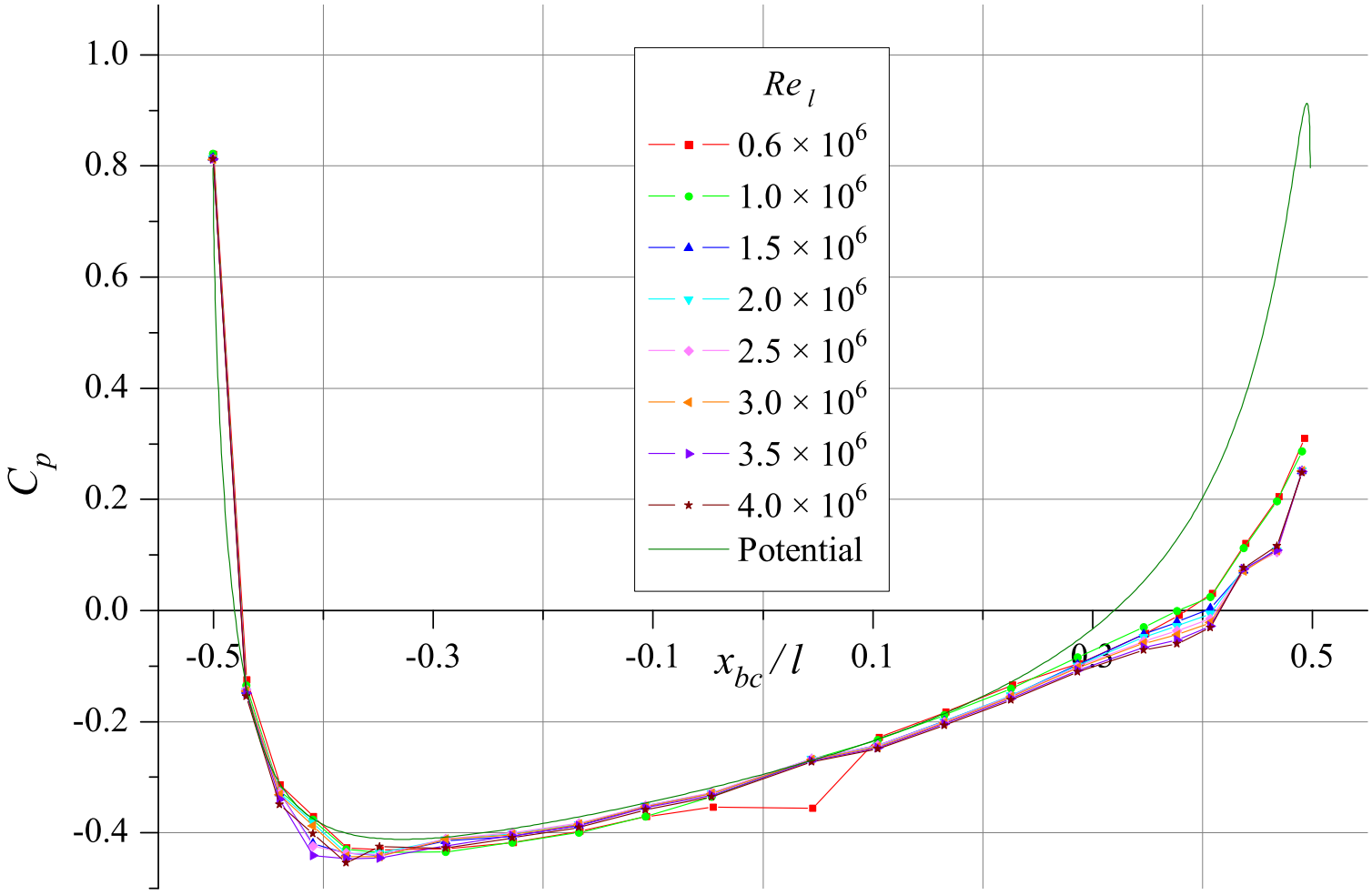

Figure D.48: Surface pressure distribution on ellipsoid at $\alpha = -10.2°$, $\varphi_e = -120°$, tripped at $x_{bc}/l = -0.3$

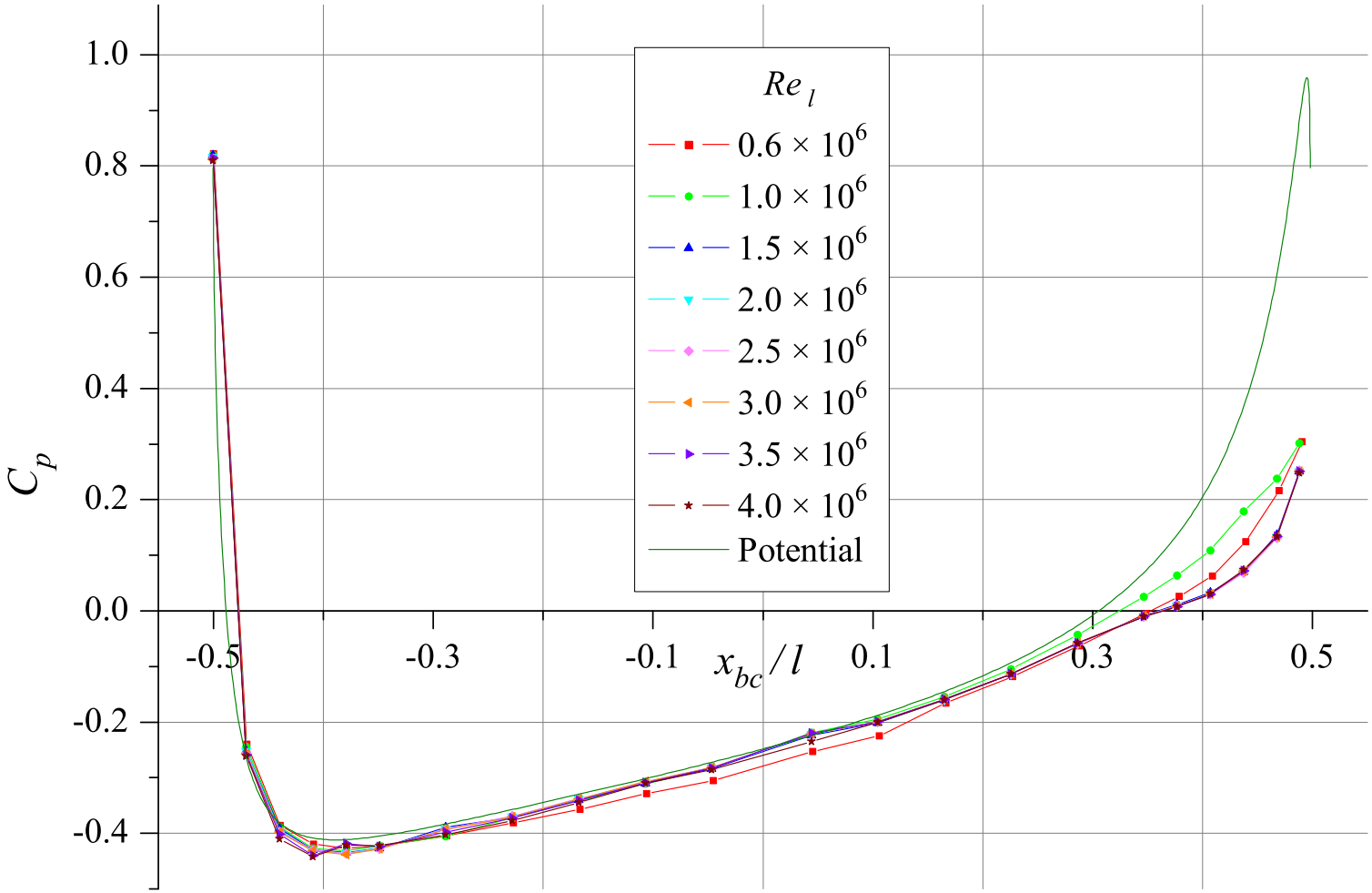

Figure D.49: Surface pressure distribution on ellipsoid at $\alpha = -10.2°$, $\varphi_e = -135°$, tripped at $x_{bc}/l = -0.3$

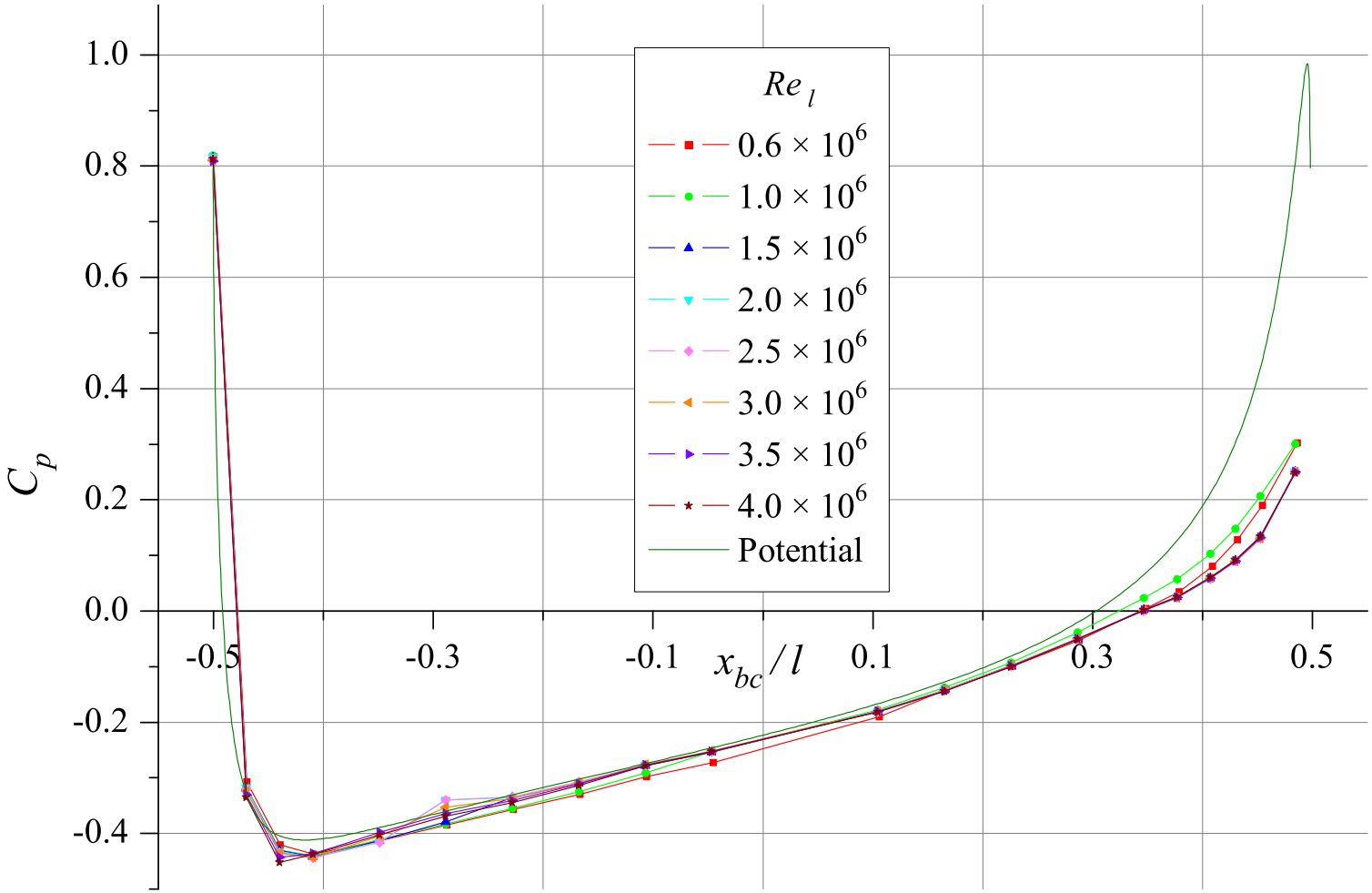

Figure D.50: Surface pressure distribution on ellipsoid at $\alpha = -10.2°$, $\varphi_e = -150°$, tripped at $x_{bc}/l = -0.3$

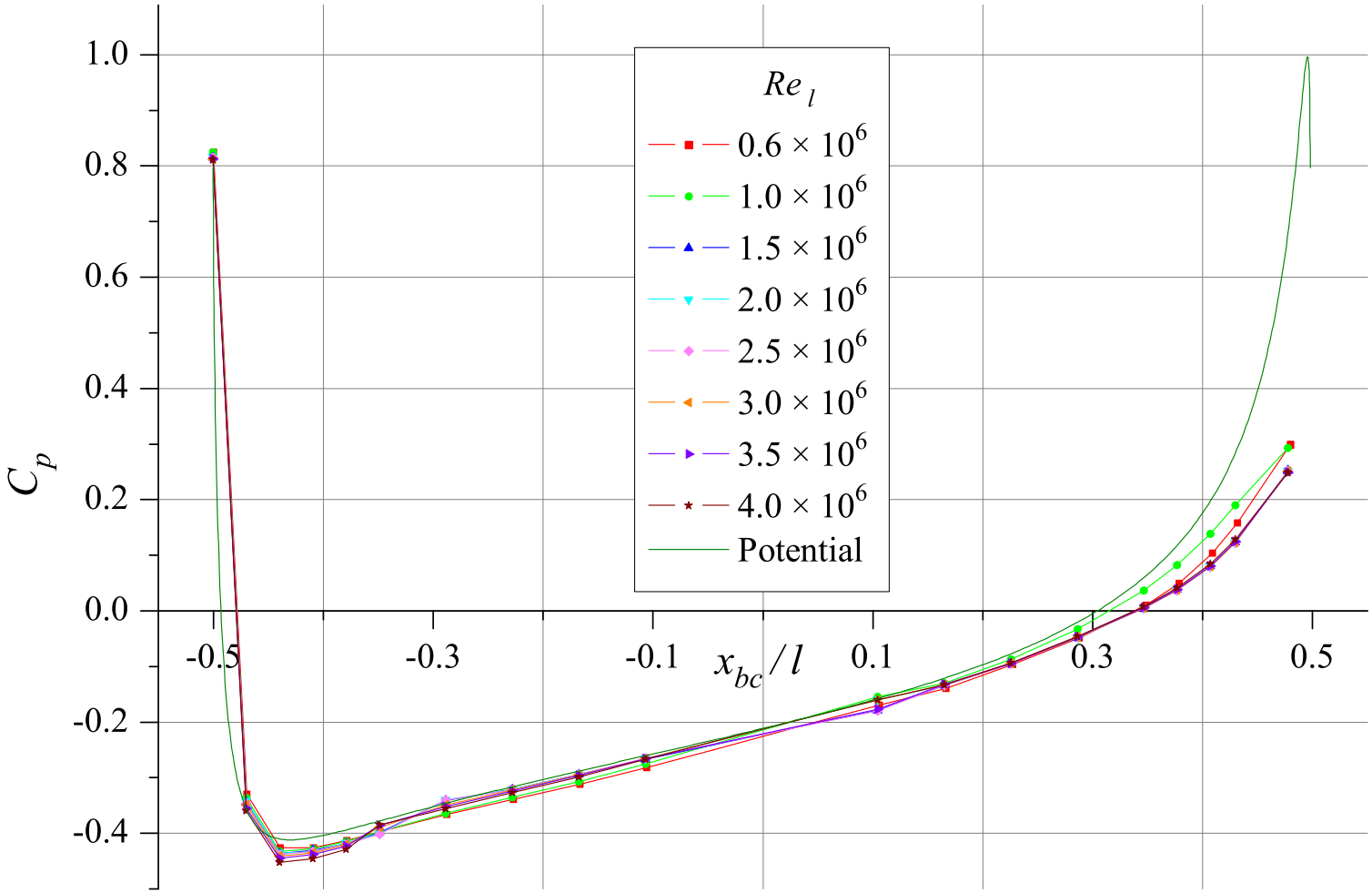

Figure D.51: Surface pressure distribution on ellipsoid at $\alpha = -10.2°$, $\varphi_e = -165°$, tripped at $x_{bc}/l = -0.3$

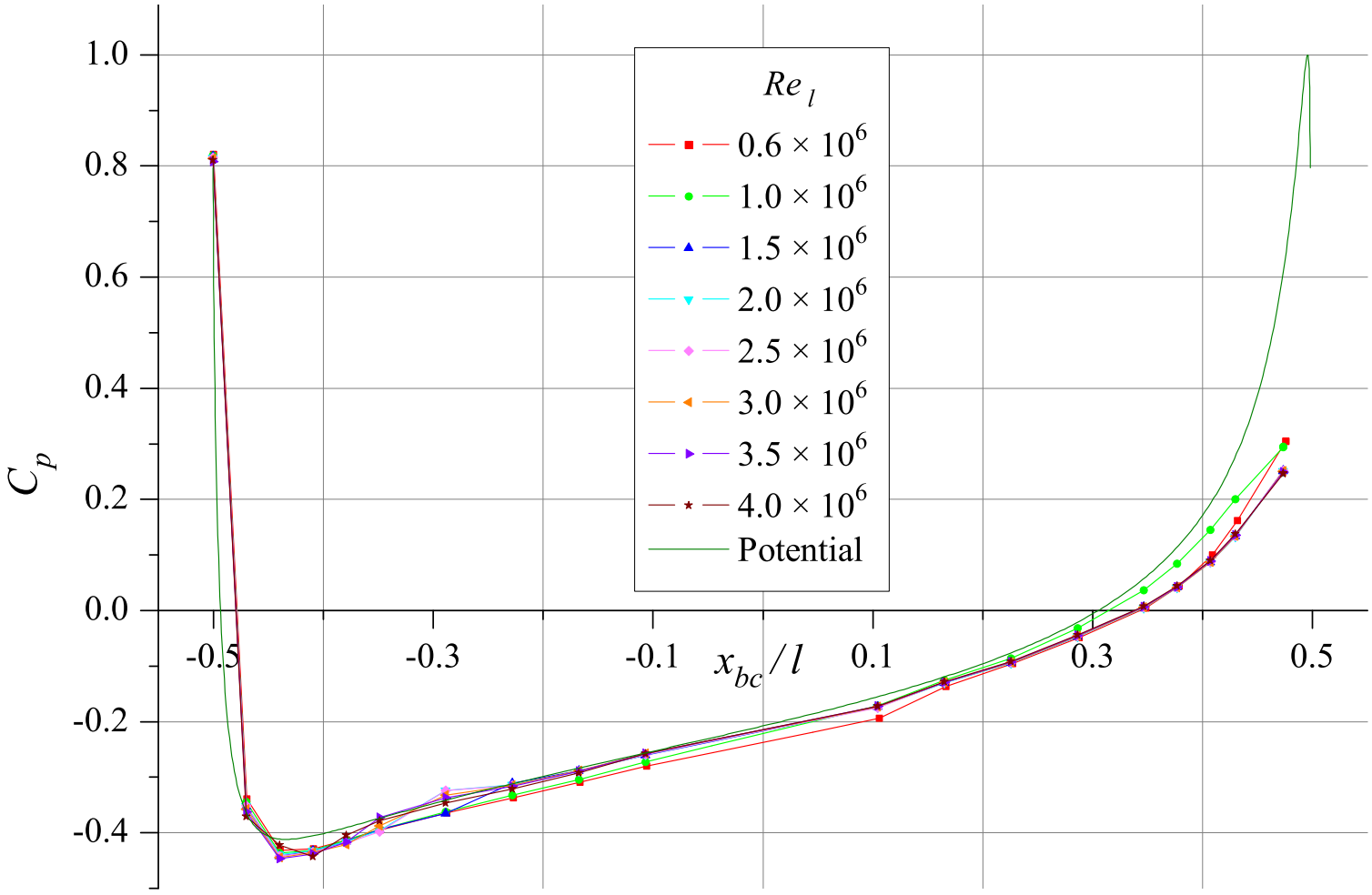

Figure D.52: Surface pressure distribution on ellipsoid at $\alpha = -10.2°$, $\varphi_e = -180°$, tripped at $x_{bc}/l = -0.3$

Appendix E

Critical Point Toplogy

This figure is not avaliable for download due to copyright, please see Figure 4 of the paper cited in the caption.

Figure E.1: Classification of the critical point in the [p,q] plane, from Délery [11]

This figure is not avaliable for download due to copyright, please see Figure 5 of the paper cited in the caption.

Figure E.2: The different critical points, from Délery [11]

Appendix F

Traverse Drawings

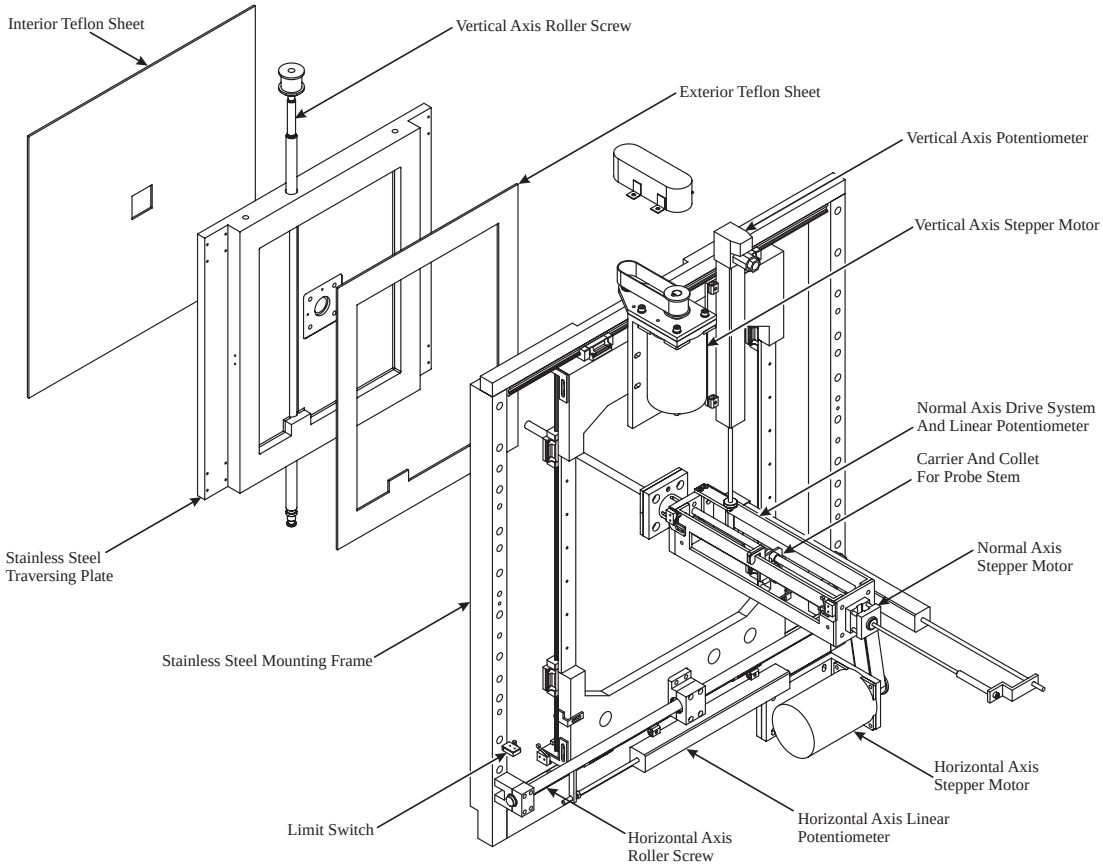

Figure F.1: Exploded external view of traverse external components (except for main window and support frame)

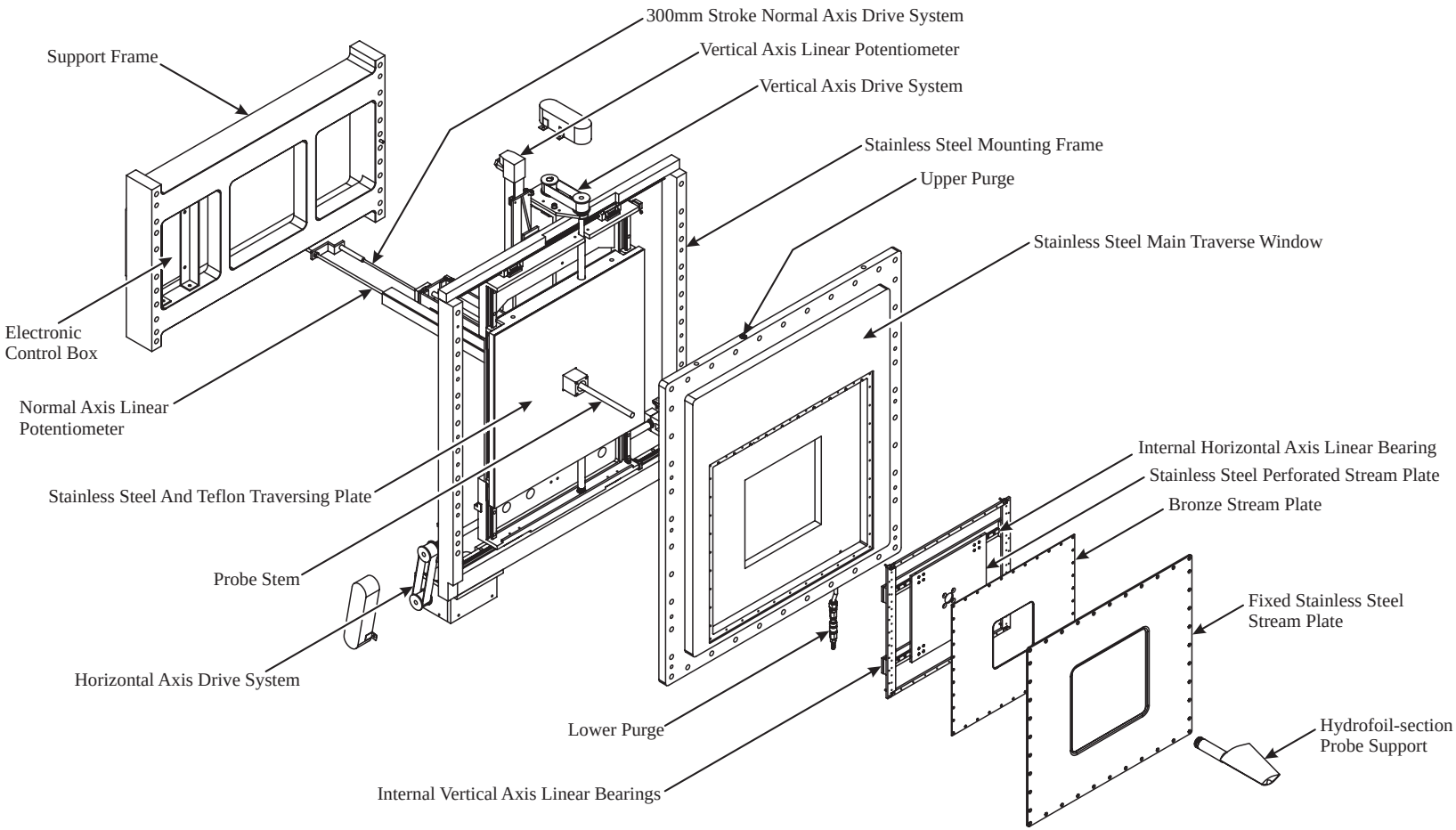

Figure F.2: Exploded internal view of traverse

Appendix G

4.2–2–1 Ellipsoid Wake Measurements

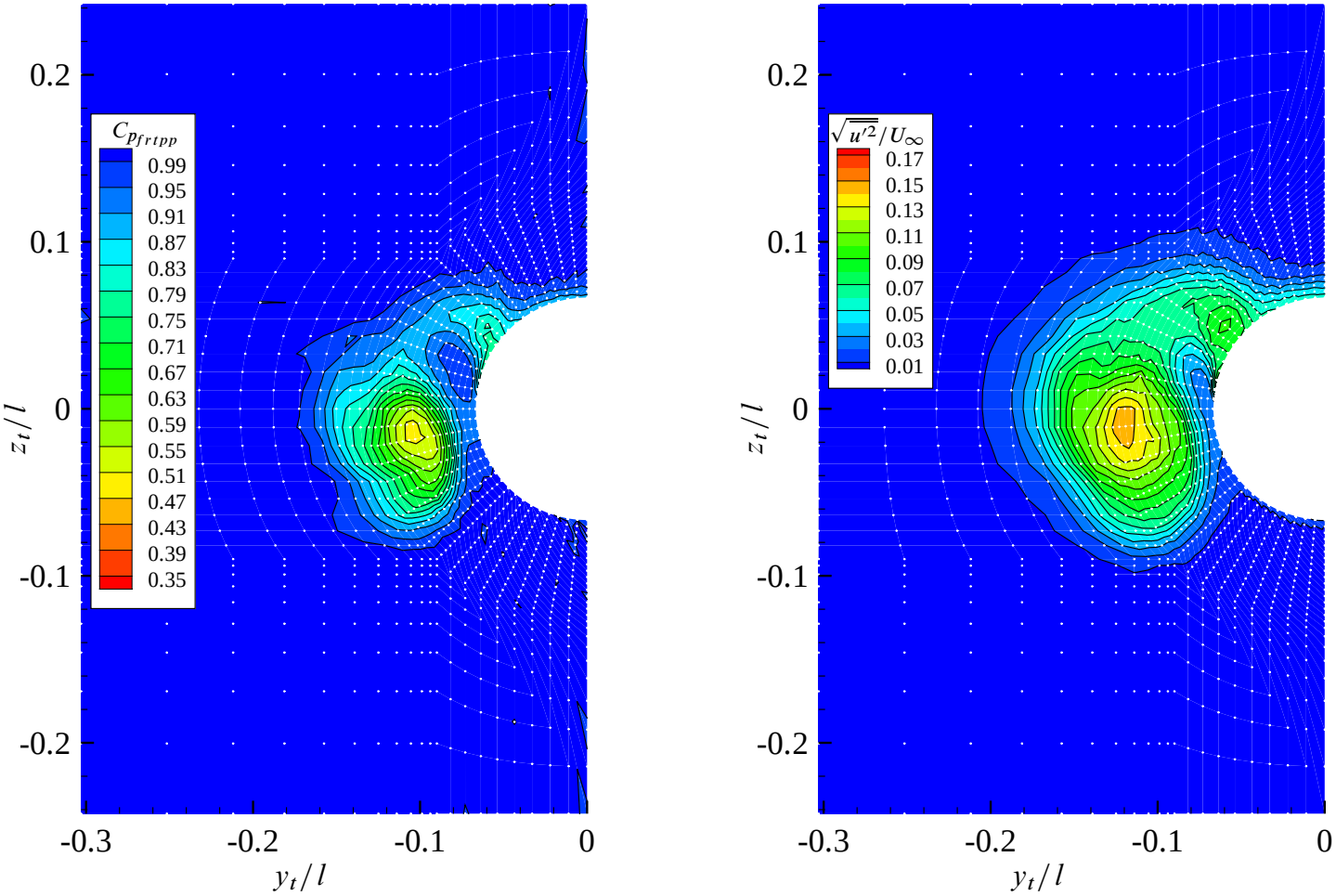

(a) Non-dimensionalised total pressure

(b) Nominal $\sqrt{\overline{u'^2}}/U_\infty$

Figure G.1: Wake measurements with the FRTPP in plane $x_t/l = 0.76$, $250mm$ downstream of ellipsoid centroid, $\alpha = -10.2°$, $Re_l = 1.0 \times 10^6$.

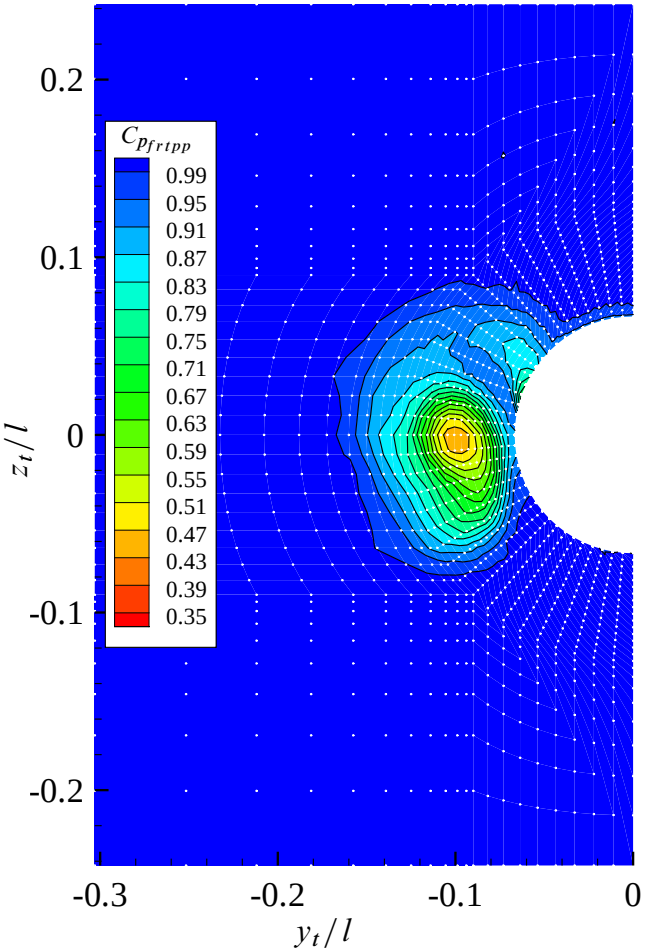

(a) Non-dimensionalised total pressure

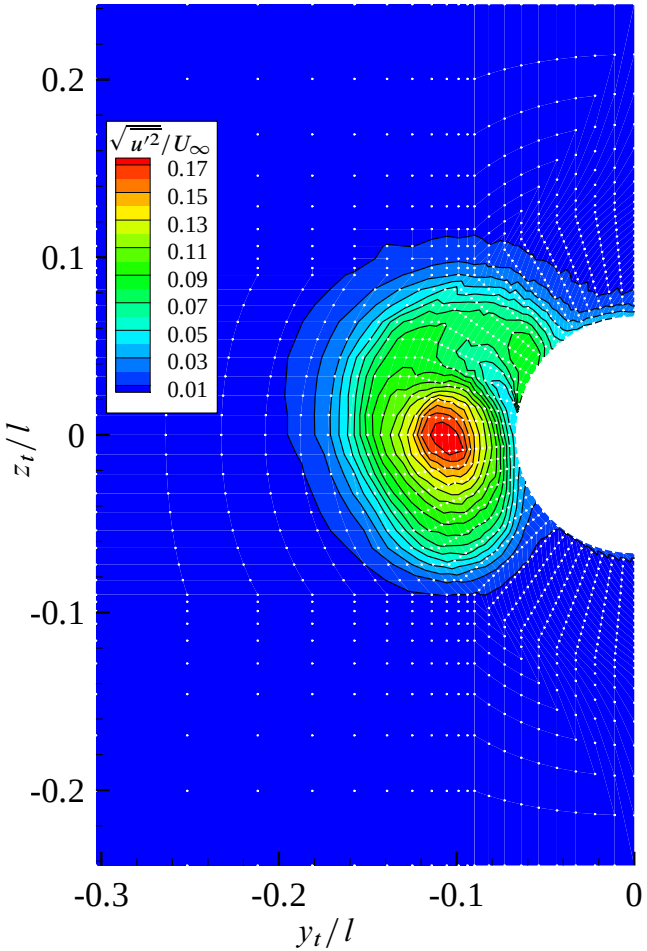

(b) Nominal $\sqrt{\overline{u'^2}}/U_\infty$

Figure G.2: Wake measurements with the FRTPP in plane $x_t/l = 0.76$, $250mm$ downstream of ellipsoid centroid, $\alpha = -10.2°$, $Re_l = 2.0\times10^6$.

Bibliography

[1] Munk, M. M., 1924, "The aerodynamic forces on airship hulls," Tech. rep., National Advisory Committee for Aeronautics, NACA Report 184.

[2] Hopkins, E. J., 1951, "A semi-empirical method for calculating the pitching moment of bodies of revolution at low mach number," Tech. rep., National Advisory Committee for Aeronautics, NACA RM-A51C14.

[3] Fink, R. D., 1976, "USAF stability and control DATCOM," Tech. rep., United States Airforce Flight Dynamics Laboratory.

[4] Fidler, J. E. and Smith, C. A., 1977, "Methods for predicting submersible hydrodynamic characteristics," Tech. rep., Nielsen Engineering and Research Inc., NEAR TR 139.

[5] Peterson, R. S., 1980, "Evaluation of semi-empirical methods for predicting linear static and rotary hydrodynamic coefficients," Tech. rep., Naval Coastal Systems Center, NCSC TM-291-80.

[6] Nahon, M., 1993, "Determination of undersea vehicle hydrodynamic derivatives using the USAF DATCOM," *OCEANS '93*, vol. 2, pp. II/283–II/288.

[7] Funnell, C., ed., 2001, *Janes Underwater Technology*, Jane's Information Group, 4th ed.

[8] Aage, C. and Wagner Smitt, L., 1994, "Hydrodynamic manoeuvrability data of a flatfish type AUV," *OCEANS '94*, vol. 3, pp. III/425–III/430.

[9] Coxhead, M., Graham, P., Neill, R., Price, P., Travers, A., Wharington, J., and Wright, G., 2002, "A report card on Wayamba, DSTO's new uninhabited undersea research vehicle," *UDT Korea 2002*, p. 10 pp.

[10] Guo, J., Tsai, J. F., and Chiu, F. C., 1995, "Design, simulation, and control of a highly maneuverable autonomos underwater vehicle testbed," *MARIENV'95, Tokyo, Japan*, p. 8 pp.

[11] Delery, J. M., 2001, "Robert Legendre and Henri Werle: Toward the elucidation of three-dimensional separation," Annual Review Fluid Mechanics, **33**, pp. 129–154.

[12] Riabouchinsky, D. P., 1921, "On the resistance of spheres and ellipsoids in wind tunnels," Tech. rep., National Advisory Committee for Aeronautics, NACA Report 121, translated from Bulletin of the Aerodynamical Institute of Koutohino.

[13] Eichelbrenner, E. A. and Michel, R., 1958, "Observations sur la transition laminaire-turbulent en trois dimensions," Recherche aeronautique, **65**, pp. 3–10.

[14] Cebeci, T. and Cousteix, J., 1999, *Modeling and Computation of Boundary-Layer Flows*, Horizons Publishing Inc, California.

[15] Han, T. and Patel, V. C., 1979, "Flow separation on a spheroid at incidence," Journal of Fluid Mechanics, **92**, pp. 643–657.

[16] Fu, T. C., Shekarriz, A., Katz, J., and Huang, T. T., 1994, "The flow in the lee of an inclined 6:1 prolate spheroid," Journal of Fluid Mechanics, **269**, pp. 79–106.

[17] Meier, H. U. and Kreplin, H. P., 1980, "Experimental investigation of the boundary-layer transition on a body of revolution," Zeitschrift für Flugwissenschaften und Weltraumforschung, **4**, pp. 65–71.

[18] Kreplin, H. P., Meier, H. U., and Maier, A., 1978, "Wind tunnel model and measuring techniques for the investigation of three-dimensional turbulent boundary layers," *Proceedings of the AIAA 10th Aerodynamic Testing Conference, San Diego, California*, pp. 93–97, paper 78-781.

[19] Cebeci, T., 1978, "Progress in the calculation of three-dimensional laminar and turbulent boundary layers on bodies of revolution at incidence," *Proceedings of the 7th US/FRG DEA-Meeting, AFFDL-TR-78-111*, pp. 237–246.

[20] Meier, H. U., Kreplin, H. P., and Vollmers, H., 1983, "Development of boundary layers and separation patterns on a body of revolution at incidence," *2nd Symposium on Numerical and Physical Aspects of Aerodynamic Flows, State University, Long Beach, California*, T. Cebeci, ed., p. 9.

[21] Vollmers, H., Kreplin, H. P., and Meier, H. U., 1983, "Separation and vortical-type flow around a prolate spheroid - evaluation of relevant parameters," *AGARD CP-342*, pp. 14–1 – 14–14.

[22] Meier, H. U., Michel, U., and Kreplin, H. P., 1987, "The influence of wind tunnel turbulence on the boundary layer transition," *Perspectives in Turbulence Studies, International Symposium DFVLR Research Center*, pp. 26–46.

[23] Kreplin, H. P. and Stäger, R., 1993, "Measurements of the Reynolds-stress tensor in the three-dimensional boundary layer of an inclined body of revolution," *Ninth Symposium on Turbulent Shear Flows, Department of Mechanical Engineering, Kyoto., Japan*, F. Durst et al., eds., pp. 2–4–1 – 2–4–6.

[24] Wetzel, T. G., 1996, *Unsteady Flow Over a 6:1 Prolate Spheroid*, Ph.D. thesis, Virginia Polytechnic Institute and State University, Virginia.

[25] Barber, K. M. and Simpson, R. L., 1991, "Mean velocity and turbulence measurements of flow around a 6:1 prolate spheroid," AIAA Paper 91-0255, p. 10.

[26] Ahn, S., 1992, *An Experimental study of flow over a 6 to 1 prolate spheroid at incidence*, Ph.D. thesis, Virginia Polytechnic Institute and State University, Virginia.

[27] Chesnakas, C. J. and Simpson, R. L., 1994, "Full three-dimensional measurements of the cross-flow separation region of a 6:1 prolate spheroid," Experiments in Fluids, **17**(1), pp. 68–74.

[28] Chesnakas, C. J. and Simpson, R. L., 1996, "Measurements of the turbulence structure in the vicinity of a 3-D separation," ASME Journal of Fluids Engineering, **118**(2), pp. 268–275.

[29] Chesnakas, C. J. and Simpson, R. L., 1997, "Detailed investigation of the three-dimensional separation about a 6:1 prolate spheroid," AIAA Journal, **35**(6), pp. 990–999.

[30] Wetzel, T. G., Simpson, R. L., and Cheesnakas, C. J., 1998, "Measurement of three-dimensional crossflow separation," AIAA Journal, **36**(4), pp. 557–564.

[31] Goody, M., 1999, *An experimental investigation of pressure fluctuations in three-dimensional turbulent boundary layers.*, Ph.D. thesis, Virginia Polytechnic Institute and State University, Virginia.

[32] Granlund, K., 2009, *Steady and unsteady maneuvering forces and moments on slender bodies*, Ph.D. thesis, Virginia Polytechnic Institute and State University, Virginia.

[33] DeMoss, J. A., 2007, *Drag measurements on an ellipsoidal body*, Master's thesis, Virginia Polytechnic Institute and State University, Virginia.

[34] Lamb, S. H., 1932, *Hydrodynamics*, Cambridge University Press, sixth ed.

[35] Milne-Thomson, L. M., 1968, *Theoretical Hydrodynamics*, MacMillan Press Ltd, London, fifth ed.

[36] Band, E. G. and Payne, P. R., 1980, "The pressure distribution on the surface of an ellipsoid in inviscid flow," Aeronautical Quarterly, pp. 70–84.

[37] Wang, K. C., 1970, "Three-dimensional boundary layer near the plane of symmetry of a spheroid at incidence," Journal of Fluid Mechanics, **43**, pp. 187–209.

[38] Wang, K. C., 1975, "Boundary layer over a blunt body at low incidence with circumferential flow," Journal of Fluid Mechanics, **72**, pp. 49–65.

[39] Patel, V. C. and Choi, D. H., 1979, "Calculation of three-dimensional laminar and turbulent boundary layers on bodies of revolution at incidence," *2nd Symposium on Turbulent Shear Flows, Imperial College London*, L. J. S. Bradbury et al., eds., pp. 15.14–15.24.

[40] Cebeci, T., Khattab, A. K., and Stewartson, K., 1980, "On nose separation." Journal of Fluid Mechanics, **97**, pp. 435–454.

[41] Cebeci, T. and Su, W., 1988, "Separation of three-dimensional laminar boundary layers on a prolate spheroid," Journal of Fluid Mechanics, **191**, pp. 47–77.

[42] Cebeci, T., Chen, H. H., Arnal, D., and Huang, T. T., 1991, "Three-dimensional linear stability approach to transition on wings and bodies of revolution at incidence," AIAA Journal, **29**(12), pp. 2077–2085.

[43] Patel, V. C. and Baek, J. H., 1985, "Boundary layers and separation on a spheroid at incidence," AIAA Journal, **23**(1), pp. 55–63.

[44] Rosenfeld, M., Israeli, M., and Wolfshtein, M., 1988, "Numerical study of the skin friction on a spheroid at incidence," AIAA Journal, **26**(2), pp. 129–136.

[45] Rosenfeld, M., Wolfshtein, M., and Israeli, M., 1992, "A numerical study of the laminar incompressible flow over a 6-1 prolate spheroid at incidence," International Journal for Numerical Methods in Fluids, **15**(2), pp. 147–173.

[46] Gee, K., Cummings, R. M., and Schiff, L. B., 1992, "Turbulence model effects on separated flow about a prolate spheroid," AIAA Journal, **30**(3), pp. 655–664.

[47] Constantinescu, G. S., Pasinato, H., Wang, Y., Forsythe, J. R., and Squires, K. D., 2002, "Numerical investigation of flow past a prolate spheroid," Journal of Fluids Engineering, **124**, pp. 904–910.

[48] Kim, S. E., Rhee, S. H., and Cokljat, D., 2003, "Application of modern turbulence models to vortical flow around a 6:1 prolate spheroid at incidence," AIAA Paper 2003-429, p. 11.

[49] Wilcox, D. C., 1998, *Turbulence Modeling for CFD*, D C W Industries Inc., California.

[50] Wikström, N., Svennberg, U., Alin, N., and C., F., 2004, "Large eddy simulation of the flow around an inclined prolate spheroid," Journal of Turbulence, **5**(1), p. 18.

[51] Karlsson, A. and Fureby, C., 2009, "LES of the flow past a 6:1 prolate spheroid." *47th AIAA Aerospace Sciences Meeting including The New Horizons Forum and Aerospace Exposition, Orlando, Florida*, p. 13, paper AIAA-2009-1616.

[52] Brandner, P. A. and Walker, G. J., 2007, "An experimental investigation into the performance of a flush water-jet inlet," Journal of Ship Research, **51**(1), p. 21.

[53] Hoerner, S. F., 1965, *Fluid-Dynamic Drag*, Hoerner Fluid Dynamics, New Jersey, second ed.

[54] Blevins, R. D., 1979, *Formulas for natural frequency and mode shapes*, Krieger Publishing Company, Malabar, Florida.

[55] Meier, H. U. and Kreplin, H. P., 1978, "Pressure distributions and flow visualisations on an ellipsoid 1:6 designed for three-dimensional boundary layer investigations," *Proceedings of the 7th US/FRG DEA-Meeting AFFDL-TR-78-111*, A. W. Fiore, ed., pp. 197–208.

[56] Bevington, P. R. and Robinson, D. K., 2003, *Data Reduction and error analysis for the physical sciences*, McGraw-Hill, New York, third ed.

[57] Cousteix, J. and Pailhas, G., 1979, "Exploratory study of a laminar-turbulent transition process close to laminar boundary layer separation," Recherche Aerospatiale - English, **3**, pp. 79–85.

[58] Brawslow, A. L. and Knox, E. C., 1958, "Simplified method for determination of critical height of distributed roughness particles for boundary-layer transition at Mach numbers from 0 to 5," Tech. rep., National Advisory Committee for Aeronautics, NACA TN 4363.

[59] Barlow, J. B., Rae, W. H., and Pope, A., 1999, *Low-Speed Wind Tunnel Testing*, John Wiley & Sons, New York, third ed.

[60] Von Doenhoff, A. E. and Horton, E. A., 1958, "A low-speed experimental investigation of the effect of a sandpaper type roughness on boundary-layer transition," Tech. rep., National Advisory Committee for Aeronautics, NACA Report 1349.

[61] Panaaras, A. G. and Steger, J. L., 1988, "A thin-layer solution of the flow about a prolate spheroid," Zeitschrift für Flugwissenschaften und Weltraumforschung, **12**, pp. 173–180.

[62] ATI Industrial Automation, 2003, *ISA F/T-16 Intelligent Multi-axis Force/Torque Sensor System, Installation and operation manual.*

[63] Tobak, M. and Peake, D. J., 1982, "Topology of three-dimensional separated flows," Annual Review Fluid Mechanics, **14**, pp. 61–85.

[64] Perry, A. E. and Chong, M. S., 1987, "A description of eddying and flow patterns using critical-point concepts," Annual Review Fluid Mechanics, **19**, pp. 125–155.

[65] Wang, K. C., 1974, "Boundary layer over a blunt body at high incidence with an open type separation," Proceedings of the Royal Society A, **340**, pp. 33–35.

[66] Simpson, R. L., 1968, "Aspects of turbulent boundary layer separation," Progress in Aerospace Sciences, **6**(3), pp. 543–545.

[67] Wu, J. K., Trammel, R. W., Zhu, F. L., and Yin, X. Y., 2000, "Boundary layer over a blunt body at high incidence with an open type separation," Physics of Fluids, **12**(8), pp. 1932–1954.

[68] Squire, L. C., 1961, "The motion of a thin sheet oil sheet under the steady boundary layer on a body," Journal of Fluid Mechanics, **11**, pp. 161–179.

[69] LightHill, M. J., 1963, *Laminar Boundary Layers.*, chap. II - Boundary Layer Theory, Oxford Clarendon Press, pp. 46–113.

[70] Biagioni, L. and d'Agostino, L., 1999, "Measurement of energy spectra in weakly compressible turbulence." 17th AIAA Applied Aerodynamics Conference, AIAA 99-3516, p. 8.

[71] Bradshaw, P., 1971, *An Introduction to Turbulence and its Measurement.*, Pergamon Press, New York.

[72] Brandner, P. A., Clarke, D. B., and Walker, G. J., 2004, "Development of a fast response pressure probe for use in a cavitation tunnel." *15th Australasian Fluid Mechanics Conference*, B. M. et al., eds., p. 4.

[73] Cebeci, T. and Cousteix, J., 1999, *Modeling and computation of boundary-layer flows*, Horizons Publishing Inc., Long Beach, California.

[74] Timoshenko, S. and Woinowsky-Krieger, S., 1959, *Theory of plates and shells*, McGraw-Hill Book Company, New York.

[75] Sirohi, R. S. and Radha Krishna, H. C., 1991, *Mechanical measurements*, Wiley, John & Sons, third ed.

[76] Mazumdar, J., 1971, "Transverse vibration of elastic plates by the method of constant deflection lines." Journal of Sound and Vibration, **18**(2), pp. 147–155.

[77] Arndt, R. E. A. and Ippen, A. T., 1970, "Turbulence measurements in liquids using an improved total pressure probe." Journal of Hydraulic Research, **8**(2), pp. 131–158.

[78] Tang, S. K., 2005, "On helmholtz resonators with tapered necks." Journal of Sound and Vibration, **279**, pp. 1085–1096.

[79] National Instruments Corporation, 2000, *LabVIEW VIs and Functions*.

[80] Emmons, H. W., 1951, "The laminar-turbulent transition in a boundary layer - part 1." Journal of the Aeronautical Sciences, **18**(7), pp. 490–498.

[81] Bull, M. K., 1996, "Wall-pressure fluctuations beneath turbulent boundary layers: Some reflections on forty years of research." Journal of Sound and Vibration, **190**(3), pp. 299–315.

[82] Hedley, T. B. and Keffer, J. F., 1974, "Turbulent/non-turbulent decisions in an intermittent flow." Journal of Fluid Mechanics, **64**, pp. 625–644.

[83] Canepa, E., 2002, "Experiences in the application of intermittency detection techniques to hot-film signals in transitional boundary layers." *The 16th Symposium on Measuring Techniques in Transonic and Supersonic Flow in Cascades and Turbomachines*, p. 10.

[84] Solomon, W. J., 1996, *Unsteady Boundary Layer Transition on Axial Compressor Blades.*, Ph.D. thesis, University of Tasmania.

[85] Dhawan, S. and Narasimha, R., 1958, "Some properties of boundary layer flow during the transition from laminar to turbulent motion," Journal of Fluid Mechanics, **3**(4), pp. 418–436.

[86] Gostelow, J. P., Blunden, A. R., and Walker, G. J., 1994, "Effect of free-stream turbulence and adverse pressure gradients on boundary layer transition," Journal of Turbomachinery, **116**, pp. 392–404.

[87] White, F. M., 1991, *Viscous fluid flow*, McGraw-Hill Inc., New York.

[88] Dryden, H. L., Schubauer, G. B., Mock, W. C., and Skramstad, H. K., 1937, "Measurements of intensity and scale of wind-tunnel turbulence and their relation to the critical

reynolds number of spheres," Tech. rep., National Advisory Committee for Aeronautics, NACA Report 581.

[89] Spangler, J. G. and Wells, C. S., 1998, "Effects of freestream disturbances on boundary-layer transition." AIAA Journal, **36**(4), pp. 557–564.

[90] Drela, M. and Giles, M. B., 1987, "Viscous-inviscid analysis of transonic and low reynolds number airfoils," AIAA Journal, **25**(10), pp. 134–1355.

[91] Stock, H. W., 2006, "Navier-Stokes airfoil computations with e^N transition prediction including transitional flow regions," AIAA Journal, **44**(1), pp. 108–118.

[92] Langtry, R. B., Menter, F. R., Likki, S. R., Suzen, P. G., Y. B.and Huang, and Völker, 2004, "A correlation-based transition model using local variables part II - test cases and industrial applications," *Proceedings of ASME Turbo Expo 2004*, p. 11.

[93] Menter, F. R., Langtry, R. B., Likki, S. R., and Suzen, P. G., Y. B.and Huang, 2004, "A correlation-based transition model using local variables part I - model formulation," *Proceedings of ASME Turbo Expo 2004*, p. 11.

[94] Fluent Inc., 2005, *Fluent 6.2 Users Guide*.

[95] Kim, S. E., Choudhury, D., and Patel, B., 1999, "Computations of complex turbulent flows using the commercial code Fluent," *Modeling complex turbulent flows*, M. D. Salas et al., eds., Kluwer Academic Publishers, pp. 259–276.

[96] Menter, F. R., 1994, "Two-equation eddy-viscosity turbulence models for engineering applications," AIAA Journal, **32**(8), pp. 1598–1604.

[97] Jongon, T., 1998, *Simulation and modeling of turbulent incompressible fluid flows*, Ph.D. thesis, EPF Lausanne, Lausanne, Switzerland.

[98] Jongen, T. and Marx, Y. P., 1997, "Design of an unconditionally stable, positive scheme for the k-ε and two-layer turbulence models," Computers & Fluids, **26**(5), pp. 469–487.

[99] Lighthill, M. J., 1958, "On displacement thickness," Journal of Fluid Mechanics, **4**, pp. 383–392.

[100] Morini, L., Chen, L.-T., and Suciu, E. O., 1975, "Steady and oscillatory subsonic and supersonic aerodynamics around complex configurations," AIAA Journal, **13**(3), pp. 368–374.

[101] Popov, A. V., Botez, R. M., and Labib, M., 2008, "Transition point detection from surface pressure distribution for control design," Journal of Aircraft, **45**(1), pp. 23–28.

[102] Clarke, D. B., Brandner, P. A., and Walker, G. J., 2007, "Computational and experimental investigation of flow around a 3-1 prolate spheroid," *16th Australasian Fluid Mechanics Conference*, P. Jacobs et al., eds., pp. 1381–1387.

[103] Curle, N., 1967, "A two-parameter method for calculating the two-dimensional incompressible laminar boundary layer," Journal of the Royal Aeronautical Society, **71**, pp. 117–123.

[104] Stock, H. W. and Haase, W., 2000, "Navier-Stokes airfoil computations with e^N transition prediction including transitional flow regions," AIAA Journal, **38**(11), pp. 2059–2066.

[105] Head, M. R. and Hayasi, N., 1967, "Approximate calculations of the incompressible laminar boundary layer," The Aeronautical Quarterly, **18**, pp. 259–272.

[106] Stock, H. W., 1980, "Laminar boundary layers on inclined ellipsoids of revolution," Zeitschrift für Flugwissenschaften und Weltraumforschung, **4**, pp. 217–224.

[107] Willmarth, W. W., 1975, "Pressure fluctuations beneath turbulent boundary layers," Annual Review Fluid Mechanics, **7**, pp. 13–38.

[108] Schlichting, H. and Gersten, K., 2000, *Boundary Layer Theory*, Springer-Verlag, Berlin, eighth ed.

[109] Dress, D., 1990, "Drag measurements on a modified prolate spheroid using a magnetic suspension and balance system," Journal of Aircraft, **27**(6), pp. 523–528.

[110] Costi, S. and Portnoy, H., 1974, "Incompressible, inviscid, symmetrical flow about ellipsoids - comparison of an approximate theory with exact results," Scientific Report 5, Department of Aeronautical Engineering, Technion - Israel Institute of Technology.

[111] Hobson, E. W., 1931, *The theory of spherical and ellipsoidal harmonics*, Cambridge University Press, London.

[112] Carlson, B. C., 1995, "Numerical computation of real or complex elliptic integrals," Numerical Algorithms, **10**, pp. 13–26.

[113] The Numerical Algorithms Group Limited, Oxford, 1994, *NAG C Library Manual, Mark 3*, vol. 3.